DANILO CALDERINI

KINETICS AND DYNAMICS FOR CHEMICAL REACTIONS IN GAS PHASE

KINETICS AND DYNAMICS FOR CHEMICAL REACTIONS IN GAS PHASE

DANILO CALDERINI

SCUOLA NORMALE SUPERIORE

Ph.D. in Chemistry

Supervisor: Vincenzo Barone
Co-supervisor: Dimitrios Skouteris
Scuola Normale Superiore

August 2016

ABSTRACT

A deep understanding of molecular reactions is a challenging task since the range of time and energy covered implies a wide and dense grid for the numerical representation of the reactive Hamiltonian.

For a computational chemist, the accurate prediction of its value starting from the definition of reactants and products is fascinating and demanding, but can be extremely useful for further investigation and optimization problems.

Several methods, all derived by the Transition State Theory, have been developed to avoid the computational cost of the Hamiltonian representation on a large, multidimensional grid; we investigate these strategies both in the time and energy domain to explore the advantages and drawbacks of these reciprocal spaces.

Since we want to increase the range of applicability of the calculation of thermal rate constants to medium size molecules, which can have floppy geometries with low frequency modes, we introduce a dedicated treatment of such modes based on the Intrinsic Reaction Path of Fukui.

In Part i, we introduce the theoretical instrument used to perform our calculation, both in energy and time domain; Part ii is devoted to the presentation of the applications, mainly focused on current issues in astrochemical studies. Appendices treat specific topics, like Möller operators, essential for the comprehension of the theory but too long to be inserted in Part i.

PUBLICATIONS

The work of my Ph.D. Thesis is based on the following publications:

- Fanny Vazart, Danilo Calderini, Dimitrios Skouteris, Camille Latouche and Vincenzo Barone: **Reassessment of the Thermodynamic, Kinetic, and Spectroscopic Features of Cyanomethanimine Derivatives: A Full Anharmonic Perturbative Treatment**. – *Journal of Chemical Theory and Computation*, Volume 11, Number 3, 1165-1171, **2015**, DOI = 10.1021/ct501147a, URL: http://dx.doi.org/10.1021/ct501147a

- Dimitrios Skouteris, Danilo Calderini and Vincenzo Barone: **Methods for Calculating Partition Functions of Molecules Involving Large Amplitude and/or Anharmonic Motions**. – *Journal of Chemical Theory and Computation*, Volume 12, Number 3, 1011-1018, **2016**, DOI = 10.1021/acs.jctc.5b01094, URL: http://dx.doi.org/10.1021/acs.jctc.5b01094

- Thiago Ferreira da Cuñha, Danilo Calderini and Dimitrios Skouteris: **Analysis of Partition Functions for Metallocenes: Ferrocene, Ruthenocene, and Osmocene**. – *The Journal of Physical Chemistry A*, Volume 120, Number 27, 5282-5287, **2016**, DOI = 10.1021/acs.jpca.6b01280, URL: http://dx.doi.org/10.1021/acs.jpca.6b01280

- Fanny Vazart, Danilo Calderini, Cristina Puzzarini, Dimitrios Skouteris and Vincenzo Barone: **State-the-art thermochemical and kinetic computations for astrochemical complex organic molecules: formamide formation in cold interstellar clouds as a case study**. – *Journal of Chemical Theory and Computation*, *Accepted*

ACKNOWLEDGMENTS

I want to express my deepest gratitude to all the members of the chemistry group of the SNS for their support and advice, especially prof. Vincenzo Barone and dot. Dimitrios Skouteris for their scientific assistance. I thank my friends Matteo, Giordano, Ivan, Michele, Danilo, Teresa, Elisa, Alberto, Marco, Emanuele, Fanny, Julien and Camille to share this great adventure with me.

Also to my friends Lorenzo, Davide, Paolo, the fighter of Santa Maria, Caterina and all the people that cross my walk and make me smile: thank you for all.

Most importantly, the continuous support of my family makes all of this possible: without you I'm nothing.

CONTENTS

LIST OF TABLES

ACRONYMS

ABC Absorbing Boundary Condition

BO Born-Oppenheimer approximation

CD Current Density

Cp Cyclopentadienyl

CRP Cumulative Reaction Probability

DOS Density of States

DOF Degree of Freedom

DFT Density Functional Theory

DFVP Dirac-Frenkel Variational Principle

DVR Discrete Value Representation

FFCF Flux-Flux Correlation Function

FBR Finite Basis Representation

GWP Gaussian WavePackets

GC Generalized Coordinate

G-MCTDH Gaussian Multi Configuration Time Dependent Hartree

JWKB Jeffreys-Wentzel-Kramers-Brillouin method

KME Kinetic Master Equation

HR Hindered Rotations

HRPF Hindered Rotor Partition Function

IRC Intrinsic Reactive Coordinate

ISM Interstellar Medium

LAM Large Amplitude Motions

LHA Local Harmonic Approximation

MC Monte Carlo

MD MetaDynamics

MEP Minimum Energy Path

MPF Molecular Partition Function

MCTDH Multi Configuration Time Dependent Hartree

PES Potential Energy Surface

QCT Quasi Classical Trajectory

RRKM Rice-Ramsperger-Kassel-Marcus theory

RPH Reaction Path Hamiltonian

RHS Right Hand Side

SPF Single Particle Function

SPT Simple Perturbation Theory

SOS Sum of States

STMD Statistical Temperature Molecular Dynamics

TS Trasition State

TST Trasition State Theory

TDSE Time Dependent Schrödinger Equation

TISE Time Independent Schrödinger Equation

VPT2 Second order Vibrational Perturbation Theory

WL Wang-Landau algorithm

ZPE Zero Point Energy

Part I

THEORY

1

THE RATE CONSTANT

Chemistry is the discipline that studies matter and its transformations; as physical chemists, our goal is to understand, describe and predict the behaviour of matter at the highest level of accuracy we can reach.

In the ensemble of all the typologies of behaviour of matter, chemical reactions are probably the most important ones, since the technological consequences of a better knowledge of reactions can improve almost every field of human activity. An atomistic description of reactions has to be used in order to obtain the details of chemical rate dependence on physical quantities such as translational motion, vibrational population, rotational orientation...

For these reasons, it is not surprising that the first experiments and theoretical investigations were made on gas phase unimolecular reactions with an inert gas (usually a noble gas, treated as an ensemble of structureless particles) as a thermal bath.

Even if common sense associates chemical reactions with the liquid phase due to the stereotype of chemistry as an empirical science done with laboratory glassware, the ability to make accurate predictions of the evolution of gas phase reactions is crucial for various fields, from astronomy to aeronautical engineering, from pharmaceutics to electronic industries [1].

From a phenomenological point of view, experiments in chemical kinetics have shown a relation between the rate of a reaction and two macroscopic variables: the concentrations of the reactants $R_1, R_2, \ldots$ that we denote using squared brackets, $[R_1], [R_2] \ldots$, and the temperature T of the system.

Even in a favourable field of investigation like gas phase molecular reactions, this dependence is cumbersome in most of the experimental cases.

This happens because in general reactions are *complex*, which means that they are constituted of an ensemble of steps, called *elementary reactions*.

An elementary reaction involves two groups of stable molecules, one that defines the reactants and one that defines the products (see Section 2.1 for a formal definition of a stable molecule).

The first step to inquire on the behaviour of the microscopic events that lead to the generic reaction is the isolation of the chain of elementary reactions that identify the *reaction mechanism*, that will be treated in Section 2.8.

Elementary reactions are divided in terms of their *molecularity*, i.e. the number of reactants involved in it:

- Unimolecular: one molecule reacts to give a product (e.g. *cis-trans* conversion) or more products (i.e. dissociation);
- Bimolecular: two molecules react to produce one or more products;
- Termolecular: three molecules react to give one or more products.

The evolution of a reaction is commonly measured by the velocity of disappearance of (one of) the reactants weighted by its stoichiometric coefficient, which has the dimension of concentration divided by time, $[\cdot]t^{-1}$.

For a unimolecular reaction,

$$R \underset{k'(T)}{\overset{k(T)}{\rightleftharpoons}} P_1 + P_2 + \dots \tag{1}$$

The rate of disappearance is found to be

$$-\frac{d[R]}{dt} = k(T)[R] - k'(T)\prod_{i=1}^{n}[P_i] \tag{2}$$

where $k(T)$ is the thermal unimolecular rate constant and $k'(T)\prod_{i=1}^{n}[P_i]$ is the rate of the inverse reaction, which depends on the concentration of the products; note that the unit of $k(T)$ is the inverse of time.

Assuming the case of an elementary bimolecular reaction where P_n are a set of products,

$$R_1 + R_2 \underset{k'(T)}{\overset{k(T)}{\rightleftharpoons}} P_1 + P_2 + \dots$$

the time evolution of a reaction can be described by a second-order law, following the rate of decrease of one of the reactant concentration:

$$-\frac{d[R_1]}{dt} = k(T)[R_1][R_2] - k'(T)\prod_{i=1}^{n}[P_i] \tag{3}$$

where we intend that the rate dependence is of the first order for both of the reactants. Here the unit of the thermal rate contant of a bimolecular reaction is the inverse of concentration $\times$ time ($([\cdot]t)^{-1}$).

Termolecular reactions follow the same structure, but they will never be discussed in this Thesis because the collision of three bodies is a rare event, therefore this kind of reactions are almost negligible.

Eq. 2 and Eq 3 are the starting points of our research and they will be always considered true. Since the concentration of molecules does

not contain any information about what is actually happening but can be experimentally measured with high level of accuracy, all the information about the physical process like energy transfer between particles, quantum effects, non-equilibrium statistics... is contained in $k(T)$.

Therefore, the calculation of thermal rate constants is a formidable task which involves the Boltzmann average over the evolution of all states available at a given temperature, while the environment exchanges energy with the reactive molecules before and after the reaction.

In this Thesis we will focus on gas phase reactions, where molecules can be treated as singular, isolated systems in vacuum that interact only with other reactants (if necessary for the reaction). The main objective is to find a computation strategy to calculate $k(T)$ in a reasonable way that limits the computational cost in order to perform the calculation on a dedicated workstation, instead of a large cluster.

The first attempt to find a formula to calculate $k(T)$ was made in 1889, when Svante Arrhenius found experimentally an exponential-type relation between temperature and rate constant, described in his well-known equation

$$k(T) = Ae^{-E_a/RT} \tag{4}$$

where A is the pre-exponential factor, E_a is the activation energy and R is the thermodynamic ideal gas constant. The previous equation can be derived from a classical treatment of hard sphere collisions [2] where the probability of reaction is always one if the particles have a relative translational energy greater or equal to the activation barrier.

Even if the Arrhenius law can be considered a fundamental step for the comprehension of chemical reactions, due to its direct and simple treatment, some drawbacks can be found:

- It neglects every information about internal state distribution of products and reactants. This could lead to vast errors in complex chains of elementary reactions, where the products become the reactants for another reaction step.
- In the low temperature regime, where quantum effects dominate, most reaction rates diverge from linearity in an Arrhenius plot, which displays the logarithm of kinetic constants $\ln(k(T))$ on the ordinate axis plotted against the inverse temperature $1/T$ on the abscissa.

The complete description of the microscopic events that lead to a chemical reaction can be studied by solving the equation of motion under the laws of non relativistic quantum mechanics, (i.e., following the dynamics of the system) in the microcanonical ensemble (i.e. for a given energy, volume and number of particles). This approach

is called *reaction dynamics*, since we technically observe the system moving.

One of the results of the investigation of the dynamics is the Cumulative Reaction Probability (CRP) $N(E)$, which allows to calculate the thermal rate constant for each temperature T with a straightforward calculation, averaging on the Boltzmann statistics

$$k(T) = \frac{1}{hQ_R(T)} \int_{-\infty}^{\infty} N(E) e^{-\frac{E}{k_B T}} \, dE \tag{5}$$

where $Q_R(T)$ is the reactant partition function per unit volume and k_B is the Boltzmann constant, while h is the Planck constant.

The CRP is the sum of probabilities that each state of the reactants α goes to a specific state β of the products [3]

$$N(E) = \sum_{\alpha,\beta} P_{\alpha,\beta}(E) \tag{6}$$

therefore, the CRP is not normalizable and does not share any properties of probability distribution, as wavefunctions do.

On the other hand, it is possible to calculate the thermal rate constant as an integral with respect to time t of the Flux-Flux Correlation Function (FFCF) $C_f(t)$, which represents the autocorrelation function of a quantum system in a reactive geometry at time zero and itself

$$k(T) = \frac{1}{Q_R(T)} \int_0^{\infty} C_f(t) \, dt \tag{7}$$

where

$$C_f(t) = i \, tr\left[\bar{F}\hat{U}(-t_c)\bar{F}\hat{U}(t_c)\right] \tag{8}$$

In the previous equation, $\bar{F}$ is a symmetrized flux operator across a generic surface that properly divides reactants and products regions in the configurational space and $\hat{U}(t_c)$ is the propagator in the complex time t_c.

The formal derivation of the CRP and the FFCF will be presented in Chapter 2 and Chapter3, respectively.

The most used levels of theory for reaction dynamics are the following:

- Classical: the molecules are particles that follow the classical equations of motion;
- Quasiclassical: the molecules follow again the classical equation of motion, but quantum mechanical properties (like tunneling) can be added with some *a posteriori* corrections;
- Semiclassical: the molecules are described using a simplified wavefunction description, which allows to treat quantum effects in a coherent, but approximate approach;

- Quantum: the molecules are described in terms of wavefunctions that follow the laws of quantum mechanics.

The choice of the level of theory is a consequence of the characteristics of the molecular system and its environment (electromagnetic radiation, presence and effects of the solvent...), the accuracy that we want to reach and the computational resources that we use.

The knowledge of the whole Potential Energy Surface (PES) (see Appendix A for more details) is a common prerequisite for the numerical implementation of almost every dynamical theory proposed [4]. Therefore, small molecular systems, such as atom-diatom reactions in the gas phase ($H + H_2$, for example) are the usual benchmark, and in general analytic PES are not available for reactions involving more than five atoms.

Due to the large number of calculations needed to create the PES and to solve the equations of motion, all these different theories, in each specific approach and approximation scheme, were applied after the introduction of modern calculators, during the second part of the last century.

At the *classical* level of theory, the trajectories are run over a PES, together with some reasonable initial conditions for the coordinates and momenta. To sample as much as possible of the initial phase space (coordinates and momenta) and to get meaningful results, many trajectories (usually thousands or tens of thousands) should be run.

Often one restricts the initial vibrational energies in the various vibrational modes to their allowed quantized values, and when this is done the method is usually called the Quasi Classical Trajectory (QCT) method [5]. QCT calculations can give accurate results when dynamical quantum effects such as zero point energy, tunneling, and resonances are not important.

Semiclassical methods, instead, are a class of approximation based on the (Jeffreys-Wentzel-Kramers-Brillouin method (JWKB)) method for differential equations [6], which provides analytic formulae for wavefunctions, energy levels, scattering cross sections... in the limiting case of $\hbar \to 0$, i.e. when the action in the corresponding classical counterpart is high enough to ignore the magnitude of $\hbar$. Since the seventies of the last century, semiclassical models for chemical reactions have been proposed and refined [7, 8, 9, 10], involving various schemes of corrections [11].

The adjective "semiclassical" is also used to define some hybrid methodologies [12, 13], where classical trajectories are propagated and successively a WKB solution of the Schrödinger equation is performed to reproduce quantum effects like the surface hopping between different PES [14].

If experiments or other sources of information suggest that the reaction is strongly non classical (for example, if we expect the presence of resonance peaks or classically forbidden events), we are forced to

treat reactions at the *quantum* level, usually in the frame of Scattering Theory [15]. In a quantum mechanics picture, the structure of a molecule is described by a multidimensional nuclear wavefunction including the rotations, the vibrations and reactions that it can accomplish: while the former two motions conserve its molecular identity, the latter allows to reach new chemical structures under the restriction of mass conservation.

Also electrons in molecules, which are coherently described only in frame of quantum mechanics laws, play a crucial role in chemical reactions. Not only does their Coulomb interaction with nuclei and themselves generate an infinite number of PES (the lowest one is, normally, the only one supposed to be populated), but they can also exchange energy through electromagnetic radiation(visible and UV) not accessible directly to nuclei.

Electrons (see Eq. 12 in Chap. 2 for a formal definition) not only absorb energy, eventually making it available to nuclear motions, but, when the energy difference between two or more of electronic states is low enough, they also permit non classical behaviour such as surface hopping [16, 17].

Another way to obtain the CRP or FFCF is by using the Trasition State Theory (TST), thanks to which the computational cost is dramatically reduced avoiding the calculation of the whole PES. The main idea under TST is that the molecular system of the reactants will move in the configurational space under the appropriate laws of motion, but the reaction will take place only if the system assumes a specific geometry called Trasition State (TS). A necessary condition to the successful application of TS is that the reaction must be elementary [18].

Almost every chemical reaction of practical interest consists of a network of elementary steps, each with its own contribution to the global kinetics, where each reactant and product of each step is the product and the reactant of another elementary reaction forming a chemical pathway (see Section 2.8 in Chapter 2 for more details).

TST moves the reaction rate calculation from a global problem (that needs a whole PES to be resolved) to a series of local problems, that involves the calculation of a smaller number of points along the PES, especially when the number of atoms rises above ten.

The TST results are called kinetic, because our goal becomes the evaluation of the rate of reaction between some reference structures.

The concepts introduced in this Chapter will be discussed in Chapter 2 and Chapter 3. Chapter 4, Chapter 5 and Chapter 6 will cover the applications to chemical reactions of astrochemical interest.

2

ENERGY FRAMEWORK

2.1 TIME INDEPENDENT SCHRÖDINGER EQUATION

Chemical reactions are a complex class of physical events that hide both theoretical and experimental problems, because both their causes and consequences involve wide time and energy scales.

From a theoretical perspective, the first step is to introduce the Time Independent Schrödinger Equation (TISE) 9 for *different geometries* of the atoms N_a and electrons N_i that constitute the molecules

$$\hat{H}(R,r)\Psi(R,r) \equiv [\hat{T}(R,r) + \hat{V}(R,r)]\Psi(R,r) = E\Psi(R,r) \tag{9}$$

where 'R' represents the nuclear coordinates and 'r' are the electronic ones. As in standard textbooks, $\hat{H}(R,r)$ is the Hamiltonian, $\hat{T}(R,r)$ is the kinetic energy operator and $\hat{V}(R,r)$ is the potential.

Thus, reactants R and products P are solutions (relative minima) of the nuclear motion described by the TISE. This definition is almost arbitrary, because polyatomic molecules have a vast ensemble of geometries that satisfy this condition. Structural isomers are the clearest examples of how many geometries satisfy the same TISE with a fixed number of atoms and electrons, but in general this number is much higher, including a variety of geometries called generically *intermediates*.

In other words, we are almost free to choose any geometry which is a minimum as our reactants and products, but normally the chemical problem itself defines R and P. Nevertheless, for fixed R and P we usually find that the molecular system passes through a number of intermediates. These geometries are crucial because it is possible to decompose a reaction into a series of elementary reactions from one intermediate to another. Section 2.8 is devoted to the description of chains of elementary reactions and their combination, called reaction mechanism.

If not differently specified, every time we talk about reaction, we refer to an elementary reaction.

The Hamiltonian in Eq. 9 can be written in atomic units as

$$\hat{H} = -\frac{1}{2}\sum_{a=1}^{N_a}\frac{\nabla_a^2}{M_a} - \frac{1}{2}\sum_{i=1}^{N_i}\nabla_i^2 + \sum_{a>b}\frac{Z_a Z_b}{|R_a\text{-}R_b|} + \sum_{i>j}\frac{1}{|r_i\text{-}r_j|} - \sum_{a,i}\frac{Z_a}{|R_a\text{-}r_i|} \tag{10}$$

The letters 'a' and 'b' label the nuclei of the atoms of the molecule, whereas 'i' and 'j' are used for electrons, which have unit mass and

charge in atomic units. In particular, the first two terms are the kinetic operators for nuclei and electrons, respectively; the other three represent the nuclear and electronic repulsion potential (both with positive sign) and the attractive potential between nuclei and electrons (with negative sign).

Eq. 10 depends on all the electrons and all the nuclei of the molecules related with the chemical reactions. In the case of bimolecular reaction or unimolecular decompositions, where the same amount of particles is shared or divided depending on the reaction stage, we treat each fragment of the whole molecule as non interacting, i.e. placed at infinity with respect to each other.

This assumption is consistent with the non-relativistic quantum mechanics used in this Thesis, where particles (nuclei and electrons) cannot be destroyed nor created.

The first strategy to decrease the complexity of Eq. 9 is to treat separately electrons and nuclei: this approach, called the Born-Oppenheimer approximation (BO) approximation [19], allows us to resolve the electronic part of Schrödinger equation for a specific, fixed geometry of the nuclei.

In the BO approximation, the Hamiltonian is separated into two parts, one for the electronic part $\hat{H}_{el}$ and another for the nuclear part $\hat{H}_{nuc}$

$$\hat{H} = \hat{H}_{nuc} + \hat{H}_{el} \tag{11}$$

where

$$\hat{H}_{el} = -\frac{1}{2}\sum_{i=1}^{N_i}\nabla_i^2 + \sum_{a>b}\frac{Z_a Z_b}{|\mathbf{R}_a - \mathbf{R}_b|} + \sum_{i>j}\frac{1}{|r_i - r_j|} - \sum_{a,i}\frac{Z_a}{|\mathbf{R}_a - r_i|} \tag{12}$$

and

$$\hat{H}_{nuc} = -\frac{1}{2}\sum_{a=1}^{N_a}\frac{\nabla_a^2}{M_a} \tag{13}$$

In Eq. 12 the use of $\mathbf{R}$ means that the nuclear positions are fixed parameters; the spectrum of eigenvalues $\epsilon_i(\mathbf{R})$, also PES, absorbs also the repulsive nuclear potential because it is an additive term which is irrelevant for the results.

The electronic part of the Schrödinger equation is

$$\hat{H}_{el}\phi_i(r;\mathbf{R}) = \epsilon_i(\mathbf{R})\phi_i(r;\mathbf{R}) \tag{14}$$

where the notation $\phi(r;\mathbf{R})$ means that the electronic wavefunctions are functions of the electronic coordinates and accept R as parameters. To obtain a more compact notation, from here to the end of the Chapter 2 we use the Dirac bracket notation.

By the Spectral Theorem [20], the eigenfunctions $\phi(r;\mathbf{R})$ of a self-adjoint operator form a complete and orthogonal basis set at each $\mathbf{R}$

$$\sum_i |\phi_i(r;\mathbf{R})\rangle \langle \phi_i(r;\mathbf{R})| = 1 \qquad \langle \phi_i(r;\mathbf{R})| \left|\phi_j(r;\mathbf{R})\right\rangle = \delta_{i,j} \tag{15}$$

where $\delta_{i,j}$ is Kronecker's delta function.

The reason under the BO approximation comes from a kinematic consideration: electrons are roughly two thousand times lighter than the hydrogenion, which is the lightest atom in the periodic table. This means that electrons respond faster than nuclei to internal or external forces, as if the latter are 'frozen' from the electron's point of view.

There are cases where the BO approximation does not work perfectly, but the error can be evaluated and even recovered with various strategies [17]. A common example of this failure is the behaviour of the nuclear motion in the neighbourhood of conical intersections [21], where two or more electronic states show some kind of degeneracy ($\epsilon_i \simeq \epsilon_j$).

Another example of process that involves more electronic states is the interaction with visible or UV photons, which can be created (via emission) or destroyed (via absorption) by molecules. In this dissertation we exclude electronic photon-induced phenomena and surface hopping, focusing our analysis on reactions where only the first (or ground) electronic state ϵ_1 of Equation 14 is populated, supposing it is well defined and not degenerate. Nevertheless, it is still possible to study the influence of photons on chemical reactions from *ab initio* methods [16].

Electronic calculations, also known as quantum chemistry calculations, can be performed with a dedicated software [22], which can yield all the information (energy, Gradient, Hessian...) we need about each nuclear geometry.

After the solution of the electronic Hamiltonian, Eq 11 can be written in the BO framework as

$$\hat{H}_{BO} \approx \hat{H}_{nuc} + \epsilon_1(\mathbf{R}) \tag{16}$$

and then used to solve the equation

$$(\hat{H}_{nuc} + \epsilon_1(\mathbf{R}))\varphi(R) = E\varphi(R) \tag{17}$$

Again, the nuclear wavefunction $\varphi(R)$ depends directly on the coordinates of the nuclei.

The product function $\varphi(R) \cdot \phi(r;\mathbf{R})$ is the BO approximated solution of Eq. 9.

2.2 CHEMICAL KINETICS

The unfeasible computational cost of the evaluation of a whole PES (see Appendix A) for medium sized molecules leads to the necessity

of a theory that can predict the rate constant using the least number of quantum chemistry calculations.

All of these theories start with the identification of a specific geometry that drives the reaction, namely the TS, since it represents the lowest energetic geometric arrangement that the molecule can reach in the motion from reactants to products.

Many different versions of TST have been proposed during the last 90 years [23, 24, 25, 26, 27, 28, 29, 30, 31] but the identification of the TS is always a crucial challenge.

Formally, the dynamics of a complex molecule can be accurately described only in the phase space using the laws of quantum mechanics, i.e. by sampling with a sufficient (normally large) number of quantum trajectories the space spanned by the 3N coordinates and 3N momenta.

We have to identify a point in the whole *phase space* that represents the dynamical bottleneck of the reaction, which in principle depends not only on the geometry of the nuclei, but also on the momenta [32, 33], which are coupled with all the coordinates.

This treatment needs again the knowledge of the global PES and expensive calculations.

On the other hand, we can easily locate in the *coordinate space* a first order saddle point, a specific geometry along a chosen reactive molecular coordinate (usually, a bond length) and define it as the Transition State, the bottleneck that the reactants have to surpass to become the products.

Under this preliminary consideration, we are going to introduce the microcanonical version of TST, called Rice-Ramsperger-Kassel-Marcus theory (RRKM) theory.

The key idea of RRKM theory starts from the concept of classical phase space, i.e. the space of 3N coordinates $\bar{q}$ (where, N is the number of atoms) and their 3N conjugate momenta $\bar{p}$. In a non relativistic description, the time is simply a parameter used to describe the motion along some trajectories in the phase space.

In the microcanonical ensemble the phase space volume is constant as a consequence of Liouville equation (Eq. 24), which is actually a n-dimensional continuity equation [34], that is true in the absence of any kind of source or sink of particles. This condition is always respected in non-relativistic quantum mechanics.

More specifically, the number of quantum states n in the infinitesimal volume element $d\bar{q} \cdot d\bar{p}$ is

$$n = \frac{1}{h^{3N}} d\bar{q} \cdot d\bar{p} \tag{18}$$

where h is Planck's constant and 6N is the dimensionality of the phase space. Eq. 18 is a correspondence rule used in statistical mechanics [34] as a *bridge* between quantum and classical partition function. The association of a phase space volume h^{3N} with each quantum

state can be thought of as a consequence of the uncertainty principle, which limits the precision with which a phase point can be specified in a quantum mechanical system [35].

The phase space volume formalism is used to *select* some specific subset of the total quantum states. The number of states with energy below a given value E is proportional to the volume of the integral

$$n(E) = \frac{1}{h^{3N}} \int \Theta(H(\bar{q}, \bar{p}) - E)\, d\bar{q} d\bar{p} \tag{19}$$

where $H(p, q)$ is the energy of the point. The Heaviside theta function $\Theta(H(\bar{q}, \bar{p}) - E)$ is used as a selector, that nullifies the contribution of the points that do not meet the condition to have the energy lower than E

$$\Theta(H(\bar{q}, \bar{p}) - E) = \begin{cases} 1, & \text{if } H(\bar{q}, \bar{p}) \leqslant E; \\ 0, & \text{if } H(\bar{q}, \bar{p}) > E. \end{cases}$$

Now, we introduce the concept of Density of States (DOS), $\rho(E)$, i.e. the number of states per unit of energy, by differentiation of Eq 19

$$\rho(E) \equiv \frac{\partial n(E)}{\partial E} = \frac{\partial}{\partial E}\left[\frac{1}{h^{3N}} \int \Theta(H(\bar{q}, \bar{p}) - E)\, d\bar{q} d\bar{p}\right] \tag{20}$$

Using the property of Heaviside function

$$\frac{d\Theta(x)}{dx} = \delta(x) \tag{21}$$

where $\delta(x)$ is the Dirac Delta function, defined as

$$\delta(H(\bar{q}, \bar{p}) - E) = \begin{cases} \infty, & \text{if } H(\bar{q}, \bar{p}) - E = 0; \\ 0, & \text{if } H(\bar{q}, \bar{p}) - E \neq 0. \end{cases}$$

the DOS can be now written as

$$\rho(E) = \frac{1}{h^{3N}} \int \delta(H(\bar{q}, \bar{p}) - E)\, d\bar{q} d\bar{p} \tag{22}$$

Similarly to Heaviside function in Eq. 19, the Dirac Delta function acts like a switch, or a projector operator, by counting only the states (or, equally, point of phase space) with energy E.

By integration over the energy range $[0, E]$, we can rewrite Eq. 19 using the DOS 22 as

$$n(E) = \int_0^E \rho(E')\, dE' \tag{23}$$

The microcanonical rate constant $k(E)$ can be roughly imagined as the probability for a microcanonical ensemble of states to evolve into another one: for this reason, we need to evaluate the flux of particles

that flow from reactant to product region of the phase space at a specific value of energy.

This quantity can be in principle calculated by defining a (hyper)surface at any point of the phace space dividing the two regions, but a wise choice of this point can greatly reduce the effort needed to calculate the flux.

This point is the TS and represents the dynamical bottleneck of the reaction. It is usually defined as the point in configurational space where the PES reaches a maximum between reactants and products, i.e. a first order saddle point [36].

Introduced simultaneously by Evans and Polanyi [37], and Eyring [38], the TST has been the most used and efficient method for the calculation of rate constants.

In the derivation and application of the formulae of the rate constant in RRKM, some approximations are made:

1. The distribution of reactants is in a microcanonical equilibrium;
2. The identification of TS is made in the configuration space;
3. The reactive mode is the normal mode of the TS with imaginary frequency [39];
4. If a particle surpasses the TS on the reactive mode into the product region, it becomes a product (no-recrossing approximation);
5. The motion along the reactive mode is separable from the others and is treated classically.

Here, we briefly derive the RRKM microcanonical rate constant; for a detailed demonstration, we refer to any book of chemical kinetics [40]. After the identification of two regions of phase space as reactants and products, the flux between them is described by the Liouville's equation

$$\frac{\partial \rho(\bar{q}, \bar{p})}{\partial t} + \nabla \cdot \rho(\bar{q}, \bar{p}) \frac{\bar{p}}{m} = 0 \tag{24}$$

where $\rho(\bar{q}, \bar{p})$ is the probability density in phase space and m is the generalized mass of the particle. Here, we note that Eq. 24 is the classical analogue of Eq. 104 in Chapter 3. By following the flow probability density between different regions in phase space, it is possible to study the course of the chemical reaction.

The microcanonical equilibrium assumes that the total phase space is populated statistically to form a microcanonical ensemble of states at total energy E, including at the TS, identified at coordinate $q' + dq'$ and $p' + dp'$. At each given energy E in the interval $[0, \infty]$, this assumption permits the ratio of molecules at the TS to the total number

of molecules, $dN(E, q', p')/N$ to be expressed as the ratio of the phase space volume at the TS to total one

$$\frac{dN(E, q', p')}{N} = \frac{dq'dp' \int \delta(H_{TS}(\bar{q}, \bar{p}) - E)\, d\tau^{\ddagger}}{\int \delta(H_R(\bar{q}, \bar{p}) - E)\, d\bar{q}d\bar{p}} \tag{25}$$

where the integration in the numerator in the Right Hand Side (RHS) of Eq. 25 is done over all the variables except for the reactive coordinate and the conjugate momentum

$$d\tau^{\ddagger} = \prod_{i \neq i'} dq_i dp_i \tag{26}$$

In Eq. 25, H_{TS} and H_R are the Hamiltonian of the TS and reactants, respectively: they are used to select, as in Eq. 22, the specific energy of each trajectory. Counting only the trajectories with positive momentum $p' + dp'$ in Eq. 25 is equivalent to the no-recrossing approximations, because we accept as *reactive trajectories* only the ones with a positive momentum in the direction of products.

The separation of the reactive mode implies that the Hamiltonian at the TS can be written as

$$H_{TS}(\bar{q}, \bar{p}) = H(\tau^{\ddagger}, q', p') = E^{\ddagger} + V(q'_0) + \frac{p'^2}{2m} \tag{27}$$

The differential dq' in Eq. 25 may be replaced with $p'dt/m$, obtaining

$$\frac{dN(E, p')}{dt} = \frac{Np'dp}{m} \frac{\int \delta(H_{TS}(\bar{q}, \bar{p}) - E)\, d\tau^{\ddagger}}{\int \delta(H_R(\bar{q}, \bar{p}) - E)\, d\bar{q}d\bar{p}} \tag{28}$$

The quantity at the right side of Eq. 28 is the flux that we want to find, $F(E, p') = dN(E, p')/dt$. By the change of variable $E' = p'^2/2m$, in Eq.28 the flux dependence on the reactive momentum is replaced by its relative energy becoming

$$F(E, E') = \frac{NdE' \int \delta(H_{TS}(\bar{q}, \bar{p}) - E)\, d\tau^{\ddagger}}{\int \delta(H_R(\bar{q}, \bar{p}) - E)\, d\bar{q}d\bar{p}} \tag{29}$$

This equation expresses the reaction rate for total energy E and energy E' in the reaction coordinate, which is equal by definition to

$$F(E, E') = k(E, E')NdE' \tag{30}$$

Using the Hamiltonian of the TS in Eq. 27, the numerator of the right hand side of Eq. 29 can be defined as the DOS at the TS and thanks to the property of the Dirac delta function

$$\int \delta(H_{TS}(\bar{q}, \bar{p}) - E)\, d\tau^{\ddagger} = \rho^{\ddagger}(E - V(q') - E') \tag{31}$$

The integral in the denominator of the right hand side of Eq. 28 is the DOS of the reactants, therefore we obtain

$$k(E, E') = \frac{\rho^{\ddagger}(E - V(q') - E')}{h\rho(E)} \tag{32}$$

This expression of the rate is specific for some value of the E'; by integration over the interval $[0, E - V(q')]$ we obtain

$$k(E) = \frac{\int_0^{E-V(q')} \rho^{\ddagger}(E - V(q') - E')\, dE'}{h\rho(E)} \tag{33}$$

which is the classical RRKM rate constant for a chemical reaction [41, 42, 43]. Note that in Eq. 33 the numerator, also called Sum of States (SOS), labeled as $N(E)$, count as reactive only the trajectories with energy $E > E' + V(q')$, which means that tunnelling is not allowed. In Section 2.4 this quantum effect will be recovered with some *ad hoc* assumptions. In the next Sections of this Chapter, we will focus on the correction of the classical RRKM in order to obtain a quantum (or semiclassical) version of RRKM thoery.

The assumption of microcanonical equilibrium at TS remains the critical approximation, but it is expected to work better as long as the molecules involved increase in complexity, which is the perfect kind of behaviour we need in order to create a computational tool for the calculation of the rate constants of reactions of medium size molecules.

The thermal rate constant finally becomes, as in Eq. 5,

$$k(T) = \frac{\int_0^{\infty} N(E) e^{-E/k_B T} dE}{Q_{reac}(T)} \tag{34}$$

and in RRKM theory it can be viewed as a Boltzmann average of energy dependent flux in microcanonical equilibrium from reactants to products passing through the TS.

2.3 SEPARATION OF DOF AND CONSERVATION LAWS

The derivation of the RRKM microcanonical rate constant in Sec. 2.2 treats each DOS equivalently, except the reactive mode: we will collectively define these orthogonal modes as "bath". In general, the bath is composed of internal motions, i.e. bonds stretching and bending, plus other kinds of particular motion (hindered rotations, ring deformations, etc. . . ; for more details, see Section 2.5). If not differently specified, we can approximately think about them as a set of harmonic oscillators.

At the same time, the hypothesis of microcanonical equilibrium at reactants and TS implies that the coupling between the bath's DOS make the energy freely flow from one DOS to another.

However, the conservation laws of linear and angular momentum lead to the necessity of further consideration in order to obtain physically consistent results.

The linear momentum is the easiest conservative quantity to preserve, because the motion of the centre of mass of a molecule (or more than one) in the gas phase is always exactly separable [39].

The translational Degree of Freedom (DOF) can be simply dropped out from the calculation of RRKM rate constants, because the total linear momentum never changes during the process.

The three external rotational DOFs are more complex to handle, because they actually exchange energy with the bath via Coriolis coupling [44] and can assist the reaction due to centrifugal contribution for a reaction with bond breaking (clearly, a normal situation for all dissociation reactions), under the constraint of angular momentum conservation.

A rotating molecule can be described as a rigid rotor, excluding the coupling with the internal vibrations; moreover, in a gas phase environment these rotations are unconstrained, therefore the Hamiltonian of these three DOF consists of a kinetic term only

$$\hat{H} = \hat{T} = \frac{1}{2}\left[\frac{\hat{j}_x^2}{I_{xx}} + \frac{\hat{j}_y^2}{I_{yy}} + \frac{\hat{j}_z^2}{I_{zz}}\right] \tag{35}$$

where $j_{x,y,z}$ are the angular momentum operators and $I_{xx,yy,zy}$ are the principal moments of inertia, obtained by diagonalization of the inertia tensor [39].

In order to simplify the problem, the space-fixed coordinate system x, y, z can be replaced by the new system x', y', z' that rotates with the molecule, called molecular-fixed system. The transformation between the two sets of variables can be defined for each atom i in the molecule and is evaluated by the following equation

$$R_{x,y,z;i} = R_{x',y',z';i} + B(\theta, \phi, \chi)_i (d^0_{x',y',z';i} + d_{x',y',z';i}) \tag{36}$$

where $R_{x,y,z}$ is the position vector in the space-fixed system, $B(\theta, \phi, \chi)$ is an orthonormal transformation matrix that rotates the position vectors in the molecule-fixed system $d^0_{x',y',z'}$ and $d_{x',y',z'}$, which are the reference and the displacement vectors, respectively.

The transformation has to meet the Eckart-Sayvetz conditions [45, 46],

$$\sum_i m_i \left(\frac{\partial d^0_{x',y',z';i}}{\partial t}\right) = 0 \tag{37}$$

$$\sum_i m_i d^0_{x',y',z';i} \times \frac{\partial d_{x',y',z';i}}{\partial t} = 0 \tag{38}$$

minimizing the interaction between rotational and vibrational motions. This is the standard treatment for the kinetic term of the Hamiltonian in polyatomic molecules [39] and we will not discuss here any more.

The total angular operator $\hat{J}^2$ and its component along the quantization axes z, j_z satisfy the following equations

$$\hat{J}^2 |j, m\rangle = j(j+1) |j, m\rangle \tag{39}$$

$$\hat{j}_z |j, m\rangle = m |j, m\rangle \qquad -j \leqslant m \leqslant j \tag{40}$$

$$\tag{41}$$

where $|j, m\rangle$ is the rotational wavefunction [47].

The total angular momentum and its projection along a space-fixed quantization axis must be conserved, therefore they are the same in every coordinate system we use and remain the same throughout the process of forming the TS from reactants.

The choice of a molecule-fixed Cartesian frame to describe free rotations and their angular momenta suffers from an unavoidable arbitrariness, since the permutation of the axes leaves all the observables unchanged. We prefer to label the orthogonal axes in molecule-fixed frame x', y', z' with the letters (a, b, c) where the choice of which axis is associated to which letter is made by the convention that the higher rotational constant is assigned to A, the second one to B and the third one to C.

Since the rotational constants are defined as

$$A = \frac{1}{2I_a} \qquad B = \frac{1}{2I_b} \qquad C = \frac{1}{2I_c} \tag{42}$$

the inertia moments are labelled such that $I_a \leqslant I_b \leqslant I_c$.

The most general case of rigid rotor is the asymmetric one, which has three different moments of inertia $I_a \neq I_b \neq I_c$, but in this case the energy levels cannot be calculated in closed form. Since the probability that a medium sized molecule is strictly a symmetric top (two equal moments) or a spherical top (all moments equal) is low, we will approximate our asymmetric top as a symmetric top, taking the geometric mean of the two nearest moments of inertia. For example, the case where $I_a \neq I_b \approx I_c$ becomes $I_a \neq \sqrt{I_b I_c} = \sqrt{I_b I_c}$

In the case of a rigid symmetric top, the rotational eigenvalues in Eq. 39 become

$$E_{rot}(j, m) = \begin{cases} j(j+1)B + k^2(A-B), & \text{if } I_a < I_b = I_c \\ j(j+1)B + k^2(C-B), & \text{if } I_a = I_b < I_c \end{cases}$$

Even though the rotational energy is a sum of two additive terms, looking separable, the constraint $-j \leqslant k \leqslant j$ couples them, see Eq 40.

We shall next uncouple the rotors, dropping the restriction on k and neglecting the term $-k^2B$, so that the energy in Eq. 35 is merely

the sum of energies of a two-dimensional rigid free rotor and of a one-dimensional rigid free rotor.

Neglecting the term $-k^2B$ in the energy has the effect of diminishing the total number of states, but the absence of a restriction on k results in the inclusion of normally disallowed states having $k > j$, which has the effect of increasing the number of states within a specified energy interval. Thus the two errors tend to compensate each other, with the result that the separated rotor approximation for the density of states is reasonable [48].

After the introduction of these approximations, we shall discuss how rotation affects the reaction. If we label B_r and B_{TS} as the rotational constants of reactants and transition state and suppose that $B_r \neq B_{TS}$, because the presence of a reactive mode implies a distortion on some bond length or angle, then we have an energy difference

$$\Delta E_{rot} = j(j+1)(B_r - B_{TS}) \tag{43}$$

ΔE_{rot} is available to drive the reaction.

A different discussion is made for the quantum number m; there are $2J+1$ values of m for a given J, which means that exists a $(2J+1)$-fold degeneracy. If m is conserved in the reaction, the $2J+1$ states cannot contribute to J-resolved microcanonical rate $K(E,J)$ [49] and are called adiabatic. If m is not conserved, both numerator and denominator in Eq. 33 should be multiplied by a constant factor $2J+1$, leaving the microcanonical RRKM rate unchanged [48].

In applications, the individual rotational DOS will be treated classically, because in medium sized molecules the value of the rotational constant is small enough to safely approximate the sum over states as an analytical integral, reaching the classical (i.e. continuum) limit.

2.4 ANHARMONICITY

Since RRKM theory is based on the microcanonical equilibrium hypothesis, which implies a strong coupling between the DOF of the bath, it seems not reasonable to accept that a pure harmonic treatment of internal modes, intrinsically orthogonal and separated, can coherently describe the system.

For this reason we use a second order perturbative vibrational Hamiltonian [50] (called Second order Vibrational Perturbation Theory (VPT2)) that allows us to describe simultaneously the coupling between the modes of the bath and gives us a suggestion about the dissociation limit, furthermore describing overtones and combination modes and handling accidental degeneracy.

A detailed discussion of the state of the art of vibrational spectroscopy is not an object of this Thesis and is beyond our goals.

Here, we just want to briefly summarize that the energy of N coupled anharmonic oscillators defined by an n-tuple $\bar{n}$ of vibrational quantum numbers $\bar{n} = [n_1, n_2, \dots n_N]$ is assumed to be

$$E(\bar{n}) = E_0 + \sum_i^N \omega_i (n_i + 1/2) + \sum_{i>j}^N \chi_{i,j} (n_i + 1/2)(n_j + 1/2) \quad (44)$$

where the term E_0, called Zero Point Energy (Zero Point Energy (ZPE)), contains all the energy contributions independent of the vibrational quantum numbers.

These equations are valid if the molecule under analysis is found at a minimum of the electronic PES, when all the frequencies ω_i and anharmonic terms $\chi_{i,j}$ are real.

In the case of a TS, one frequency is imaginary [51] and the associated state is metastable (see Chapter 3). We can associate it with the complex eigenvalue $E(\bar{n})$, where the real part is the energy of the $N-1$ normal modes, defined $n^\ddagger$, while the imaginary one is related with the reactive one, defined here as n_r.

The total complex energy associate with the TS is

$$E(n^\ddagger, n_r) = E(n^\ddagger) + i\left(\omega_r - \sum_i \bar{\chi}_{i,j} n_i n_r\right) \quad (45)$$

where $\chi_{i,r} = -i\bar{\chi}_{i,r}$.

Metastable states have a finite lifetime inversely proportional to the imaginary part of their energy; this is the reason why it is possible to define a semiclassical action θ as function of the energy of the n-tuple [52, 53]

$$n_r + \frac{1}{2} = i\frac{\theta}{\pi} \quad (46)$$

where n_r is the quantum number related to the imaginary frequency.

Now, substituting Eq. 46 in Eq. 45 we obtain

$$E(n^\ddagger, \theta) = E(n^\ddagger) + i\left(\omega_r - i\frac{\theta}{\pi}\sum_{i\neq i_r} \bar{\chi}_{i,j} n_i - i^2 \frac{\theta^2}{\pi^2} \bar{\chi}_{i_r,i_r}\right) \quad (47)$$

Solving the previous second order equation leads to an expression of $\theta(E)$ that can be used for tunnelling probability in the frame of the JWKB approximation

$$P(E) = \frac{1}{1 + e^{2\theta(E)}} \quad (48)$$

where $\theta(E)$ becomes [3]

$$\theta(E) = \frac{\pi \Delta E}{\Omega_r (1 + \sqrt{1 + 4\bar{\chi}_{r,r}\Delta E/\Omega_r^2})} \quad (49)$$

with

$$\Delta E = E - E(n^{\ddagger}) \tag{50}$$

$$\Omega_R = \omega_r - \sum_{i \neq r} \bar{\chi}_{i,r}(N_i + \frac{1}{2}) \tag{51}$$

Now, we introduce the semiclassical tunnelling probability $P(E)$ in Eq. 48, the previous definition of the microcanonical rate constant $k(E)$ expressed in Eq. 33 of Section 2.2.

Since the tunnelling probability depends on the energy difference ΔE in Eq 50, where $E(n^{\ddagger})$ is the energy of the TS, in order to be consistent with the notation os Section 2.2 we write

$$k(E) = \frac{\int_0^{\infty} \rho^{\ddagger}(E - V(q') - E')P(E - E')\,dE'}{h\rho(E)} \tag{52}$$

$$\Delta E = E' - E \tag{53}$$

The actual integration limit E_{max}, is chosen such that $E_{max} \gg E$, because the tunneling correction makes the DOS of the TS at energies higher than E relevant for the calculation of the SOS at a lower energy [54].

2.5 LARGE AMPLITUDE MOTION

The harmonic treatment of vibrational modes, as well the VPT2, is based on the hypothesis that the potential is correctly described as a Taylor series, which is truncated at second order, in the case of pure harmonic vibration, or up to fourth order, in the VPT2 case.

The Taylor series is intrinsically *local*, in the sense that it assumes to describe the behaviour of the potential at infinity from the knowledge of the PES in the neighbourhood of a point, chosen as reference (minimum or TS). Some kinds of potentials, however, cannot be correctly described by a Taylor series: for example, if the potential is n times periodic, as in the case of Hindered Rotations, the Taylor series converges slowly.

The failure in the description of the multidimensional PES as a set of harmonic oscillators, moreover, implies that the normal modes themselves, which are obtained by diagonalization of the GF product matrix in Wilson's method for the calculation of the molecular vibrational Hamiltonian [39], cannot describe the vibrations of the molecule properly [55]. Normal modes are also called *rectilinear* because they are expressed as linear combinations of the mass-weighted Cartesian coordinates.

We will define these special modes Large Amplitude Motions (LAM) and treat them separately from the others, which implies that also the terms that couple the LAM with the other "standard" normal modes must be ignored in the calculation of $\chi_{i,j}$ matrix in Eq. 44.

To surpass this poor description of vibrational modes, which leads to a incorrect evaluation of DOS and SOS, we need to use some coordinates which follow the real movements of the molecule: for this purpose, internal coordinates are the natural choice. Internal coordinates are a set of *curvilinear* (i.e. non linear) combinations of Cartesian coordinate [56]. Three kinds of *primitive* internal coordinate [57] exist:

- bond lengths $r_{i,j}$;
- valence angles $\alpha_{i,j,l}$;
- dihedral angles $\gamma_{i,j,l,m}$.

where the bond lengths are the usual Cartesian distances between atoms i and j sharing a chemical bond. Valence and dihedral angles are defined by the following equations

$$\cos(\alpha_{i,j,l}) = \frac{r_{i,j} \cdot r_{j,l}}{|r_{i,j}| \cdot |r_{j,l}|} \tag{54}$$

$$\cos(\gamma_{i,j,l,m}) = \frac{(r_{i,j} \times r_{j,l}) \cdot (r_{j,l} \times r_{l,m})}{\sin \alpha_{i,j,l} \sin \alpha_{j,l,m}} \tag{55}$$

From now until the end of the Section, we focus on the Hindered Rotations (HR) because they represent an easy internal mode that can be identified unequivocally by a single primitive internal coordinate, whereas other, more complex internal modes, like ring deformations, should be expressed as a linear combination of primitive internal modes.

We are interested in a computational strategy that allows us to find the energy spectrum of the vibrational Hamiltonian of the system beyond the harmonic oscillator [58]: following the formalism of the Reaction Path Hamiltonian (RPH) [59], based on the Intrinsic Reactive Coordinate (IRC) [60, 61], we define a path $\zeta(s)$ that obeys the following differential equation

$$\frac{d\zeta(s)}{ds} = \zeta'(s) = \frac{g}{\sqrt{g^\dagger \cdot g}} \tag{56}$$

where $\zeta(s)$ is a curve in the configurational space and s is the arc length that can be viewed as a variable that determinates univocally the position of each point $\in \zeta$ (see. Appendix B): thus, $\zeta'(s)$ is the tangent line to $\zeta(s)$ in s, i.e. its derivative. g is the energy gradient in mass-weighted Cartesian coordinates, whose elements, labelled as g_i, are defined as

$$g_i = \frac{\partial V(\bar{x})}{\partial x_i} \tag{57}$$

Note that the denominator of Eq. 56 is a normalization factor to keep the velocity vector equal to one.

Equation 56 becomes indeterminate at any extremum point along the closed curve $\zeta(s)$, but it can be shown [62] that even at these points the solution can be deduced from the knowledge of the second and third coefficients of the Taylor expansion of the PES, that we can perform automatically in the frame of VPT2 [50]. The mass-weighted Cartesian space $\mathbf{X}$ can be parametrized by the curve; therefore, each point $\mathbf{x}$ in $\mathbf{X}$ is identified by a value of s and its displacement from the curve ξ_i. For each component the relation

$$x_i = \zeta_i(s) + \xi_i \tag{58}$$

holds. We need a practical way to evaluate the curve $\zeta(s)$ that associates to each value of s a point $\mathbf{x}$ in $\mathbf{X}$: we first note that Eq. 56 has six solutions that are identically zero, related to translations and external rotations, plus another one related to the curve itself, because we expect that the energy of the internal rotation varies slowly along the curve (otherwise, it should be treated as a vibration).

Since it is always possible to diagonalize the reduced $3N-7$ Hessian, we can rewrite the displacement ξ_i from the curve $\zeta(s)$ as

$$x_i = \zeta_i(s) + \sum_{k=1}^{3N-7} L_{i,k}(s) Q_k \tag{59}$$

where $\mathbf{L}_k(s)$ (whose components are $L_{i,k}(s)$) are the eigenvectors of the non-zero eigenvalues of the Hamiltonian (i.e. the vibrations) and Q_k are the normal modes [59].

Eq. 59 is the reference for the numerical identification of the curve solution of Eq 56.

The first step to obtain it is to perform a relaxed scan along the primitive internal coordinate, i.e. the HR, obtaining a series of geometries that we label as $j = [1, \dots N]$: the relaxation on the other vibrational modes minimizes the coupling with the HR, satisfying (at least variationally) Eq. 189.

Imposing the Eckart-Sayvetz conditions to two consecutive, optimized geometries and then superimposing their Eckart frames, we are able to minimize the rototranslational displacement between them. Again this computational strategy is the best numerical solution to satisfy Eq. 187 and Eq. 188 If the two geometries, actually two points $\mathbf{x}$ in the configurational space $\mathbf{X}$, are close enough, the vibrational displacement (i.e. the second part of the RHS in Eq. 59) is negligible and we can calculate pointwise $\mathbf{a}(s)$ as the distance in mass-weighted coordinate between the two points $\mathbf{x}$

$$|ds|^2 = |\mathbf{a}_{i+1}(s) - \mathbf{a}_i(s)|^2 = |\mathbf{x}_{j+1} - \mathbf{x}_j|^2 \tag{60}$$

In this scheme, the reduced mass is equal to unity and any information about kinematic coupling is stored in the discrepancy between the closed curve s [63], parametrized pointwise by the map $\mathbf{a}(s)$, and its geometrical counterpart, i.e. the dihedral angle that defines the internal rotation.

2.6 DISCRETE VALUE REPRESENTATION

Since we are interested in the DOS of a molecular system composed of a number of harmonic (or anharmonic) oscillators and some LAM, we need to find a practical way to calculate the energy spectrum of the one dimensional Hamiltonian of the latter, in order to introduce it coherently in an equation like Eq. 44. For this reason we use the Discrete Value Representation (DVR) basis set [64] $|x_i\rangle$, a finite basis of the $L^2(\mathbb{R})$ build up using localized functions on an interval $\Delta x = x_{i+1} - x_i$ of the uniform grid on $\mathbb{R}$ formed by N points in the interval (a, b) such that

$$x_i = i\Delta x + a \qquad i = [1 \dots N-1] \tag{61}$$

where

$$\Delta x = \frac{b-a}{N} \tag{62}$$

Due to their localized nature in $\mathbb{R}$, DVR functions have some remarkable properties that make them useful for quantum calculation in low-dimensional problem; DVR are dense in $L^2(\mathbf{R})$, are orthogonal with respect to the grid points and therefore complete

$$\langle x_j | x_i \rangle = \delta_j, i \qquad \sum_i |x_i\rangle \langle x_i| = 1 \tag{63}$$

If we are interested in some property, represented by the operator $\hat{F}(x)$ of a wavefunction built using the DVR basis set $\psi(x) = \sum c_i |x_i\rangle$, we need to use a discrete summation in place of the standard integral of the relative operator representation

$$\langle \psi(x)| \hat{F}(x) |\psi(x)\rangle = \sum_i^N c_j^* c_i \left\langle x_j \right| \hat{F}(x) |x_i\rangle = \sum_i^N F(x_i)|c_i|^2 \tag{64}$$

The momentum counterpart of the DVR basis set, $|k_i\rangle$ [65], is called Finite Basis Representation (FBR) basis set and is orthogonal and complete itself

$$\langle k_i | k_j \rangle = \delta_{i,j} \qquad \sum_i |k_i\rangle \langle k_i| = 1 \tag{65}$$

As expected, the momentum range Δk is inversely proportional to the shortest wavelength that can be represented on a grid of length $N\Delta x$

$$\Delta k = \frac{2\pi}{N\Delta x} \tag{66}$$

DVR and FBR basis sets allow a diagonal representation of operators that act on position or momentum, respectively. The superposition

between them should respect the Uncertainty Principle, a discrete version of Fourier Transform

$$\langle x_i|k_j\rangle = c_{i,j} = \sqrt{\frac{2}{b-a}}\sin\left(\frac{k_j x_i \pi}{b-a}\right) \tag{67}$$

where $c_{i,j}$ are the coefficients of the linear combination

$$\left|k_j\right\rangle = \sum_i c_{i,j}\left|x_u i\right\rangle \tag{68}$$

The energy spectrum of the Hamiltonian can be now evaluated by diagonalization of its matrix representation

$$\langle x_i|\hat{H}\left|x_j\right\rangle = \langle x_i|\hat{T}\left|x_j\right\rangle + \langle x_i|\hat{V}\left|x_j\right\rangle \tag{69}$$

$$= \sum_{l,m}\langle x_i|k_l\rangle\langle k_l|\hat{T}|k_m\rangle\langle k_m|x_j\rangle + V(x_i)\delta_{i,j} \tag{70}$$

$$= \sum_{l}\langle x_i|k_l\rangle\hat{T}_{ll}\langle k_l|x_j\rangle + V(x_i)\delta_{i,j} \tag{71}$$

The kinetic operator in FBR $|k_i\rangle$ is simply

$$\hat{T}_{ll} = \frac{\hbar^2}{2m}k_l^2 \tag{72}$$

Evaluating the kinetic part of the Hamiltonian $\hat{T}_{i,i'} = \sum_l \langle x_i|k_l\rangle\hat{T}_{ll}\langle k_l|x_j\rangle$ is an analytic procedure [66] that leads to exact (analytic) representation of the kinetic operator on the DVR basis set

$$\hat{T}_{i,i'} = \begin{cases} \frac{\pi^2}{4(b-a)^2}\left(\frac{2N^2+1}{3} - \frac{1}{\sin^2(\pi i/N)}\right) & \text{if } i = i', \\ \frac{\pi^2(-1)^{i-i'}}{2(b-a)^2}\left(\frac{1}{\sin^2(\pi(i-i')/2N)} - \frac{1}{\sin^2(\pi(i+i')/2N)}\right) & \text{if } i \neq i' \end{cases}$$

On the other hand, the diagonal representation of the potential is approximated in the DVR basis set, since it is exact only in the limit of an infinite number of points, while in applications the grid will always be finite [67]. Nevertheless, we can increase the number of points until numerical convergence of the vector of eigenvalues $\epsilon(n)$.

Finally, the energy of an ensemble of quantum anharmonic oscillator with k LAMs can be described as function of their quantum numbers $\bar{n}$

$$E_{vib}(\bar{n}) = E_0 + \sum_{i=1}^{3N-6-k}\omega_i n_i + \sum_{i,j=1}^{3N-6-k}X_{i,j}n_i n_j + \sum_{l=1}^{k}\epsilon_l(n_l) \tag{73}$$

where n_l is the quantum number of the l-th LAM and $\epsilon_l(n_l)$ is its relative eigenvalue.

2.7 RANDOM SAMPLING OF PHASE SPACE

We are interested in an accurate description of the vibrational DOS $\rho(E)$ starting from a functional form of the energy depending on the vibrational quantum numbers as in Eq. 73, but the presence of a quadratic term that couples the modes makes the analytic solutions used for the pure harmonic case incorrect [34]; also numerical algorithms for harmonic vibrations are useless [68, 69].

To achieve the highest level of accuracy in the calculation of the vibrational DOS, which is important also for the calculation of the SOS in Eq 52 avoiding the unfeasible direct count of each possible combination of quantum numbers, we use the WL algorithm [70], a Monte Carlo sampling of the phase space described by the Hamiltonian in Eq. 73.

The method is based on a random walker, i.e. a random generator of vibrational states, that moves along the phase space creating new states with energy E_{new} which are counted (or "accepted") with a probability $P(E_{old}, E_{new})$ that is inversely proportional to the DOS itself [70]

$$P(E_{old}, E_{new}) = \min\left(\frac{\rho(E_{old})}{\rho(E_{new})}, 1\right) \tag{74}$$

In the previous equation, $\rho(E_{old})$ is the DOS of the energy interval where we start the current step of the sampling and $\rho(E_{new})$ is the DOS of energy interval E_{new} where the new n-tuple belongs. Since the probability of the random step is inversely proportional to the DOS of the step that we want to jump in, the high energy region of the DOS will be statistically less visited, compensating for the fact that there are more combinations of quantum numbers $\bar{n}$ within that specific energy interval. This strategy produces a flat histogram as Metropolis-Hastings algorithm [71], that is used to check the convergence of the sampling.

The exact DOS $\rho(E)$ is then used to calculate the partition function at every temperature [58]

$$Q(T) = \int \rho(E) e^{-E/k_B T} \, dE \tag{75}$$

This approach, also called multicanonical in statistical papers, has been proved [72] to give results of the same quality as MetaDynamics (MD) [73] and Statistical Temperature Molecular Dynamics (STMD) [74] in the limit of a satisfactory sampling.

Widely used in many areas of physics and chemistry, the WL algorithm has been improved by Barker and coworkers [75] by the addition of a filter which automatically discards any non-bounded state, which has negative partial derivatives $\partial E(\bar{n})/\partial n$.

The results show excellent agreement with exact counting DOS for small molecules, while the linear scaling of CPU time versus the num-

ber of DOF and the possibility of massive parallelization due to the statistical nature of WL sampling makes it possible to handle molecular systems with thousands of DOF [76].

The other thermodynamic properties, enthalpy, entropy and Gibbs free energy can be calculated by the well known equations

$$H = E_0 + k_B T + k_B T^2 \left(\frac{\partial Q(T)}{\partial T}\right) \tag{76}$$

$$S = k_B T \left(\frac{\partial Q(T)}{\partial T}\right) + k_B T \ln Q(T) \tag{77}$$

$$G = H - TS = E_0 + k_B T(1 - \ln Q(T)) \tag{78}$$

In order to avoid numerical instabilities and errors due to numerical differentiation, in our applications we prefer to use the completely equivalent expression

$$H = RT\left(\frac{Q'(T)}{Q(T)}\right) \tag{79}$$

$$S = R\left(\ln Q(T) + \frac{Q'(T)}{Q(T)}\right) \tag{80}$$

where $Q'(T)$ is

$$Q'(T) = \int E\rho(E) e^{-E/k_B T}\, dE \tag{81}$$

is the first moment distribution of the partition function.

2.8 KINETIC MASTER EQUATION

By Kinetic Master Equation (KME) we mean a series of coupled first order differential equations of the form

$$\frac{d\rho_i(E)}{dt} = \sum_j k_{i,j}(E) c_j(E) - \sum_{j'} k_{j',i}(E) c_i(E) \tag{82}$$

where $k_{i,j}(E)$ are the rate constants of j reactants that produce the i-th molecule, the system that we are investigating, and $k_{j',i}(E)$ are the rate constants of the reactions where i are the reactants, with negative contribution. In addiction to these reactive terms, collisional terms representing energy transfer between states at different energy E can be added if the environment conditions are compatible with this kind of phenomena, that depend on the density of particles, both reactive or the thermal bath.

A KME is called monodimensional if it depends only on the total energy E; if we use J-resolved rate constant, $k(E, J)$, we have to calculate a two dimensional KME.

In previous Sections, we referred to the reaction mechanism as the chain of elementary reactions that compound a given reaction. The reaction mechanism consists of a series of N stable molecular systems,

reactants, products and intermediates, usually separated by one or more TS, the metastable configurations that allow the reaction to proceed.

The reaction mechanism gives us the connection to build up N equations like Eq. 82: if they are divided by a TS, the RRKM microcanonical rate constants $k(E)$ are used.

Some reactions have some barrierless step: in this case, often regarding radical reactions, specific techniques have to be used to obtain the reaction cross sections [77, 78].

Since the rate constants are time independent, the time evolution of the DOS, also called population or concentration, is defined *Markovian*, i.e. does not conserve any information about his past populations, continuously evolving to equilibrium.

Markovian process are based on the same assumption of microcanonical equilibrium in RRKM theory and is always satisfied if the intramolecular energy transfer in faster than reaction, always true in dilute gas phase [79].

Moreover, microcanonical equilibrium implies that direct and inverse rates must be equal. This property is also called *detailed balance* and implies that the for a generic reaction $A \rightarrow B$ (unimolecular or bimolecular, A, B are generic labels)

$$k\rho(A) = k_{-1}\rho(B) \tag{83}$$

where k and k_{-1} are the direct and inverse rate constant respectively and $\rho(\cdot)$ is the DOS of reactants or products. The matrix formalism is the most used approach to solve this set of coupled linear equations.

Therefore, if we call the $\mathbf{c}$ the vector of population and $\mathbf{K}$ the matrix of rate constants, we have to resolve the vectorial differential equation

$$\dot{\mathbf{c}} = \mathbf{K} \cdot \mathbf{c} \tag{84}$$

for each energy interval.

The elements $k_{i,j}$ of $\mathbf{K}$ satisfy the following properties:

- Diagonal terms are negative, since, as shown in Eq. 82, the rate of inverse reactions for the i-th population are proportional to its number of states.
- The sum of each column is zero, because the rate of descruction is equal to the sum of the rates of its reactions.

Defined in this way, $\mathbf{K}$ is not hermitian and therefore its eigenvalues are not real. Different strategies have been proposed to solve the previous equation, with or without symmetrization of the $\mathbf{K}$ matrix [80].

By diagonalization we find the eigenvectors $\boldsymbol{\Lambda}$ and thus the time evolution of the population vector

$$\mathbf{c}(t) = \mathbf{U} e^{\boldsymbol{\Lambda} t} \mathbf{U}^{-1} \mathbf{c}(0) \tag{85}$$

where $\mathbf{c}(0)$ is the initial population vector determinated by the physics of the reaction or simply taken from the microcanonical equilibrium DOS.

3 TIME FRAMEWORK

3.1 TIME DEPENDENT SCHRÖDINGER EQUATION

In Chapter 2, we introduced the concepts of reactants, products and Transition States as minima or first order saddle points of the TISE.

In the latter case, we anticipated the concept of *metastable* states, that are characterised by a finite lifetime, contrary to the reactants and product which are stable (infinite lifetime).

How does the molecular system evolve from a stable to a metastable state? In the absence of external forces the necessary energy is provided by the bath by random collisions; this process is known as thermal activation.

In Section 2.2 we postulated a microcanonical equilibrium to estimate the population at the TS, but is it always true?

As an example, the rate of a chemical reaction can be influenced, while the molecule walks the path from reactants to products passing through the TS, by the formation of a geometrical configuration where the hypothesis of intramolecular strong coupling fails, leading to a non-RRKM reaction [81, 82, 83].

Van der Waals complexes, relative minima of the PES not identified as intermediates, are another example of troublesome molecular structures which are not satisfactorily treated in RRKM theory.

The information about the exact evolution of molecules is contained in the Time Dependent Schrödinger Equation (TDSE), written in atomic units as

$$i\frac{\partial}{\partial t}\Psi(\bar{r},t) = \hat{H}\Psi(\bar{r},t) \tag{86}$$

where $\hat{H}$ is the same of Eq. 10. Eq. 86 describes the evolution of all the particles (nuclei and electrons) at each time, making possible the study of the properties of a molecule under the laws of quantum mechanics: the collective variable $\bar{r}$ represents the ensemble of $3N$ spatial DOF of interest of the system $(3N_a + 3N_i)$.

The BO approximation is postulated to be true at each instant in Eq 86 leading to

$$i\frac{\partial}{\partial t}\psi(R,t) = \hat{H}_{nuc}\psi(R,t) \tag{87}$$

where $\psi(R,t)$ is the time dependent nuclear wavefunction. The notation used here is consistent with the one used in Section 2.1.

Separating the time from the spatial coordinates $\psi(R,t) = \chi(t)\varphi(R)$, we obtain two equations

$$i\frac{\partial\chi(t)}{\partial t} = E\chi(t) \tag{88}$$

$$\hat{H}_{BO}\varphi(R) = E\varphi(R) \tag{89}$$

which are true if the Hamiltonian does not depend on time, but in general it is not possible.

Eq. 88 is a first order differential equation and its solution is written as

$$\chi(t) = \chi(0)e^{-iEt} \qquad \chi(0) \equiv \chi(t_0) \tag{90}$$

where the initial time is $t_0 = 0$ for simplicity of the notation.

The total wavefunction becomes

$$\psi(R,t) = \chi(0)\varphi(R)e^{-iEt} \tag{91}$$

but the multiplicative factor $\chi(0)$ is usually absorbed in $\varphi(R)$ and then its magnitude is calculated remembering that the wavefunction is a probability distribution with normalization condition

$$\int_{-\infty}^{\infty} |\psi(R,t)|^2 \, dR = 1 \tag{92}$$

Now we introduce the evolution operator (also called propagator) $\hat{U}(t,t')$, which takes a time dependent wavefunction as in Eq. 91 at time t' and transform it in the same wavefunction at time t

$$\hat{U}(t,t')\psi(R,t') = \psi(R,t) \qquad \hat{U}(t,t') \equiv e^{-iH(t-t')} \tag{93}$$

Normally, $t' = 0$, therefore the evolution operator is rewritten as $\hat{U}(t,0) = \hat{U}(t)$. By differentiation with respect to time of Eq. 93, we can notice that $\hat{U}(t)$ satisfies the TDSE

$$i\frac{\partial\hat{U}(t)}{\partial t} = \hat{H}\hat{U}(t) \qquad \hat{U}(0) \equiv I \tag{94}$$

where I is the identity operator. The propagator does not change the norm of a stationary state and must be consistent with time symmetry and the wavefunction superposition principle [84].

If we define a generic operator $\hat{A}$, supposed to be time independent, the evolution of its expectation value $\langle a(t)\rangle$ as a function of time is

$$\langle a(t)\rangle = \langle\psi(R,t)|\, A\, |\psi(R,t)\rangle \tag{95}$$

$$= \left\langle\psi(R,0)e^{iHt}\right|\, A\, \left|e^{-iHt}\psi(R,0)\right\rangle \tag{96}$$

$$= \langle\psi(R,0)|\, e^{iHt}Ae^{-iHt}\, |\psi(R,0)\rangle \tag{97}$$

$$= \langle\psi(R,0)|\, \hat{U}(-t)A(t)\hat{U}(t)\, |\psi(R,0)\rangle \tag{98}$$

$$= \langle\psi(R,0)|\, \hat{A}(t)\, |\psi(R,0)\rangle \tag{99}$$

When operators are time independent, only the wavefunction shows a dependence on time: this is called Schrödinger picture and is represented in Eq. 95.

On the other hand, the use of the evolution operator makes clear that it is completely equivalent to think about the time dependence of the expectation value as a time dependent operator $\hat{A}(t)$

$$\hat{A}(t) = \hat{U}(-t)A\hat{U}(t) \tag{100}$$

that operates on stationary wavefunctions, as in Eq. 99: this approach is called Heisenberg picture.

One of the most useful quantities that can be evaluated in the time dependent frame of quantum mechanics is the autocorrelation function of a wavefunction, namely

$$C(t) = \langle \psi(0) | \psi(t) \rangle \tag{101}$$

The autocorrelation function is a well known instrument used in many scientific and engineering fields. In quantum mechanics, it is strictly related to the spectra of the molecular system; the reader is invited not to confuse $C(t)$ with the flux autocorrelation function $C_f(t)$ of Eq. 114, defined later in Section 3.2.

Since we focus our treatment on nuclear dynamics, the region of the spectra that we reproduce is the infrared region (IR), associated with vibrations. Nevertheless, the same formalism can be applied to electronic wavefunctions to obtain electronic spectra, in the visible and Ultra Violet portion of the electromagnetic field (VIS-UV).

In order to use the TDSE to predict the motion and the observables of a molecular system of a generic dimension, we need to know a functional form of the potential as a function of each DOF, provided by quantum chemistry calculation in the BO approximation. But even in the cases where the PES is known, the analytic solutions for multi-dimensional problems are unknown.

For this reason the TDSE cannot be used directly to calculate and propagate a time dependent wave function wavefunction as it is. We need to impose some analytic form, physically reasonable, to the functions, to the operators or both of them. These numerical methods will be discussed in Section 3.3 and Section 3.4.

Before the presentation of the numerical methodologies for the calculation of thermal rate constants and partition functions in time dependent quantum mechanics, we need to introduce the concept of quantum Current Density and the flux operator, which are the fundamental concepts to obtaining information about the thermal rate constant of a reacting molecular system with a reasonable computational effort.

3.2 THE CURRENT DENSITY AND FLUX OPERATOR

While the TDSE in Eq. 87 describes the evolution in time of the wavefunction, we are interested in the evolution of density of probability, i.e. the square of its norm

$$\rho(R,t) = |\psi(R,t)^* \psi(R,t)| \tag{102}$$

which is normalized to unity,

$$\int \rho(R,t)\, dR = 1 \tag{103}$$

Again, R represents the generalized spatial coordinate, which collects all the nuclear variables: the electronic ones are not involved in nuclear motion thanks to the BO approximation.

Now, we are interested in the evolution of the density, also known as Liouville-VonNeumann equation or quantum mechanical continuity equation. For simplicity of the notation, here we drop the time and space dependence of the wavefunction, thus $\psi \equiv \psi(R,t)$.

$$\begin{aligned}
\int_\Omega \frac{\partial \rho}{\partial t}\, dR &= \int_\Omega \psi^* \left(\frac{\partial \psi}{\partial t}\right) + \left(\frac{\partial \psi *}{\partial t}\right)\psi \, dR \\
&= \int_\Omega \psi^* \left(-i\hat{H}\psi\right) + \left(i\hat{H}\psi^*\right)\psi \, dR \\
&= \frac{i}{2m}\int_\Omega \psi^* \left(\nabla^2\psi\right) - \left(\nabla^2\psi^*\right)\psi \, dR \\
&= \frac{i}{2m}\int_\Omega \nabla \cdot \left(\psi^*\nabla\psi - \left(\nabla\psi^*\right)\psi\right) dR \\
&= \frac{i}{2m}\int_\Sigma \left(\psi^*\nabla\psi - \left(\nabla\psi^*\right)\psi\right) \cdot n \, d\sigma
\end{aligned} \tag{104}$$

where Ω is the volume of the space, Σ is a closed surface that contains Ω and n is the normal vector at the surface $d\sigma$.

Now we can define the quantity $S(R,t)$, the Current Density (CD) [15] as

$$\begin{aligned}
S(R,t) &= \frac{1}{2im}\left(\psi^*\nabla\psi - \left(\nabla\psi^*\right)\psi\right) \\
&= \mathrm{Im}\left\langle\psi^*\right| \frac{\nabla}{m} \left|\psi\right\rangle = \mathrm{Re}\left\langle\psi^*\right| \frac{\nabla}{im} \left|\psi\right\rangle
\end{aligned} \tag{105}$$

and obtain a compact form for the evolution of the flux of probability density through the surface Σ

$$\int_\Omega \frac{\partial \rho}{\partial t}\, dR = -\int_\Sigma S \cdot n \, d\sigma \tag{106}$$

Equation 106 is the conceptual starting point of all strategies to calculate the rate constant on time dependent approach, but cannot be used directly, because the integrand region Ω or the closed surface Σ cannot be defined easily in practical cases.

Before discussing how we can find the rate constant for a chemical reaction from the quantum flux, we have to make some considerations about the physical meaning of $S(R,t)$.

If the volume of integration Ω is chosen such that it covers all the configurational space and the closed surface Σ that contains Ω is properly set, the probability density ρ is a conservative quantity: the flux is constant and therefore the right part of Eq. 106 is always equal to zero. In other word, it implies that Equation 103 will be constantly satisfied. On the other hand, we can think of $S(R,t)$ as a CD operator, and associate the operator $1/m\,\nabla$ to a *velocity* operator.

Eq. 106 cannot be used directly since is numerically difficult to define a closed surface Σ that covers an infinite volume. The existence of a first order saddle point on the PES, a TS, can be used to localize the calculation of the CD only in one specific point of the configurational space, as in Sec. 2.2; this assumption introduces the concept of flux operator $\hat{F}$.

The flux operator is strictly related with the CD in Eq. 105, since they operate on the same set of wavefunctions but with the difference that, while the CD is computed by integration on the closed surface Σ, the flux operator $\hat{F}$ is integrated over the vibrational normal modes of the TS perpendicular to the reactive mode, written with the Dirac bracket notation.

We define a generic coordinate s such that the region of space where $s < 0$ is associated with reactants and $s > 0$ with products.

The main advantage of the flux operator is that the TS is our reference choice as generating point for the surface, set at $s = 0$, and its vibration modes define a dividing *hyperplane* that separates reactants from products, a $3N-7$ space embedded in the $3N-6$ space obtained when we drop out the 6 dimensions related to translation and external rotation in our 3N configurationl space).

The plane can be defined as

$$f(R)_{s=0} = 0 \tag{107}$$

The flux operator $\hat{F}$ is defined with respect to the dividing surface $f(R,s)$ as [85]

$$\hat{F} = \frac{\partial h(f(R)_{s=0})}{\partial t} = \delta(s)\frac{\partial f(R)_{s=0}}{\partial R}\cdot\frac{p}{m} \tag{108}$$

where $h(f(R)_{s=0})$ is Heaviside function and its derivative $\delta(f(R)_{s=0})$ is the Dirac delta function.

The derivative of the surface, $\partial f(R)_{s=0}/\partial R$, is the normal vector to TS plane in the product direction.

As in Section 2.2, we have to project out the contribution of negative momentum that moves in the reactant space by the introduction of a projection operator $\mathcal{P}$ which consists in a Heaviside function $h(k)$

that takes into account all states that have positive momentum in the infinite future

$$\mathcal{P} = \lim_{t\to\infty} \hat{U}(-t)\hat{U}_0(t)h(p)\hat{U}_0(-t)\hat{U}(t) = \Omega_+\mathcal{P}_0\Omega_- \tag{109}$$

where

$$P_0 = \sum_{n_a} \int_{-\infty}^{\infty} h(k) \left|\chi_{\pm k,n_r}\right\rangle \left\langle\chi_{\pm k,n_r}\right| \tag{110}$$

In the previous equations, $\Omega_\pm$ are the Möller operator [84] and $\chi_{\pm k,n_r}$ are the scattering eigefunctions [86].

The thermal rate constant can be evaluated using the Flux operator starting from the definition of CRP as the sum of the squares of the S-matrix elements [86], leading to

$$k(T) = \frac{1}{Q_r(T)} \sum_{n_a} \int \left\langle \Psi_{p',n_a} \right| \hat{F} e^{-\beta H} \mathcal{P} \left| \Psi_{p',n_a} \right\rangle dp' \tag{111}$$

In the previous equation, $Q_r(T)$ is the partition function of the reactants, $\beta = (k_B T)^{-1}$, where k_B is the Boltzmann constant, p' is the momentum of the reactive mode perpendicular to the surface and $\left|\Psi_{p',n_a}\right\rangle$ are the scattering wavefunctions of the reactants.

In Eq. 111, the rate constant is expressed as a Boltzmann average of the reactive flux operator $\hat{F}\mathcal{P}$, i.e. a trace; but quantum mechanical traces are independent of the basis set in which they are calculated, therefore, it can be rewritten more generally as

$$k(T) = \frac{1}{Q_r(T)} \mathrm{Re}\left[\mathrm{tr}\left[\hat{F} e^{-\beta H} \mathcal{P}\right]\right] \tag{112}$$

With a series of calculations [87] the thermal rate constant is finally expressed as the time integral of the flux autocorrelation function $C_f(t)$, as anticipated in Eq.7

$$k(T) = \frac{1}{Q_r(T)} \int_0^{\infty} C_f(t)\, dt \tag{113}$$

$$C_f(t) = \mathrm{tr}\left[\bar{F}\hat{U}(-t_c)\bar{F}\hat{U}(t_c)\right] \tag{114}$$

where $\bar{F} = (\hat{F} + \hat{F}^\dagger)/2$ is the symmetrized flux operator and $t_c = t - i\beta/2$ is the complex time which thermalizes the molecular system at temperature $T = 1/k_B\beta$ and then propagates it for time t.

Eq. 113 makes possible to calculate the thermal rate constant as a time integral; on the other hand, in Eq. 5, we propose to find the same quantity by a Boltzmann average of CRP, namely $N(E)$. The relationship between the CRP and the flux operator becomes explicit if we use the identity

$$\hat{U}(t_c) = e^{-iHt_c} = \int e^{-iHt_c} \delta(H - E)\, dE \tag{115}$$

and insert it in Eq. 113 obtaining [88]

$$k(T) = \frac{1}{2Q_r(T)} \int dt \int dE \int dE' e^{-\beta(E+E')/2} \\ e^{i(E-E')t} \mathrm{tr}\left[\bar{F}\delta(H-E)\bar{F}\delta(H-E)\right] \quad (116)$$

From the property of Dirac delta function, the time integral becomes

$$\int e^{i(E-E')t}\, dt = 2\pi\delta(E-E') \quad (117)$$

which cancels out every contribution in Eq. 116 for $E \neq E'$, leaving

$$k(T) = \frac{\pi}{Q_r(T)} \int dE e^{-\beta E} \mathrm{tr}\left[\bar{F}\delta(H-E)\bar{F}\delta(H-E)\right] \quad (118)$$

By comparison with 5, we finally find

$$N(E) = 2\pi^2\, \mathrm{tr}\left[\bar{F}\delta(H-E)\bar{F}\delta(H-E)\right] \quad (119)$$

Here, we followed the derivation of Miller [87], but a similar result was proposed by Yamamoto [89] using Kubo linear response analysis. Before a deeper investigation on the flux autocorrelation function, we focus on the symmetrized flux operator, since its evaluation is crucial for any further purpose.

If we resolve the scalar product in Eq. 108 between the normal vector from the surface and the positive momentum vector in the product space, we obtain the reactive momentum perpendicular to the surface, namely p'. Then we obtain

$$\hat{F} = \delta(s)\frac{p'}{m} \quad (120)$$

Since the flux operator is designed to return the value of the momentum in a specific position, due to the Heisenberg uncertainty principle it is an unbounded operator, i.e. the magnitude of its eigenvalues diverges in the limit of a complete basis set [90].

From the quantum definition of linear momentum, $p = -i\partial/\partial x$ we find

$$\hat{F} = \frac{1}{im}\left(\delta(s)\frac{\partial}{\partial x}\right) \quad (121)$$

The symmetrized flux operator becomes

$$\bar{F} = \frac{1}{2im}\left(\delta(s)\frac{\partial}{\partial x} + \frac{\partial}{\partial x}\delta(s)\right) \quad (122)$$

If we represent the symmetrized flux operator on an arbitrary basis set $\mathbf{n} = [\phi_1, \ldots, \phi_N]$ and its spatial derivatives $\mathbf{d} = [\phi_1', \ldots, \phi_N']$ we found that its secular equation becomes

$$\bar{\mathbf{F}} \cdot \mathbf{c} = \frac{1}{2im}\left(\mathbf{n}(\mathbf{d}^\top \cdot \mathbf{c}) - \mathbf{d}(\mathbf{n}^\top \cdot \mathbf{c})\right) = f\mathbf{c} \quad (123)$$

where $\mathbf{c}$ are the eigenvectors and f are the eigenvalues.

$\bar{\mathbf{F}}$ is an imaginary, antisymmetric matrix and its associated secular equation [91] is

$$\begin{pmatrix} \langle \mathbf{n}|\,\bar{F}\,|\mathbf{d}\rangle - f & \langle \mathbf{d}|\mathbf{d}\rangle \\ \langle \mathbf{n}|\mathbf{n}\rangle & \langle \mathbf{d}|\,\bar{F}\,|\mathbf{n}\rangle - f \end{pmatrix} \times \begin{pmatrix} a \\ b \end{pmatrix} = 0$$

where a and b are the coefficients of the linear combination of the basis set and its derivatives to form the eigenvectors $\mathbf{c}$

$$\mathbf{c} = a\mathbf{n} + b\mathbf{d} \tag{124}$$

The associated eigenvalues can be found analytically and consist of a pair of solutions, one positive and one negative

$$f_{\pm} = \pm\frac{1}{2m}|\mathbf{n}| \cdot |\mathbf{d}| \tag{125}$$

while the two eigensolutions are complex conjugate

$$\mathbf{c} = |F_{\pm}\rangle = \frac{1}{\sqrt{2}}\left(\frac{\mathbf{n}}{|\mathbf{n}|} \pm \frac{i\mathbf{d}}{|\mathbf{d}|}\right) \tag{126}$$

Using this property, the symmetrized flux operator can be rewritten by spectral decomposition as a simple sum

$$\bar{F} = \sum |F_{\pm}\rangle\, f_{\pm}\, \langle F_{\pm}| \tag{127}$$

The flux autocorrelation function allows to calculate the rate constant of a molecular system for any surface we choose, but the convergence with respect to time is not the same.

More interestingly, the two flux operators in Eq. 114 do not have to share the same surface, therefore we can think of the $C_f(t)$ as a function that returns, depending on time, how much probability density $\rho(R, t)$ escapes from the interval along the reactive coordinate defined by the two surfaces in the product region [92].

The optimal choice for the two surfaces should be in the proximity of the TS, where the DOS is minimal and can be represented by a limited number of wavefunctions. Moreover, since the TS is a saddle point, it induces fast dynamics in the reactive coordinate and therefore a short propagation is sufficient for a converged calculation.

The formalism of flux autocorrelation function has been successfally implemented in several different ways depending on the information needed.

Here, we briefly summarize two different strategies:

- if we are interested on the total rate of the reaction, we can use Absorbing Boundary Condition (ABC) to guarantee the convergence of the calculation [93, 94, 95];

- if we need a state-selected rate, because the same PES has a bifurcation in the product region that leads to two different arrangements (in other words, there is one single TS for different products) or, otherwise, we know that only one specific reactant state is available to perform the reaction, we can settle one of the dividing surfaces far in the product or in the reactant region, respectively [96, 97].

Since the dividing surfaces are constant in time, the flux operator is independent of the choice of computational methods we use to propagate the wavefunction: at each time step, we have to calculate $|F_{\pm}\rangle$ and $f_{\pm}$ and build *a posteriori* the flux autocorrelation function or the CRP in the time domain. Propagation methods will be discussed in the next Section.

3.3 NUMERICAL PROPAGATION OF THE TDSE

In the previous two Sections we have seen that every result about the reaction of a molecular system in the TDSE entails the propagation of wavefunctions.

The propagation is always possible and exact by the application of the evolution operator $\hat{U}(t)$ of Eq. 93.

Unfortunately, the exact knowledge of the time dependent wavefunction is confined in only a few, standard textbook cases like free particle motion or harmonic oscillator.

Since we are now focusing on the general time behaviour of the wavefunction, we drop every reference on the spatial coordinates.

Two different numerical strategies are proposed for the propagation of wavefunctions in quantum mechanics, depending on the knowledge of the PES.

The first approach is used if the PES is known in the whole interval of interest. However, in real simulations we approximate the continuous potential surface to a grid and calculate the PES pointwise, exactly in the same way as in Section 2.6.

For a supposed small, discrete time interval dt, the solution of TDSE is

$$\psi(t+dt) = \hat{U}(t+dt,t)\psi(t) = e^{-i\hat{H}dt}\psi(t) \tag{128}$$

but the evaluation of the propagator is more complex than $\hat{H}$ because the position and momentum operator of the Hamiltonian are coupled by the exponentiation [84].

Expanding the propagator in a Taylor series

$$e^{-i\hat{H}dt} = 1 - i\hat{H}dt + \dots \tag{129}$$

leads to unstable results, because this scheme does not conserve the time reversal symmetry of the Schrödinger equation [98]. Using a symmetric numerical differentiation

$$\psi(t+dt) - \psi(t-dt) = (e^{-i\hat{H}dt} - e^{i\hat{H}dt})\psi(t) \tag{130}$$

leads to an iterative propagation scheme

$$\psi(t+dt) = \psi(t-dt) - 2i\hat{H}dt\psi(t) \tag{131}$$

Anyway, every propagation scheme based on a local evaluation of the propagator (for example, by a chosen truncation of the Taylor series) must be repeated several times, accumulating errors during the calculations.

For this reason, when the potential has been calculated, the Chebyshev series, proposed by Kosloff [99, 100], avoids this source of error permitting us to perform a propagation over an indefinite time interval in a single step.

We define a reduced Hamiltonian H_{red} by the contraction of the range of its eigenvalues $\Delta E = E_{max} - E_{min}]$ in the interval $[-1, 1]$

$$H_{red} = \frac{2(H - E_0)}{\Delta E} \qquad E_0 = \frac{E_{min} + E_{max}}{2} \tag{132}$$

Since we work on a grid of N points that correspond to the number of single quantum chemistry calculations, the range of eigenvalues is

$$E_{min} = V_{min} \qquad E_{max} = \frac{P^2_{max}}{2m} + V_{max} \tag{133}$$

where P^2_{max} is determined by the grid, as in Section 2.6.

The reduced Hamiltonian H_{red} becomes the argument of the Chebyshev polynomials and the propagator is written as

$$e^{-i\hat{H}\,dt} = \sum_{n=0}^{\infty} (2 - \delta_{n,0}) J_n(\Delta E\, dt) T_n(-iH_{red}) e^{-iE_0 t} \tag{134}$$

where $\delta_{n,0}$ is the Kronecher Delta function, $J_n(H)$ are Bessel functions of the first kind and $T_n(t)$ are Chebyshev polynomials, which are generated from the recurrence relation

$$T_{n+1}(H_{red}) = 2H_{red}T_n(H_{red}) + T_{n-1}(H_{red}) \tag{135}$$

with the starting conditions

$$T_1(H_{red}) = 1 \qquad T_2(H_{red}) = H_{red} \tag{136}$$

In Chapter 4, we use the Chebyshev expansion to evaluate the trace of the Boltzmann operator

$$e^{-H/k_b T_c} = \sum_{n=0}^{\infty} (2 - \delta_{n,0}) I_n(\Delta E/k_B T_c) T_n(H_{red}) \tag{137}$$

i.e. the partition function of the molecular system described by the Hamiltonian. The difference between the propagator, an exponential operator that contains only an imaginary part, and the Boltzmann operator, a real operator, is reflected on the type of Bessel function used in the expression. In the previous equation, $I_n(\Delta E/k_B T_c)$ is a modified Bessel function of the first kind.

Even if the polynomial expansion of the Hamiltonian looks artificially complicated, the series in Eq. 134 and Eq. 137 decay exponentially when the index of the summation becomes higher than the argument of the pertinent Bessel function. This means that the error in propagation can be kept lower than a chosen value that can be evaluated *a priori* of the calculation, depending on the accuracy that we want to reach.

Instead, when the potential is globally unknown, as in the BO approximation, we can express the total wavefunction as a linear combination of *wavepackets* [101], localized wavefunctions, that evolve following Eq. 86.

In the field of molecular reaction dynamics, where an ensemble of harmonic or anharmonic oscillators evolves through a TS to another molecular species, the most common potential can be imagined as a multidimensional "near to quadratic" function, coupled between the different DOF.

For this reason the Gaussian WavePackets (GWP) [8] are usually used as time dependent functional forms of the wavefunction, since they are similar to the eigenfunctions of the Schrödinger equation in harmonic potential.

Before approaching the multidimensional case, it is useful to review the monodimensional case of a GWP in a harmonic potential as a benchmark [102]. This particular kind of GWP are called frozen because the width (called sigma in statistics, $\sigma = (2a)^{-1/2}$) cannot change

$$g(x,t) = Ne^{a(x-x_t)^2 + ik_t(x-x_t)} \qquad a, b \in \mathbb{R}, a > 0 \tag{138}$$

where N is the normalization factor

$$N = \sqrt[4]{\frac{2a}{\pi}} e^{k_t^2/4a} \tag{139}$$

x_t is the time dependent centre of the wavepacket and k_t is the momentum.

Now, we consider the motion of a GWP on a harmonic potential $V(x) = m\omega^2 x^2/2$, exactly expanded as a Taylor series; we need to calculate the Hamiltonian and the time derivative of the GWP, obtaining

two coupled equations for the variable of motion, position and momentum, and a condition on the width that must be satisfied, namely

$$a = \frac{m\omega}{2} \tag{140}$$

$$\frac{\partial k_t}{\partial t} = -\frac{\partial V(x)}{\partial x} = -\frac{\partial H}{\partial x} \tag{141}$$

$$\frac{\partial x_t}{\partial t} = \frac{k_t}{m} \tag{142}$$

In other words, under the constraint of a specific value for the width, the GWP moves under the classical laws of motion.

Another remarkable property of GWP is that they remain GWP under the Fourier Transform

$$\psi(k) = \frac{1}{\sqrt{2\pi}} \int g(x,0) e^{-ikx}\, dx \tag{143}$$

$$= \frac{1}{\sqrt{2\pi}} \int e^{-ax^2 - i(k_0 - k)x}\, dx \tag{144}$$

$$= \frac{1}{\sqrt{2\pi}} \sqrt{\frac{\pi}{a}} e^{(k_0-k)^2/4a} \tag{145}$$

$$= \frac{1}{\sqrt{2a}} e^{(k_0-k)^2/4a} = g(k,0) \tag{146}$$

$g(k,0)$ is the momentum representation of $g(x,0)$. The general time dependent GWP in the momentum representation can be evaluated with the help of propagator in Eq. 93

$$g(k,t) = \hat{U}(t) g(k,0) = \frac{1}{\sqrt{2a}} \int e^{(k_0-k)^2/4a} e^{-ik^2 t/2m} dx \tag{147}$$

If we calculate the variance in coordinate and momentum space, Δx and Δk, we find

$$\Delta x = \frac{1}{\sqrt{2a}} \qquad \Delta k = \sqrt{\frac{a}{2}} \tag{148}$$

which satisfies the Uncertain Principle

$$\Delta x \Delta k = \frac{1}{2} \tag{149}$$

This property comes directly form the fact that Gaussian distributions are eigenfunctions of the Fourier Transform.

3.4 GAUSSIAN MULTI CONFIGURATION TIME DEPENDENT HARTREE

In the case of a molecular system with many modes coupled between them, the nuclear Hamiltonian can be written as

$$\hat{H}_{nuc} = -\sum_i \frac{\nabla^2}{2m_i} + V(x_1, x_2 \dots x_n) \tag{150}$$

The Multi Configuration Time Dependent Hartree (Multi Configuration Time Dependent Hartree (MCTDH)) is a numerical methodology developed in the last forty years to perform the propagation of wavefunction expressed as [103, 104]

$$\psi(\bar{x}, t) = \sum_j a_j(t) \prod_i \phi_{i,j}(x_i, t) \tag{151}$$

namely a product of monodimensional Single Particle Function (SPF) $\phi_{i,j}(x_i, t)$, linearly combined with a time dependent coefficient $a_j(t)$ that weights the importance of each configuration j. Since each DOF x_i is not limited to be described by one SPF, but n_i, then j is a multi-index which runs over each SPF n_i of each DOF i; therefore, the number of configurations j and time dependent coefficients $a_j(t)$ is equal to

$$j = \prod_i n_i \tag{152}$$

The presence of different configurations is needed to recover the correlation (or at least some of it) introduced by the nonseparability of the PES in the Hamiltonian in Eq 150. If we are propagating the wavefunction using a single configuration, the Hartree product that we use to describe the wavefunction in Eq. 151 will miss any correlation effects.

The analytic structure of the primitive function used is strictly related to the physics of the particular DOF: a Gaussian wavepacket for translational motion, associated Legendre functions for angular coordinate, spherical harmonics for a combined rotation over two angles... All of these functions must be orthonormalized in order to maintain the square norm of the total wavefunction $\psi(t)$ normalized to unity.

The use of a time dependent basis set reduces the computational cost because the grid, formed by the SPF, adapts itself during the propagation. On the other hand, in a time independent grid the wavefunction has to be calculated at each point at each time. Moreover the time independent grid should be significantly larger in order to allow long time propagation.

The best way to propagate wavefunctions like in Eq. 151 is using the Dirac-Frenkel Variational Principle (DFVP) [105, 106]

$$\langle \delta\psi | \hat{H} - i\partial_t \psi \rangle = 0 \tag{153}$$

where ∂_t is the partial time derivative.

The DFVP asserts that any variation $\delta\psi$, which can be viewed as a tangent plane to the subspace that contains the wavefunction ψ, must be orthogonal to the approximated solution of the TDSE, the ket of Eq. 153.

In order to quantify the evolution of the wavefunction, we write it in terms of an ensemble of time dependent parameters: note that

DFVP is true in the finite dimensional space $\tilde{\mathcal{H}}$ spanned by the time dependent basis set $[\phi(x_i, t)]$.

If the space was complete, and the variations unrestricted (i.e. if the number of parameters, configurations and wavepackets are infinite) the solution of Eq. 153 is equivalent to the solution of the TDSE.

Even if the computational cost of the propagation in MCTDH scales favourably with the number of DOF, the main disadvantage remains the request of the total PES as a precondition of the propagation [107] which need to be fitted in a product representation [108] to be efficiently propagated.

This undesired feature of MCTDH comes from the use of non localized primitive functions as SPF in the expression of the total wavefunction in Eq. 151.

What we need is an efficient method to evaluate the effect of time on the wavefunction of a molecular system. In this contest, *efficiency* is strictly related with two requests that the method must satisfy:

- The computation cost has to scale favourably with the number of degrees of freedom, in order to save CPU time;
- The propagation does not need the knowledge of the whole PES to be performed, in order to save memory storage and long quantum chemistry calculations.

The Gaussian Multi Configuration Time Dependent Hartree (G-MCTDH) satisfies both requirements because the local nature of GWP implies that we can treat the PES locally by the Local Harmonic Approximation (LHA), using the gradient and the Hessian to perform the propagation. The computational cost is minimized thanks to the flexibility of a time dependent basis set.

In G-MCTDH the SPF are always frozen Gaussian functions as in Eq. 138, obtaining a similar expression to Eq. 151 for the total wavefunction

$$\psi(t) = \sum_j a_j(t) \prod_i g_{i,j}(x, t) \tag{154}$$

Actually, this is a Gaussian similar to Eq. 138

$$g_{i,j}(x, t) = N e^{-a(x-x_t)^2 + b_t(x-x_t)} \tag{155}$$

where $a \in \mathbb{R}$ and $b_t \in \mathbb{C}$. The real and complex part of the parameter b_t are built so that

$$\Re(b_t) = -2ax_t \qquad \Im(b_t) = p \tag{156}$$

The normalization constant N is defined so that each GWP is normalized. Is it also possible to compress more than one physical DOF in one SPF, which are called *logical variables* to avoid misunderstanding;

this computational strategy is called *mode combination* and helps to treat molecular systems with tens to hundreds of physical DOF that are less important for the dynamics.

In the following presentation, we suppose that mode combination is not used, anyway, this extension is straightforward.

This approach is also called *direct dynamics* since we can interface the nuclear propagation with the electronic calculations directly [109].

Appling the DFVP to a wavepacket such as Eq.154 leads to two coupled differential equations, one for the coefficients and one for the wavefunction [110]

$$\begin{cases} i\mathbf{S}\dot{\mathbf{A}} = (\mathbf{H} - i\boldsymbol{\tau})\mathbf{A} \\ i\mathbf{C}^{(\kappa)}\dot{\boldsymbol{\lambda}}^{(\kappa)} = \boldsymbol{\Upsilon}^{(\kappa)} \end{cases}$$

In the previous equations we use a vectorial notation, consistent with the following definition of G-MCTDH wavefunction

$$\psi(x,t) = \sum_j A_j G_j = \mathbf{AG} \tag{157}$$

where j is the index that label the N configurations, A_j is the vector of the coefficients and G_j is the product of GWP. In the next presentation, however, N is the number of DOF and n_κ is the number of GWP for each DOF [111]:

- $\mathbf{S}$, $(N \times N)$, is the configurational overlap matrix $\langle G_i | G_j \rangle$ between each configuration G_j, since GWP are not orthonormal;
- $\dot{\mathbf{A}}$, (N), is the time derivative vector of the coefficients;
- $\mathbf{H}$, $(N \times N)$, is the Hamiltonian matrix which elements are $\langle G_i | H | G_j \rangle$;
- $\boldsymbol{\tau}$, $(N \times N)$, is the overlap matrix between configurations and their time derivatives, $\langle G_i | \partial_t G_j \rangle$;
- $\dot{\boldsymbol{\lambda}}^{(\kappa)}$, (n_κ), is time evolution vector of the λ parameters in GWP;
- $\mathbf{C}^{(\kappa)}$, $(n_\kappa \times n_\kappa)$, which elements are

$$C^\kappa_{j\lambda,j'\lambda'} = \rho^\kappa_{j,j'} \left\langle \partial_\lambda g_j \right| 1 - P^\kappa \left| \partial_{\lambda'} g_{j'} \right\rangle \tag{158}$$

  where $\rho^\kappa_{j,j'} = \langle \psi^\kappa_j | \psi^\kappa_{j'} \rangle$ is the reduced density matrix defined by the single-hole wavefunction ψ^κ_j of the configuration j, obtained by elimination of the SPF κ , and P^κ is the projection operator spanned by it

$$P^\kappa = \sum_{i,j} \left| g^{(\kappa)}_i \right\rangle \mathbf{S}^{-1}_{i,j} \left\langle g^{(\kappa)}_j \right| \tag{159}$$

- $\mathbf{Y}^{(\kappa)}$, (n_κ), is defined as

$$\mathbf{Y}^{(\kappa)}_{j,\lambda} = \sum_{j'} \langle \partial_\lambda | \, (1 - P^\kappa) H^\kappa_{j,j'} \, | g_{j'} \rangle \tag{160}$$

  where $H^\kappa_{j,j'} = \langle \psi^\kappa | \, H \, | \psi \rangle^\kappa$ is the mean field Hamiltonian.

For a detailed introduction to G-MCTDH, the interested reader can find more details in many reviews [108] and books [107].

3.5 FLUX OPERATOR IN G-MCTDH

The final stage of our analysis for the calculation of time dependent thermal rate constants is the evaluation of the flux operator in the frame of G-MCTDH, to obtain a general theoretical tool for the evaluation of thermal rate constant in the time frame for molecules with tens or even hundreds of DOF.

Using the property that the symmetrized flux operator $\bar{F}$ has only two eigenvalues [90, 91], we obtain

$$\bar{F} = \frac{i}{2m}[\hat{p}, \delta(s)] \tag{161}$$

where the Dirac delta function is the derivative of the Heaviside step function that defines the surface. The delta function can be obtained as the limit of a narrow Gaussian function [112]

$$\delta(s) = \lim_{\gamma \to \infty} \sqrt{\frac{\gamma}{\pi}} e^{-\gamma s^2} \tag{162}$$

for a given parameter γ. This approximation makes possible the evaluation of the flux operator as the superposition of the G-MCTDH wavepacket with another Gaussian, fixed in the configuration space, that represent the surface.

The symmetrized flux operator becomes

$$\bar{F} = \frac{i}{2m}(|g\rangle \langle g'| - |g'\rangle \langle g|) \tag{163}$$

where $|g\rangle'$ has been approximated by the finite difference of Gaussians

$$|g\rangle' = \frac{\gamma}{2\sqrt{\pi}}\left(e^{\gamma(x+1/\sqrt{\gamma})^2} - e^{\gamma(x-1/\sqrt{\gamma})^2}\right) \tag{164}$$

Now, we can apply the symmetrized flux operator to the G-MCTDH wavepacket rewritten as $\Psi = g^\ddagger \psi^\ddagger$, where $\psi^\ddagger$ is the single-hole function obtained by dropping the GWP in the reactive mode $g^\ddagger$, obtaining

$$\bar{F}\Psi = \psi^\ddagger \bar{F} g^\dagger = \psi^\ddagger \langle g' | g^\ddagger \rangle - \psi^\ddagger \langle g | g^\ddagger \rangle \tag{165}$$

Part II

APPLICATIONS

4

PARTITION FUNCTION OF HINDERED ROTATIONS

In this second part of the Thesis we will focus on computational strategies and numerical results obtained in a series of study cases.

The calculation of thermal rate constants, both in energy (Eq. 5) and time domain (Eq. 7), needs the knowledge of the Molecular Partition Function (MPF), but the evaluation of this crucial quantity is not trivial, since it contains the full thermodynamical information on systems in the canonical ensemble.

The MPF is defined as the trace of the Boltzmann operator

$$Q(T) = \mathrm{tr}[e^{-H/k_B T}] = \sum_i e^{-E_i/k_B T} \tag{166}$$

The total MPF per unit volume is usually written, following the separation of the Hamiltonian, as a product of translational, rotational, vibrational and electronic contributions

$$Q(T) = Q_{trans}(T)\, Q_{rot}(T)\, Q_{vib}(T)\, Q_{el}(T) \tag{167}$$

The considerations and the approximations made during the separation of these modes in Chapter 2 are the same here; therefore, the total MPF accuracy can be lowered when some conditions (like the separation of the electronic states in BO approximation) are not satisfied.

Nevertheless, since the separation of the centre of mass is always exact in gas phase, the reference equation for the translational partition function is

$$Q_{trans}(T) = \left(\frac{2\pi\mu}{\hbar^2\beta}\right)^{3/2} \tag{168}$$

and it will always be considered true: μ is the reduced mass of the translational motion and $\beta = (k_B T)^{-1}$.

Since we are focused on electronic ground states with the same number of electrons between reactants and Transition State, the electronic partition function $Q_{el}(T)$ is simply the multiplicity of the electronic ground state.

The standard approach for the remaining two parts of the total MPF, $Q_{rot}(T)$ and $Q_{vib}(T)$, consists in the treatment of the molecules as rigid rotors and a series of harmonic, uncoupled oscillators. At a higher level of accuracy, it is possible to include the coupling of rotations and vibrations with a quasi-rigid description of rotations and the coupling between vibrational modes with a perturbative approach [113].

As a working definition, a floppy-geometry molecule contains one or more LAM which must be treated separately with the computational strategy presented in the Theory part. Molecules with floppy geometries cannot be treated by the perturbative approach, for the reasons presented in Section 2.5. Moreover, while the size of molecules grows, the probability that it contains one or more LAM grows as well, making it impossible to be accurately described in the approximation of anharmonic vibrations.

As anticipated in Section 2.5, we focus on the Hindered Rotation because it is a common LAM that corresponds to a single, well defined primitive internal coordinate. Nevertheless, both the methods presented, the Chebyshev expansion of the propagator presented in Section 3.3 and diagonalization of the DVR Hamiltonian presented in Section 2.6 can be applied, with the proper generalizations, to the study of multidimensional LAM, like a series of coupled hindered rotors or the complex motions described by a linear combination of internal coordinates, like ring deformations.

However, specific studies demonstrate that the coupling between different hindered rotations is weak in most molecules of practical interest [44, 114, 115] and therefore we focus only on monodimensional Hindered Rotor Partition Function (HRPF).

Methods based on the vibrational perturbation theory, like Simple Perturbation Theory (SPT) [116], cannot be applied for the same reason that forces us to use the Generalized Coordinate (GC) method: the Taylor series does not converge fast enough, therefore the anharmonic contributions suffer from numerical instability.

4.1 NUMERICAL IMPLEMENTATION FOR HRPF

While in Sections 2.6 and 3.3 we had presented the general features of the GC and the Chebyshev expansion, in this Section we present the computational strategies used to maximize the efficiency of their respective algorithms.

It must be stressed that both methods require a relaxed scan to a be performed, i.e. they need the whole PES of the LAM, which usually is just a small subset of the total modes, here equal to one.

In the Chebyshev expansion of the Hamiltonian (Eq. 137 in Section 3.3), defined as "time propagation" in the following graphs, the result of the propagation is directly the HRPF, which can be multiplied by the partition function of the other motions to obtain the total MPF.

It has been implemented, following the idea of Manthe and coworkers [117], by propagation of a initial real wave function $|\psi_r\rangle$, defined as

$$|\psi_r\rangle = \sum_i^N (-1)^{R_i} |\phi_r\rangle \tag{169}$$

where $(-1)^{R_i}$ is the overlap with the corresponding DVR function at each point around the 1-D rotor configuration space; R_i is a random integer number.

In this way, the norm of $|\psi_r\rangle$ is equal to N and the trace of the Boltzmann operator (i.e. the HRPF) can be approximated by the formula

$$Tr(e^{-\beta H}) = \frac{1}{N}\sum_{i=1}^{N}\langle\psi_i \mid e^{-\beta H} \mid \psi_i\rangle \tag{170}$$

In the case of HR, an upper bound of the eigenvalues range, E_{max} of Eq. 133, is

$$E_{max} = AN_p^2 + V_{max} \tag{171}$$

where A is the rotational constant of the HR and N_p is the number of points of the grid. Thus, the number of points should be increased to ensure a converged partition function: we choose to cut the Hamiltonian spectrum when the argument of the exponential $E_{max}/K_B T$ is greater than three, which corresponds to a maximum absolute error of $9 \cdot 10^{-2}$.

For this reason, the PES obtained with the relaxed scan with a limited number of quantum chemistry calculations along the dihedral angle are fitted using cubic spline in order to obtain a representation of the PES with a flexible number of points.

While the value of N_p does not influence drastically the computational cost of the Chebyshev algorithm, in the GC approach it represents the computational bottleneck, since it increases the size of the Hamiltonian matrix.

In the GC method two considerations must be made on the distribution of the eigenvalues obtained by the diagonalization of the Hamiltonian matrix:

1. whenever the free rotor limit is reached the corresponding eigenvalues show the typical progression of K^2 with a double degeneracy and do not contain any more valuable information about the LAM;

2. since we use a random walker to sample the phase space by the use of Eq. 73, a finite number of eigenvalues does not ensure a complete description of the DOS of the LAM.

For these reasons we fit the discrete energy spectrum for the HR obtained by GC method as a function of the quantum number (interpreted as a running integer spanning the Hamiltonian eigenvalues).

Since for a free rotor the energy is a quadratic function of the quantum number, a polynomial fitting procedure up to the second order can describe properly the progression of the eigenvalues.

However, for low energies, a polynomial performs rather poorly in reproducing the energies as a result of the (quasi)- degeneracies

arising from tunnelling across the torsional potential maxima. Thus, for every HR, we define two limits:

1. The minimum quantum number n_0, below which all energies are taken to have their exact (variational) values;
2. A limiting quantum number n_{fr}, above which the free rotor limit is assumed to have been reached and the energies are assumed to follow a quadratic expression.

The intermediate region (between n_0 and n_{fr}) is fitted to a quartic polynomial expression; as the quantum number n_0 corresponds semiclassically to a certain value of the action around the torsional loop, it is chosen to be proportional to the curvilinear integral

$$n_0 \propto \oint \sqrt{(V_{max} - V(s)}\,ds \tag{172}$$

where V_{max} is the maximum value of the potential; s is the generalized coordinate, presented in Appendix B, whose length is proportional to the reduced mass of the HR.

Thus, the quantum number n_0 will be higher for systems with a higher reduced mass, where the generalized coordinate s runs over a wider interval, and for molecules with higher torsional variation of the potential. However, whenever the semiclassical integral gives a value less than 10 we have chosen to assume $n_0 = 10$ in order to avoid numerical difficulties associated with a large state spacing.

We have found that a good value for the limiting quantum number n_{fr} is essentially $3n_0$, since all the reflection effects of the hindering potential on the eigenstates with an energy higher than V_{max} vanish rapidly. Thus, between n_0 and n_{fr} the eigenvalues were fitted using a quartic polynomial and above n_{fr} the free rotor limit is assumed to have been reached and a quadratic polynomial is obtained through fitting of the last three doubly-degenerate state pairs below n_{fr}.

Here, we examine a few test cases that illustrate a representative subset of various combinations of rotational constants and hindering potentials, presented in Table 1.

Table 1: Molecules of interest

Potential	Rotational Constant	
	Low	High
Low	Biphenyl	Methanol
High	1,2-Dichloroethane	Fluoromethanol

Since all these HRs arise from the rotation around a single bond, as a further test case we also treat a series of metallocenes, presented in Section 4.6. Metallocenes show moments of inertia even higher than

the examples in Table 1 and a symmetry number $\sigma = 5$; therefore, these characteristics make the metallocenes a stress case for GC and time propagation methods.

In Table 2, we show the minimum quantum number n_0 needed for the fitting procedure, the size of the Monte Carlo (Monte Carlo (MC)) sample for the Chebyshev expansion and the minimum number of eigenvalues that we have to use to obtain a fully convergent partition function.

Table 2: Minimum rotational quantum number, Monte Carlo sample size and DVR number of basis functions for each molecule

Molecule	n_0	MC sample	Min. N_p
Methanol	3	160	56
Fluoromethanol	8	80	59
Biphenyl	37	80	456
1,2-Dichloroethane	56	80	252

All the electronic calculations have been performed at the Density Functional Theory (DFT) level, using the B3LYP functional and the SNSD basis set; in the case of biphenyl, dispersion contributions have been evaluated using the empirical correction proposed by Grimme [118]. The anharmonic corrections have been obtained using VPT2 as implemented in the quantum chemistry package GAUSSIAN09 [22]. Each point along the internal rotation coordinate has been adiabatically relaxed.

These choices for the quantum chemistry calculations were made to optimize both the accuracy of the anharmonic frequencies, compared with experimantel IR and Raman spectra, and the computational cost [50], since our final objective is to create an flexible algorithm which can runs over a wide range of molecules with different sizes.

In all cases, the MPF has been calculated using four different schemes:

1. Wang-Landau full anharmonic treatment of vibrations and hindered rotations, with fitting of the hindered rotation quantum numbers
2. Wang-Landau full anharmonic treatment of vibrations with imaginary time propagation of hindered rotation
3. Wang-Landau full anharmonic treatment of vibrations with exact (variational) treatment of hindered rotation
4. Harmonic treatment of all vibrations

4.2 BIPHENYL

In Fig. 1 is shown the torsional potential for the biphenyl molecule. Although the symmetry number $\sigma = 2$, the potential surface of biphenyl has four peaks: the interaction of hydrogen atoms in the coplanar configurations causes the first and the third ones, while the second and the fourth peaks are related to the repulsion of π molecular orbitals.

Figure 1: Biphenyl potential: the first and the third peak are around 780 cm^{-1} (0.0034 hartree) while the second and the fourth about 810 cm^{-1} (3.7×10^{-3} hartree).

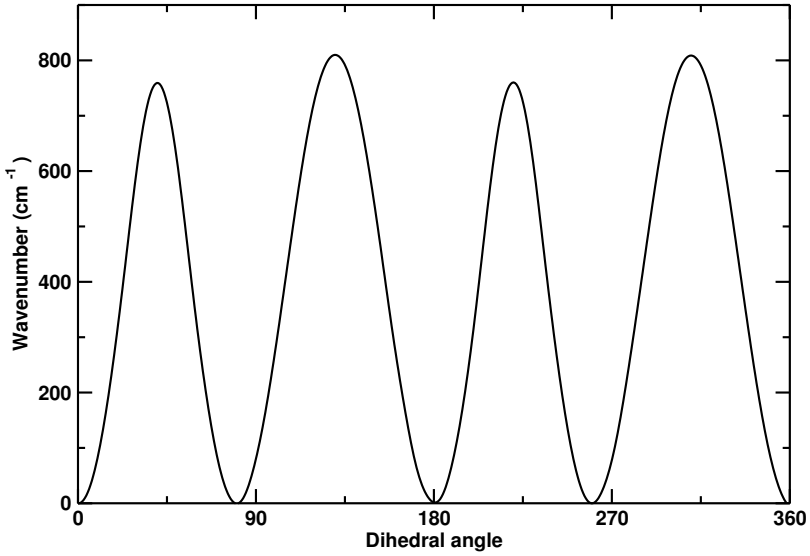

Due to the combination of a low rotational constant ($\approx 1.7 \times 10^{-6}$ hartree) and a difference between maximum and minimum value of hindering potential of $\approx 3.7 \times 10^{-3}$ hartree (i.e. $\approx$ 800 cm^{-1}), the biphenyl molecule is a quantum system very close to the classical hindered rotor limit.

In Fig. 2 is shown the partition function of biphenyl, calculated in the four different modes shown previously. As expected, the harmonic treatment underestimates the total partition function (due to the higher spacing of the vibrational manifold). On the other hand, both the time-propagation and the fitting schemes do an excellent job of approximating the variational results, although they slightly appear to overestimate and underestimate the partition function respectively. The underestimation by the fitting scheme can conceivably be traced to an overestimation of the quadratic "free rotor" rotational constant by the fitting, a minimal residue of the influence of the torsional potential. It is more difficult to assess the precise effect of the time-propagation convergence because of its fundamentally stochastic nature. Nevertheless, all methods appear to perform excellently at all temperatures considered.

Figure 2: Biphenyl partition functions. The continuous black line refers to the variational results, the blue continuous line where hindered rotation has been treated through imaginary time propagation, the dotted red line where hindered rotation eigenvalues have been fitted and the continuous green line where the harmonic vibrational scheme has been used.

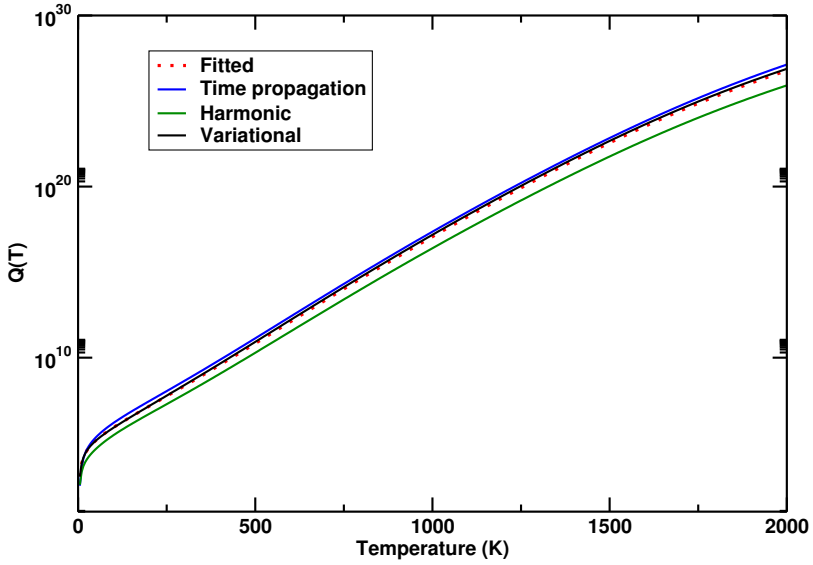

The minimum fitting quantum number for biphenyl was found to be 37. Its relatively high value can be traced to the high reduced mass and torsional rotational constant, which confines a large number of states in the torsional potential. On the other hand, the torsional free rotor limit was assumed to be reached after around 110 states.

4.3 1,2-DICHLOROETHANE

The potential energy profile in Fig. 3 shows a global minimum for the *anti* conformation and two symmetric local minima for the two *gauche* rotamers. The presence of the two vicinal chlorine atoms in 1,2-Dichloroethane produces a single peak in the torsional profile of about 3200 cm^{-1} or 1.45×10^{-2} hartree, that corresponds to an equivalent temperature of about 4000 K.

However, the other two peaks have a height of 7×10^{-3} hartree. This kind of torsion can be viewed literally as a large amplitude motion with a single barrier due to the eclipsing repulsion of the two chlorine atoms. Figure 4 shows the canonical partition functions. The agreement with the exact results is seen to be excellent again. The only appreciable deviation at high temperatures is due to the time-propagation treatment of the hindered rotation (which still, nevertheless, is essentially coincident with the exact results). As the deviation at low temperatures is essentially zero, the slight high-T deviation is

Figure 3: 1,2-dichloroethane potential: the first and the third peaks lie at 3200 cm^{-1} while the second one lies at 1600 cm^{-1}

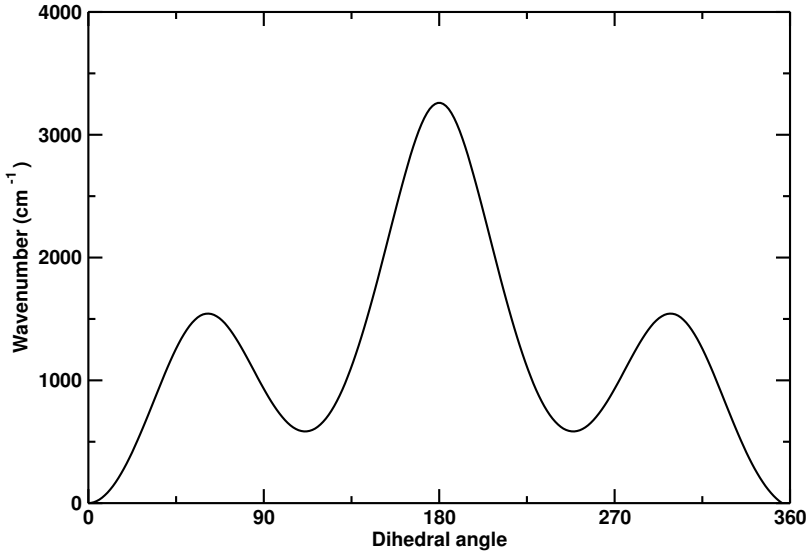

probably due to incomplete Monte Carlo sampling of the configuration space.

Interestingly, at low temperatures the harmonic partition function appears to be slightly higher than the other ones. Presumably this is due to a negative anharmonicity coefficient and/or coupling between modes which serves to increase the anharmonic spacing of some low-lying states.

The minimum fitting quantum number in this case is 56, with the free rotor limit reached around 160. Even though the rotational constant of 1,2-Dichloroethane is higher, the torsional potential is so much higher than in the case of biphenyl that more states need to be taken into account variationally. We remind that this is all indicated by the semiclassical integral in Eq. 172.

4.4 METHANOL

The methanol molecule has been extensively studied [119, 120] and, moreover, represents a prototype of hindered rotation. The small potential barrier, of about 360 cm^{-1} (or $1.5 \cdot 10^{-3}$ hartree), suggests that the free rotor limit is reachable even for medium temperatures, as shown in Fig. 6.

On the other hand, at lower temperatures (50-100 K) quantum effects become strong and the classical and harmonic HRPFs underestimate the exact one: the ground state is a quasi-degenerate triplet, because the potential energy surface has a symmetry number $\sigma = 3$, as the energy profile shows in Fig. 6. The high rotational constant of methanol means that, at moderate temperatures, the phase space is adequately sampled with only a few wavefunctions and, moreover,

Figure 4: As in Fig. 2 for 1,2-Dichloroethane.

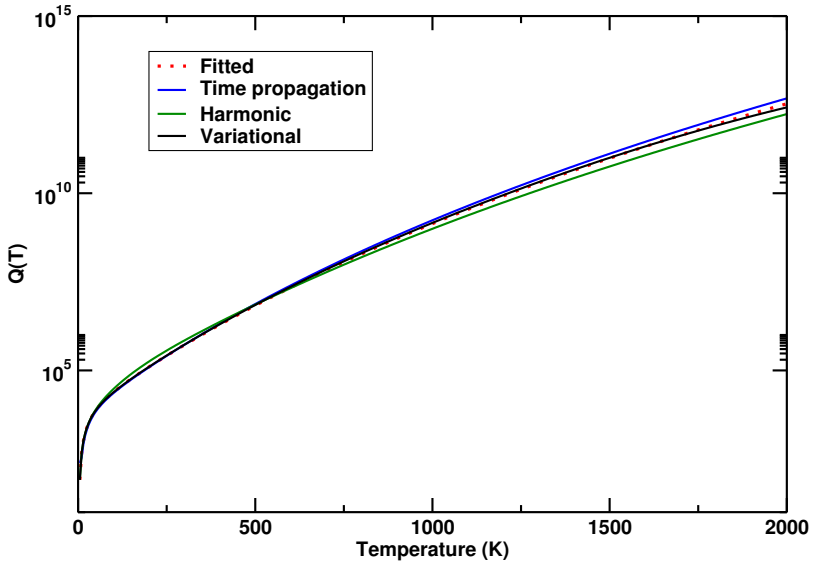

these wavefunctions have a relatively high spatial coherence length. The case of methanol, therefore, is among the ones least amenable to a Monte Carlo approach and more to an exact one.

Figure 5: As in Fig. 2 for methanol.

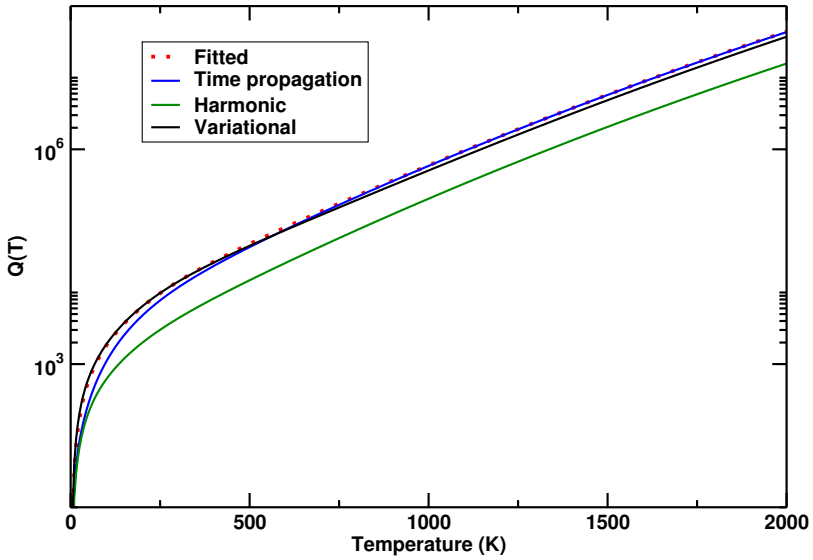

At high temperatures, both hindered rotation schemes approximate the variational partition function rather well, if slightly overestimating it. On the other hand, at low temperatures, the time propagation approach seriously underestimates the partition function. As mentioned before, this can be traced to the highly "quantum", delocalized nature of methanol low torsional levels. On the other hand, the fitting scheme does excellently at low temperatures (as expected, since low levels are taken with their variational values).

Figure 6: Methanol potential: the three degenerate maxima have a value of 360 cm^{-1}.

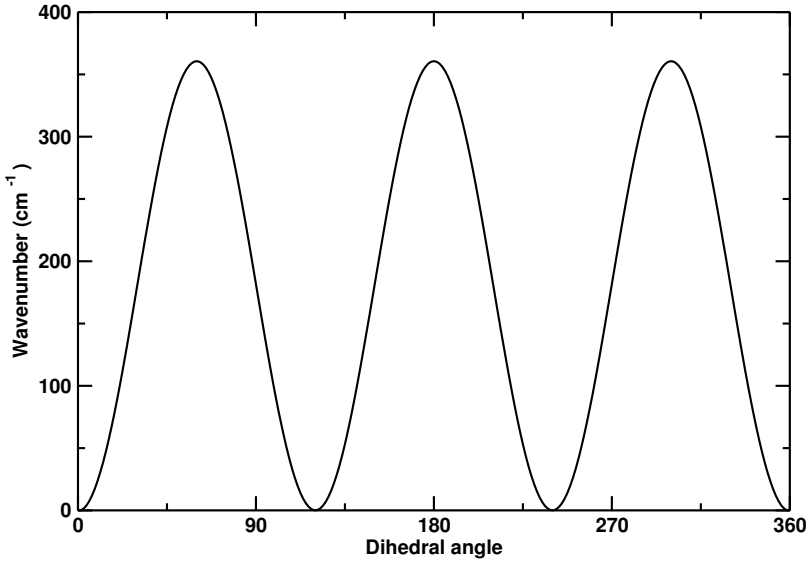

The minimum fitting quantum number for methanol was found to be 3 by the semiclassical integral and, as mentioned before, we have taken it to be 10 in order to avoid numerical problems. This is both an effect of the low torsional potential and the high rotational constant.

4.5 FLUOROMETHANOL

In order to assess the effect of a high torsional barrier (1750 cm^{-1}, $\approx 7.6 \cdot 10^{-3}$ hartree) on a hindered rotor with a high rotational constant, we have also studied fluoromethanol.

Even though the molecular structure suggests the presence of three asymmetrical minima (Fig. 6 and Fig. 8), the potential energy surface shows only two minima associated with the two *gauche* rotamers. The *anti* conformation is actually the highest maximum (the second peak in Fig. 8) and the *syn* conformation is the lower maximum, i.e. the first peak.

This behaviour is presumably associated to an interplay between eclipsing interactions between the O-H and the C-H and C-F bonds and an intramolecular O-H...F hydrogen bond.

The fluoromethanol partition function converges relatively slowly with the number of initial wavepackets. An explanation for this fact lies in the higher torsion potential profile: the resulting eigenfunctions have a relatively localized structure and are therefore less easily represented with sample eigenfunctions whose amplitude is uniform throughout the configuration space. This is also reflected in the fact (as in the case of methanol) that, at low temperatures, the time-propagation partition function seriously underestimates the variational

Figure 7: As in Fig. 2 for fluoromethanol

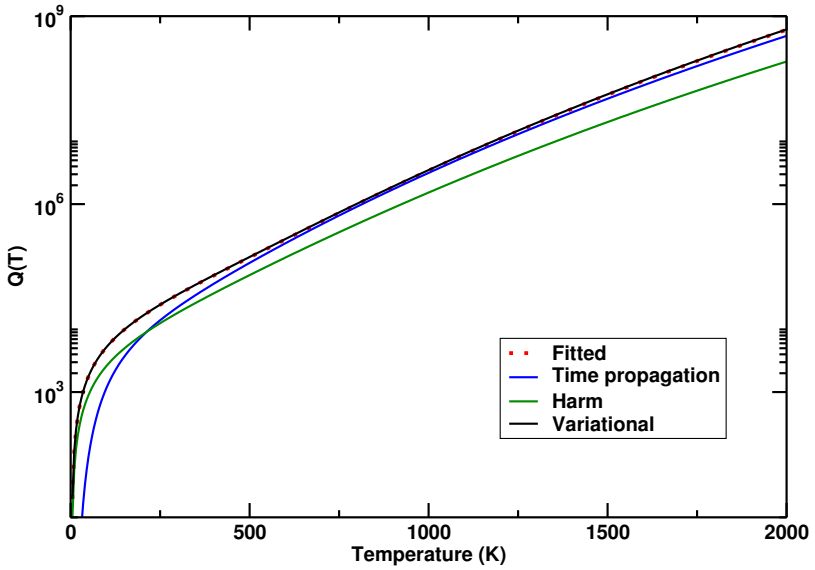

one. On the other hand, the fitting partition function does well at all temperatures.

From the interplay of a medium rotational constant and a relatively high torsional potential, a minimum fitting quantum number of 8 is calculated (therefore, again, the value of 10 is adopted).

Figure 8: Fluoromethanol potential: the two maxima correspond to 1000 cm^{-1} and 1750 cm^{-1}.

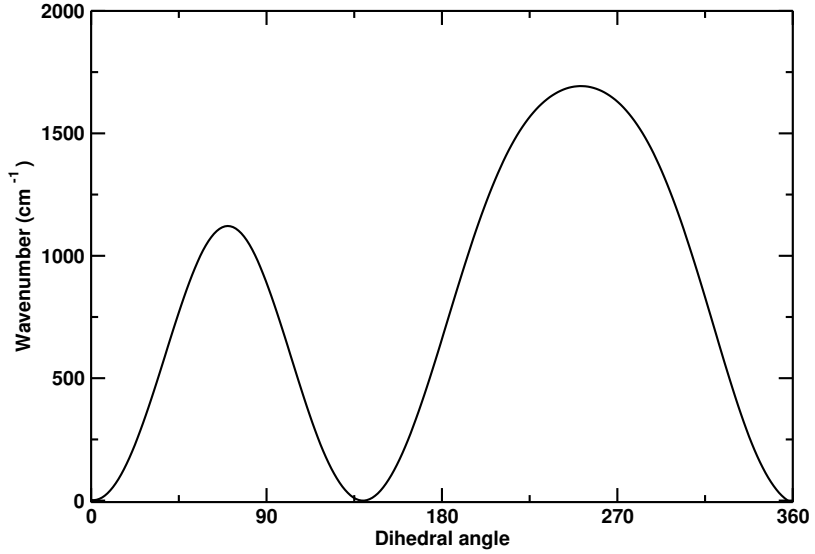

It can be seen that the harmonic model can be very inadequate and, for accurate results, anharmonicity as well as coupling between normal vibrational modes is indispensable.

Table 3: Maxima of the torsional potential (in cm^{-1}), metal-carbon distance (in Å) and harmonic frequencies (in cm^{-1})

	METALLOCENES		
	Ferrocene	Ruthenocene	Osmocene
V_{max}	293	245	361
$\bar{d}(M, C)$	2.04	2.18	2.18
ω_{harm}	30.5061	44.3077	52.3460

4.6 METALLOCENES

Another interesting application of GC and time propagation methodologies is the study of HR in metallocenenes, extending the range of our investigation to organometallic compounds with high symmetric hindering potentials ($\sigma = 5$).

Metallocenes are formed by a pair of cyclopentadienyl (Cyclopentadienyl (Cp)) anions (C_5H_5) and a transition metal atom in oxidation state II, wherein the metal atom stays between the two Cp units, forming a sandwich-like structure.

A large class of metallocenes have been analyzed by various spectroscopic techniques, obtaining accurate information about their crystallographic structures, molecular geometries and potential energy surfaces. Such studies include X-ray diffraction experiments, as well as vibrational spectroscopy, both Raman and infrared [121, 122, 123]

The ferrocene, ruthenocene and osmocene molecules have been recently analyzed from a computational point of view [124], finding the best results at DFT level of theory with the combination of the B3PW91 functional [125] and the LANL2DZ basis set [126], including polarization functions on all atoms (H (p; 0.800), C (d; 0.587), Fe (p; 0.135), Ru (f; 1.235), Os (f; 0.886)). These parameters have previously produced satisfactory agreement with experimental spectra for all three metallocenes considered.

Interestingly, as shown in Table 3, the potential maximum energies V_{max} (Fig.9) (taking 0 as the potential minimum) do not obviously correlate with the distance between metal and the carbon $\bar{d}(M, C)$ in the optimized geometry; also the harmonic frequencies, which are sensitive only to the curvature of the potential at the minimum, are not directly related with the global behaviour of the PES. This confirms the necessity of quantum chemistry calculations to obtain accurate PES for internal rotation.

As the energy increases, the eigenfunctions of the Hamiltonian are expected to switch from a localized nature among the five potential minima to the delocalized nature of the free rotor levels. However, at all energies (and for all kinds of fivefold symmetric potentials) a 5-cycle permutation of the carbon and hydrogen atoms in a Cp unit is a

Figure 9: Comparison of the torsional potential in cm^{-1} of metallocenes. The red line refers to ferrocene, the black line to ruthenocene and the blue line to osmocene.

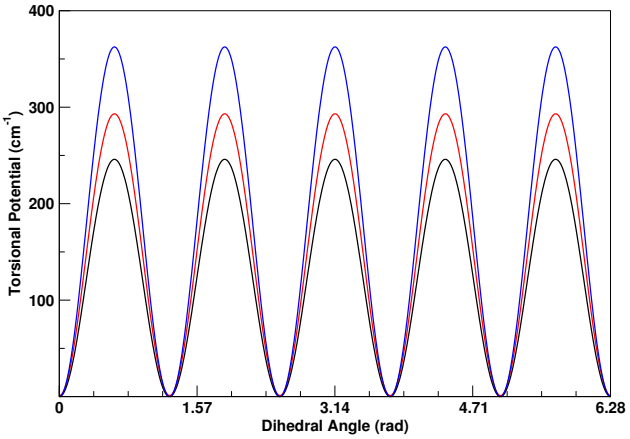

symmetry operation. Briefly, this implies that, in all cases, the energy levels can be classified into three categories:

1. Totally symmetric nondegenerate wavefunctions, A
2. Doubly degenerate wavefunctions, whose character under a 5-cycle is $2\cos(2\pi/5)$, E_1.
3. Doubly degenerate wavefunctions, whose character under a 5-cycle is $2\cos(4\pi/5)$, E_2.

In the free rotor case, these correspond respectively to K being a multiple of 5, congruent to ± 1 modulo 5 and congruent to ± 2 modulo 5 (in this case there is also the additional degeneracy for K being a nonzero multiple of 5). On the other hand, for an infinitely high potential, all three cases merge into a 5-fold degeneracy.

In Table 4 are shown the first 15 eigenvalues for all three cases and the transition of regimes can be seen. The lowest 5 eigenvalues have approximately the same energy (although the totally symmetric among them are already seen to be splitting away). This is the case also for the highest eigenvalues shown apart from the case of ruthenocene, where the $1-2-2$ splitting pattern starts being visible.

In order to compare our results with other methods for the inclusion of anharmonicities, we compute the partition function using the equation proposed by Mc Clurg and all [127]

$$Q(T) = Q_c(T)\frac{Q_q^h(T)}{Q_c^h(T)}e^{(\hbar\omega)^2/kT(2\hbar\omega+16V_0)} \tag{173}$$

Table 4: First 15 eigenvalues in the Variational Approach(cm^{-1}).

	METALLOCENES		
	Ferrocene	Ruthenocene	Osmocene
0	22.579	19.864	23.982
1	24.615	21.005	25.523
2	24.615	21.006	25.525
3	24.616	21.007	25.525
4	24.616	21.008	25.525
5	67.229	59.540	72.252
6	70.258	61.795	75.339
7	70.260	61.796	75.343
8	70.266	61.811	75.343
9	70.267	61.812	75.343
10	110.087	97.944	119.498
11	113.400	100.637	123.168
12	113.401	100.639	123.174
13	113.402	100.666	123.174
14	113.403	100.668	123.174

where V_0 is the half height of the potential maximum and $Q_c(T)$ is the classical hindered rotor partition function

$$Q_c(T) = \left(\frac{2\pi IkT}{\hbar^2}\right)^{1/2} \int_0^{2\pi} e^{-\beta V(\phi)} d\phi \tag{174}$$

Q_c^h and Q_q^h are the classical and quantum mechanical partition function of the harmonic oscillator, respectively

$$Q_c^h = \frac{kT}{\hbar\omega} \tag{175}$$

$$Q_q^h = \sum_{n=0}^{\infty} e^{-((n+1/2)\hbar\omega/kT} \tag{176}$$

In the following figures, we refer to the partition functions obtained by this equation as the 'Mc Clurg' results.

The potential maximum of ferrocene (Table 3) is equivalent to a temperature of about 420K. On the other hand, the derivative of the partition function does not show a significant change around that value, starting to decrease after 500K. The energy gap between the quasidegenerate quintets slowly decreases from 40 to 20 $cm^{-}1$, while

Figure 10: Ferrocene partition functions: the continuous line refers to the time dependent Chebyshev expansion and the dotted line refers to the variational results, while the dashed and dash-dotted are the harmonic and the corrected one.

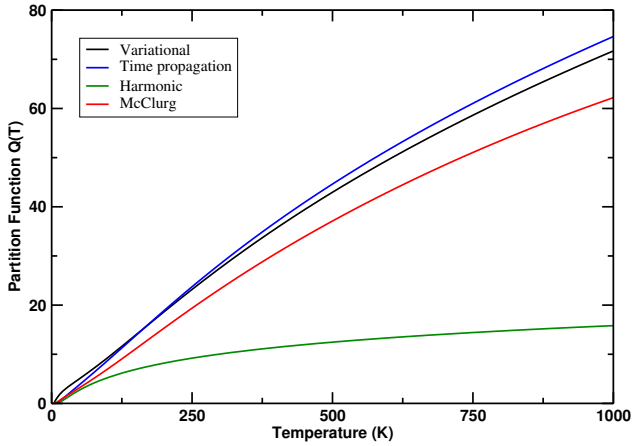

the E_1, E_2 doublets are separated from each other at the beginning of the free rotor region (around 300cm^{-}1), by a difference of 10 cm^{-}1. For this reason ' the derivative of the partition function starts to decrease significantly when the spectrum becomes similar to the free rotor one.

Figure 11: Ruthenocene partition functions: the continuous line refers to the time dependent Chebyshev expansion and the dotted line refers to the variational results, while the dashed and dash-dotted are the harmonic and the corrected one.

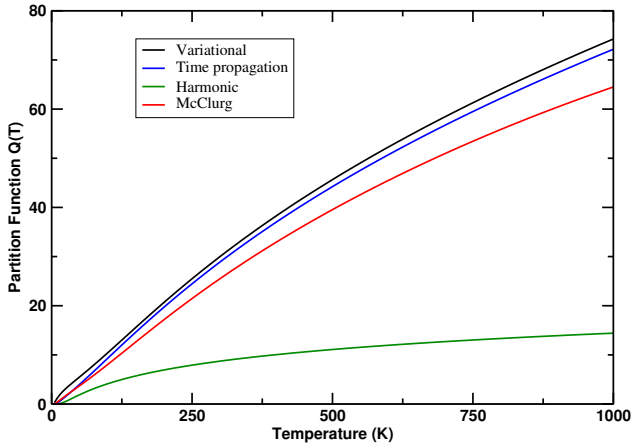

Ruthenocene (Fig. 11) shows a transition to the free rotor limit at an equivalent temperature of 352 K, which makes it an interesting molecule because it exhibits this transition at a temperature near the ambient one. As can be seen, this molecule has the highest partition function (see also Table 4), even though at high temperatures this difference becomes less significant.

Figure 12: Osmocene partition functions: the continuous line refers to the time dependent Chebyshev expansion and the dotted line refers to the variational results, while the dashed and dash-dotted are the harmonic and the corrected one.

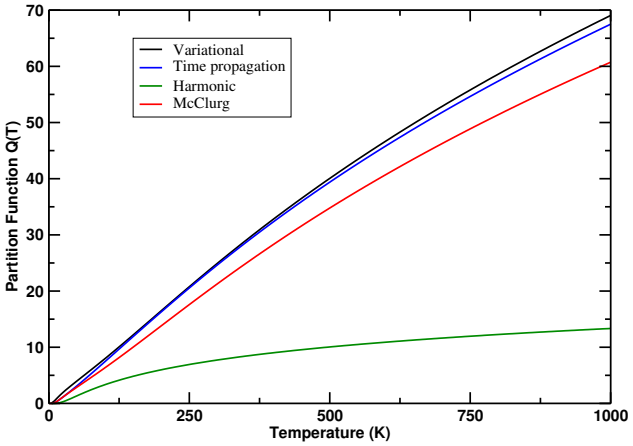

Osmocene, which has the highest potential variation, has the lowest partition function. This trend should be confirmed by further investigations on the field of organometallic molecules.

At the end of this Section about the calculation of MPF for floppy molecules, which implies the knowledge of the HRPF, we can conclude that the two hindered rotor schemes turn out to be complementary in their range of applicability.

- The time propagation scheme performs nicely in the case of large, classical-like molecules where, on the one hand, the quantum phase space is efficiently sampled by a MC scheme and, on the other hand, the calculation (and subsequent fitting) of a large number of discrete levels would be cumbersome.
- The GC scheme does well for smaller, quantum-like molecules where only a small number of discrete levels needs to be taken into account and MC sampling tends to perform poorly at low temperatures.

The main drawback of the time dependent approach, as is common with all MC approaches, where random sampling of a large population is involved, is the absence of a unique way to estimate the error when the exact solution is not available. However, we expect that its advantages far outweigh the disadvantages in the treatment of the partition functions and thermodynamics of large systems.

5

RATE CONSTANTS OF UNIMOLECULAR REACTIONS

As an example of a gas phase unimolecular reaction, we focus on the isomerization of C-cyanomethanimine between the Z and E isomers as in Fig. 13, due to the interest of these compounds as presumed intermediates in reactions involving purines and proteins [128] and in prebiotic chemistry [129].

These molecules have been detected in molecular clouds, a part of the Interstellar Medium (ISM) where the conditions of density, radiations and temperature are compatible with the formation of such kind of organic molecules. Most of the computations were performed with

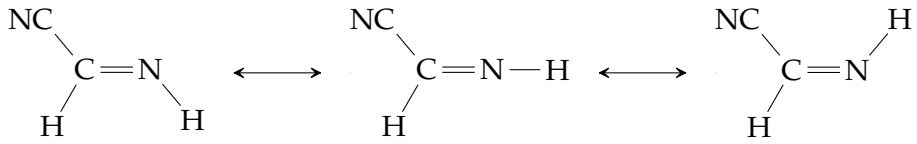

Figure 13: Form left to right: the E isomer, the transition state and the Z isomer

the B3LYP hybrid density functional, in conjunction with the SNSD basis set [130]. Additional computations were performed with the double-hybrid B2PLYP functional and with the second-order Møller-Plesset perturbative many body treatment (MP2), in conjunction with the m-aug-cc-pVTZ basis set, where d functions on hydrogen atoms have been removed. Semiempirical dispersion contributions were also included into DFT computations by means of the D3 model of Grimme [131], leading to B3LYP-D3 and B2PLYP-D3 models.

On these quantum chemistry calculations, performed with a development version of Gaussian09 [22], a full kinetic investigation has been undertaken in order to compute the rate constant using the RRKM theory presented in Section 2.2. Due to the absence of low frequency modes (i.e. LAM), the GC approach has not been used in this study.

We have computed the total density of states $\rho(E)$ of both isomers, as well as the transition state connecting them, by convolution of the 3D classical rotational DOS

$$\rho_{rot,3D} = \frac{2}{\sigma}\sqrt{\frac{E}{ABC}} \tag{177}$$

where σ is the rotational symmetry number and ABC is the product of the three rotational constants, while the anharmonic vibrational DOS is obtained by the WL algorithm.

The enthalpy and entropy of the Z and E isomers are calculated as functions of temperature and plotted as the unitless quantities H/k_BT in Fig. 14 and S/k_B in Fig. 15, using Eq. 79 and Eq. 80, respectively. In order to assess the effects of anharmonicity, these quantities are

Figure 14: Variation of the unitless quantity H/k_BT: the black line is the anharmonic WL result, while the red line is the harmonic calculation.

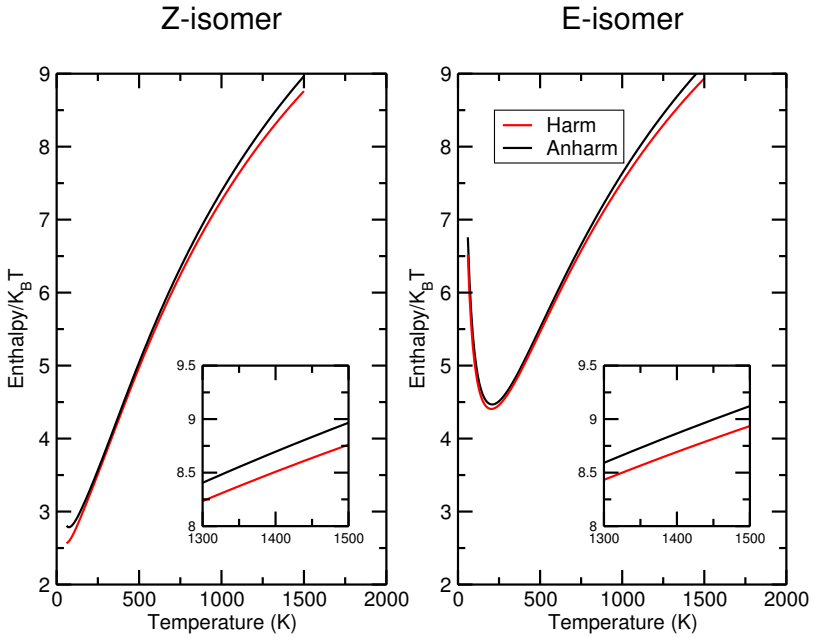

compared with the ones obtained using the harmonic vibrational density of states evaluated by the Stein-Rabinovitch modification of the Beyer- Swinehart algorithm [69].

It must be stressed that, even though the Wang-Landau algorithm is valid for any energy interval, the quadratic approximation for vibrational energy levels issuing from the VPT2 model loses reliability at high energies (corresponding to high temperatures) when the various dissociation limits of the vibrational modes are reached since, beyond the quadratic extremum, the energy tends to (unphysically) diminish with the quantum number.

Consequently, as a reasonable compromise between reliability of the quadratic energy level formula and temperature range of the data reported, we have chosen a temperature of 1500 K as our upper limit.

The chosen direction of the reaction is $Z \rightarrow E$, while the most stable isomer is always Z at every level of theory used in our investigation. In Table 5, we report the ZPE corrected energy difference, ΔE between Z, E and TS and ΔG, where the zero is fixed at the reactant value.

Figure 15: Variation of the unitless quantity S/k_B: as in Fig 14 for entropy.

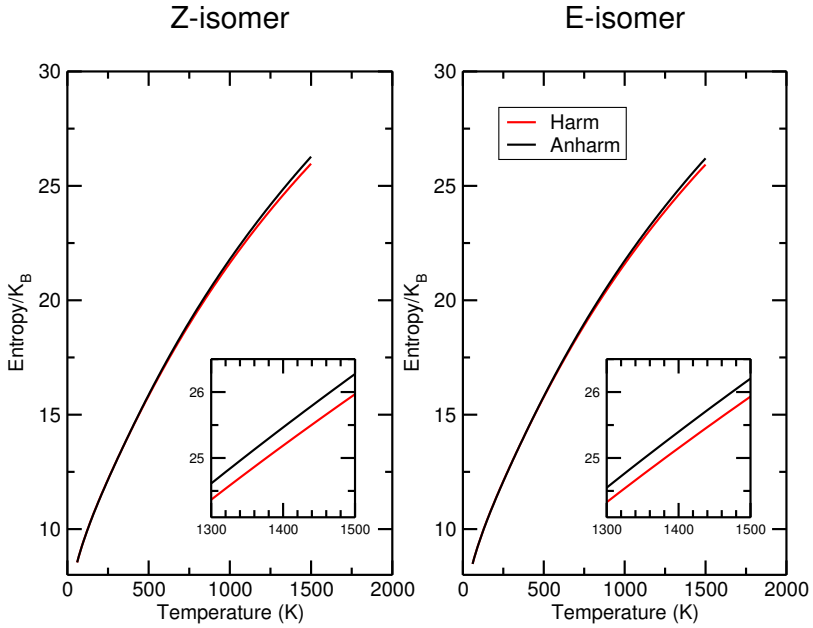

Table 5: Energy difference and Gibbs free energy difference in kJ/mol

	ΔE (kJ/mol)	ΔG (kJ/mol)
Z	0.0	0.0
TS	106.27	101.88
E	2.30	2.47

The trends of the two thermodynamic functions with temperature are very similar. The next step to understand how the introduction of anharmonicity affects the reaction is to evaluate the reaction enthalpy ΔH and entropy ΔS as a function of the temperature, as shown in Fig. 16 and Fig. 17. The reaction enthalpy is always positive. The main factor responsible for this is the higher zero-point energy of the E isomer. On the other hand, the entropy change in Fig. 17 is negative for the same reason, since fewer states are available to the E isomer. In the harmonic case, the enthalpy increases steadily and almost linearly with temperature, indicating an almost constant difference in heat capacities. This changes at very low temperatures, where the relative sparsity of E states diminishes its heat capacity and ultimately reverses the trend. Inclusion of anharmonicity has the effect of rendering the entropy change more negative, indicating that it increases the Z density of states more than the E one.

Figure 16: Reaction enthalpy $\Delta H/k_B T$: the black line is the anharmonic WL result, while the red line is the harmonic calculation.

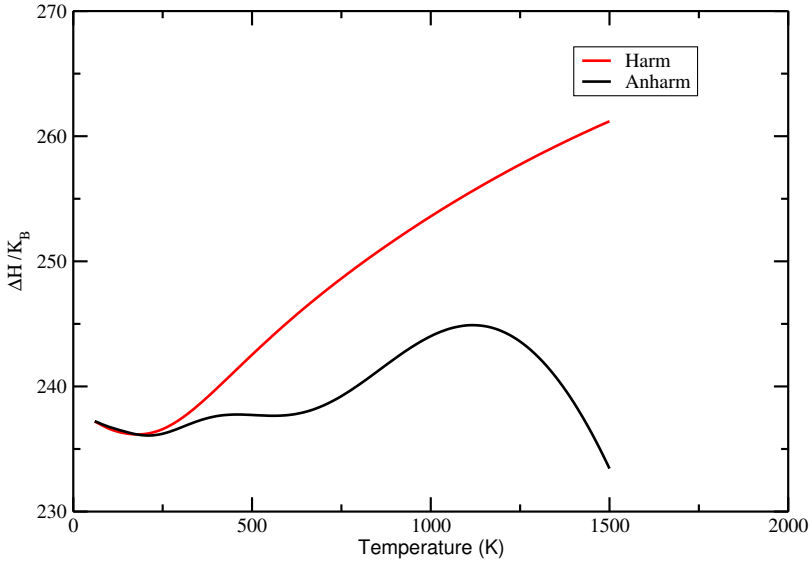

Figure 17: Reaction entropy $\Delta S/k_B$: the black line is the anharmonic WL result, while the red line is the harmonic calculation.

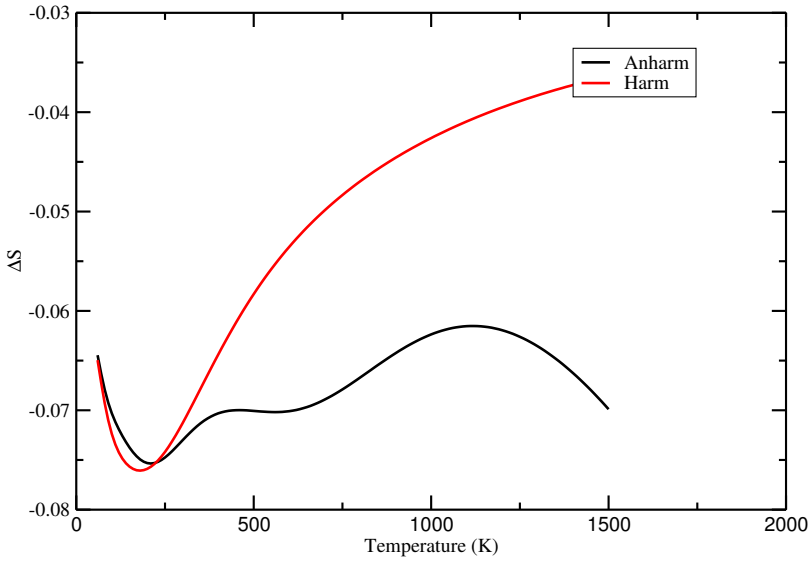

The effect of introducing anharmonicity in the DOS can be better evidenced in terms of the so-called anharmonic factor, defined as the ratio of the corresponding densities of states

$$F(E) = \frac{\rho_{anh}(E)}{\rho_{har}(E)} \tag{178}$$

As shown in Figure 18, the anharmonic factor varies almost linearly with the energy. A similar trend was found by Troe et al. [132], who

Figure 18: Energy dependence of the anharmonic factor $F(E)$

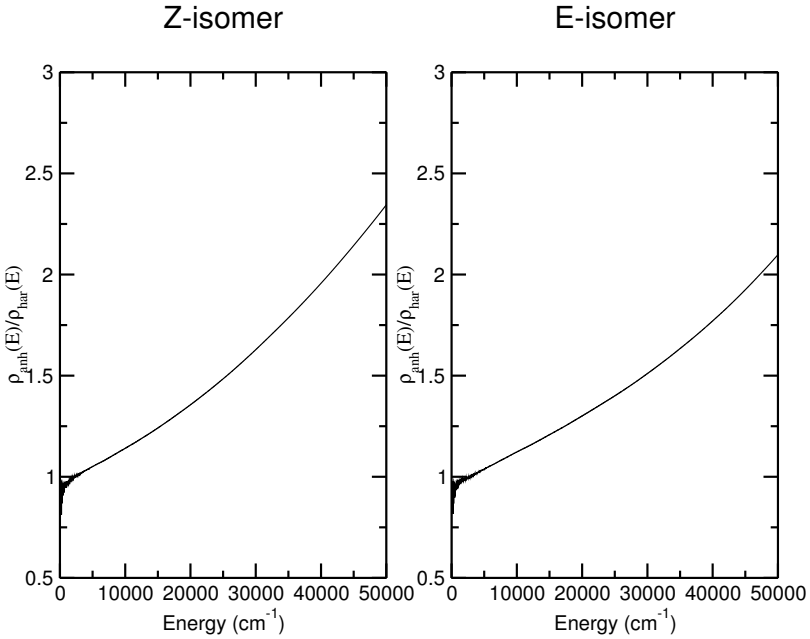

compared harmonic and anharmonic DOS for various small molecules. The high-frequency deviation in the low-energy region is related to the statistical sampling of the WL algorithm.

It can be seen that the slope in the case of the Z-isomer is higher, indicating that anharmonicity increases the DOS more for the Z isomer than for its E counterpart. This trend is in agreement with the enthalpy and entropy curves shown above.

Fig. 19 shows the natural logarithm of the equilibrium constant for the $Z \rightarrow E$ isomerization, written as usual

$$K(T) = \frac{k(T)}{k_{-1}(T)} \tag{179}$$

where $k(T)$ and $k_{-1}(T)$ are the thermal rate constants of the direct and inverse reaction, calculated as in Eq. 5 At all temperatures considered, the equilibrium constant is less than one, and this effect is more pronounced at low temperatures where the enthalpy term dominates. As the temperature increases, the difference in zero point energies becomes increasingly less important, and the equilibrium constant approaches unity. Introducing anharmonicity lowers slightly the

Figure 19: Logarithm of the thermal equilibrium constant K(T)
Thermal Isomerization Z → E

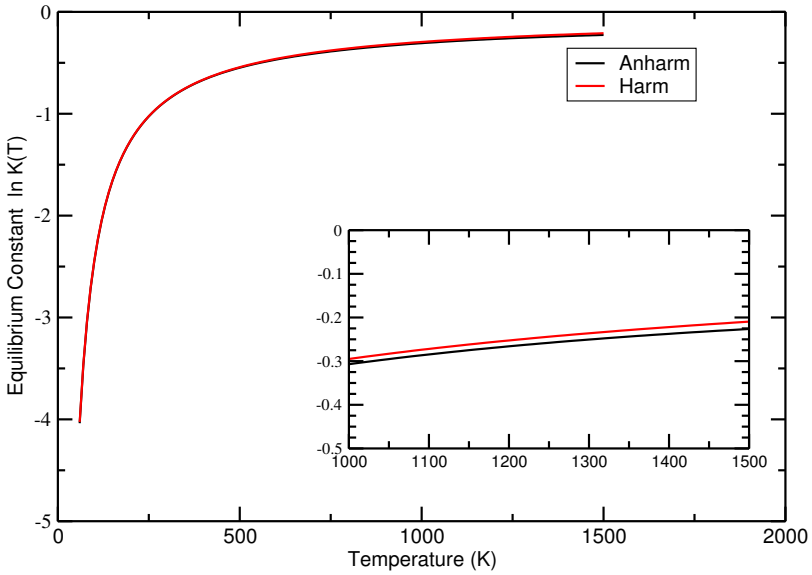

equilibrium constant. This appears principally to be an entropy effect since, as shown before, the entropy of the Z isomer is substantially larger than that of E, while the enthalpy contributions are very similar. Fig. 20 shows the microcanonical and canonical rate constants for the direct reaction. It can be seen that the anharmonic rates are lower than the harmonic ones at all energies and temperatures considered. It has already been shown how anharmonicity lowers the Gibbs free energy of the reactants. This effect more than compensates for the corresponding effect on the transition state, thus reducing the rate constant. From the Arrhenius plot, it is seen that the slope of the curve is essentially the same both in the harmonic and anharmonic case. Thus, the activation energy remains invariant on introduction of anharmonicity, which seems primarily to decrease the pre-exponential factor. The activation energy calculated from the slope of the Arrhenius plot is 100.0 kj/mol, which is in nice agreement with the potential barrier of the system (106.27 kj/mol).

Figure 20: In the left graph, the microcanonical rate constant $k(E)$ is plotted against the energy, expressed in cm^{-1}; in the right, the Arrhenius plot of the thermal rate constant of the direct reaction.

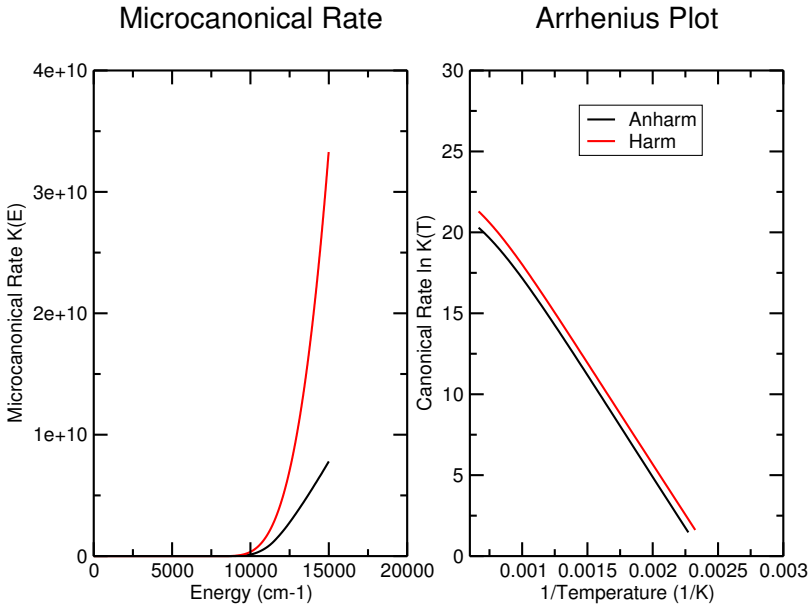

6

MASTER EQUATION APPROACH FOR COMPLEX REACTIONS IN GAS PHASE

As discussed in Section 2.2, in gas phase reactions quantum effects play a crucial role at low temperatures, when only a small range of energies are important to describe the thermal rate constant. An accurate treatment of tunneling can enhance the microcanonical rate constant at low energy (see Eq. 52) and allows classically forbidden states to contribute to the reaction.

As in Chapter 5, the molecular clouds in the ISM is the environment where the condition of low temperature and low density should make quantum effects in molecular reactions important.

Formamide, the simplest amide, has attracted increasing attention in the field of prebiotic chemistry [133, 134], has been chosen as a study case, since it has the ability to act as a precursor in the abiotic amino acid synthesis and perhaps also in that of nucleic acid bases [135].

Formamide is, therefore, a central compound to connect metabolism (conversion of energy), which is ruled by proteins, and genetics (passage of information), ruled by RNA and DNA.

The question that leads our investigation is: how was formamide formed in space?

Several reaction mechanisms have already been investigated for formamide in the gas phase:

- ion-molecules reactions [136];
- radical-molecule reactions with the assistance of ice grains as a third body [137].

The former reactions were discarded as a source of formamide in the ISM by the authors themselves, while the latter has been experimentally proved to be possible.

However, this second network of reactions needs the presence of ice grains, which has the role of hosting the reactants on its surface, and supplementary energy, necessary for the reaction. This external energy is provided by the inelastic scattering of protons of the Galactic cosmic-ray field.

Since three-body collisions are quite unusual in the low density environment of the ISM, we want to study the reaction probability of radical-molecule path for the formation of formamide in a two body collision, focusing on the tunneling effects at the TS.

Therefore, to resolve this issue, we have undertaken a comprehensive quantum mechanical investigation, focusing on the addition of

the ·OH radical to methanimine, as suggested in a study by Ali and Barker [138] and showed in Fig 21. When looking carefully at the

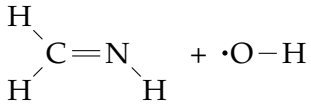

Figure 21: Addition of ·OH radical to methanimine

system, one can envisage an additional plausible path involving the addition of the $\cdot NH_2$ radical to formaldehyde in Fig 22, already sug-

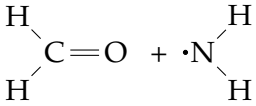

Figure 22: Addition of the $\cdot NH_2$ radical to formaldehyde

gested in a study by Kahane and coworkers [139].

In these two cases, the initial association is barrierless and capture theory has been implemented to calculate the rate: the first step is to calculate, as in GC approach for LAM, a monodimensional PES for the approach of the two fragments, fitted to a long range potential [140] functional form

$$V(r) = -\frac{C_6}{r^6} \tag{180}$$

Adding the centrifugal contribution due to angular momentum, we obtain the effective potential

$$V_{eff}(r) = -\frac{C_6}{r^6} + \frac{J(J+1)}{2mr^2} \tag{181}$$

The rate constant of the radical addition is

$$k_{capt}(E) = \sqrt{\frac{2E}{\mu}}\sigma(E) \tag{182}$$

where μ is the reduced mass of the molecular system and $\sigma(E)$ is the capture cross section

$$\sigma(E) = \frac{3\pi}{2^{2/3}}\sqrt[3]{\frac{C_6}{E}} \tag{183}$$

Due to the conservation of the total angular momentum J, we also obtain the maximum $J_{max}(E)$, used later in the RRKM calculation of the following reaction step. It must be stressed that the distribution of the reactive energy E, the translational energy of the two fragments, is assumed to be in Boltzmann distribution at the temperature of the ISM ($> 10K$). The back-dissociation rate is calculated using the detailed balance principle, as in Eq. 83.

On the other hand, when a well-defined transition state existed, we have performed a RRKM calculation as presented in Section 2.2, semiclassically corrected to introduce the tunneling contributions.

Computations were mainly performed with the double-hybrid B2PLYP functional in conjunction with the m-aug-cc-pVTZ basis set, where d functions on hydrogens have been removed. Semiempirical dispersion contributions were also included into DFT computations by means of the D3BJ model of Grimme, thus leading to the so-called B2PLYP-D3 computational model.

For all stationary points, intermediates and TSs, improved electronic energies were obtained by means of a composite approach based on Coupled Cluster theory employing the single and double excitations approximation (CCSD) augmented by a perturbative treatment of triple excitations, CCSD(T) [141], and implemented in CFOUR [142]. Here we briefly summarize the components of our composite strategy in electronic calculations:

- the first level is the Hartree-Fock self-consistent-field (HF-SCF) energy extrapolated to the complete basis-set (CBS) limit;
- the valence correlation energy at the CCSD(T) level extrapolated to the CBS limit and the core-valence correlation correction (CV);
- for some TSs, a full treatment of triple (fT) and quadruple excitations (fQ) was also added.

We label the electronic energies obtained by the composite method by simply adding the relative acronyms: thus, the most accurate results are defined as (CBS+CV+fT+fQ).

For more details about quantum chemistry calculation, the interested readers will find an accurate dissertation in Ref. [140].

6.1 METHANIMINE AND ·OH ADDITION

In Fig. 23, one can see plausible paths concerning the approach of ·OH to methanimine. Starting from the separated reactants, a complex stabilized by the formation of a hydrogen bond (RI0), more stable by 30.4 kJ/mol than the reactants, is formed. If we add zero-point corrections, this complex is found to be more stable than the precursors by 22.2 kJ/mol. Fig. 24 depicts the possible full paths of the CH_2NH + ·OH reaction and reports the relative electronic (at the CCSD(T)/CBS+CV level) and zero-point corrected energies (electronic CCSD(T)/CBS+CV energies + ZPE issuing from B2PLYP-D3/m-aug-cc-pVTZ anharmonic vibrational calculations) of all minima and TSs. If we focus on the possible products, formamide + H is the most stable one, with a relative energy of -89.5 kJ/mol. The following ones are E-methanimidic acid + H and formaldehyde + NH2,

Figure 23: Proposed path for the approach of ·OH and methanimine. Relative electronic CCSD(T)/CBS+CV energies in black. Energies in kJ/mol

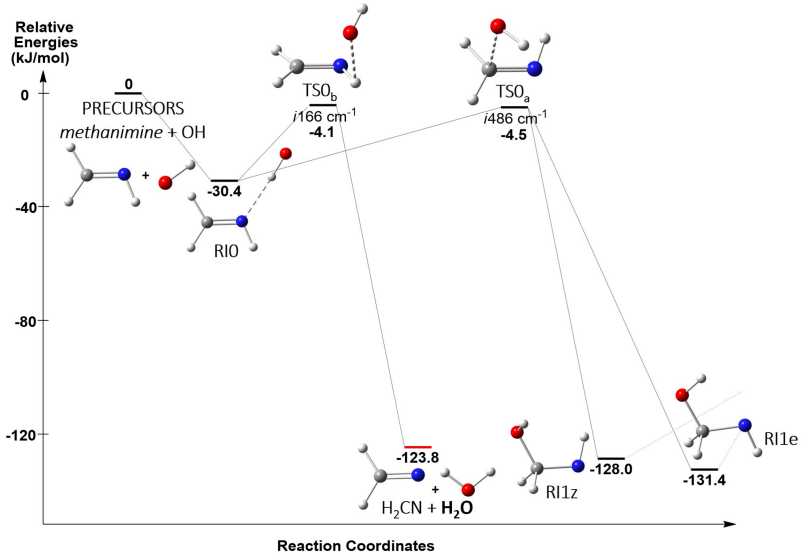

at -44.8 and -43.5 kJ/mol respectively, and then the less stable product is Z-methanimidic acid + H that exhibits a relative energy of -30.1 kJ/mol.

It is noteworthy that all compounds involved in the reaction scheme of Figure 24 are lower in energy than the reactants, which makes the entire path viable in the ISM.

Together with the channels shown in Fig. 24, we investigated also addition of OH to the N atom of methanimine, together with other possible abstractions of hydrogen atoms (linked to the C atom). However the energies of the transition states governing the first steps were so high (of the order of 15 kJ/mol) that we decided to consider those channels closed.

6.2 FORMALDEHYDE AND ·NH_2 ADDITION

Starting from the reactants either a weak van der Waals complex (RIob-vW) or an intermediate stabilized by a hydrogen bond (RIob-Hbond) can be formed, as shown in Fig. 25.

Both of them are followed by a low lying, first order saddle point (TS5) having an energy very close to that of the reactants, which then leads to an intermediate (RI3).

Once again, one can notice that this first step, leading to RI3, is nearly barrier-less, our best estimate for the transition state height with respect to reactants being 3.8 kJ/mol. Inclusion of the full-T (CBS+CV+fT) and full-Q (CBS+CV+fT+fQ) corrections further lowers this barrier to 2.05 and 1.67 kJ/mol, respectively.

Figure 24: Proposed full reaction path of ·OH and methanimine addition. Electronic energies (black) are at the CCSD(T)/CBS+CV level and the ZPE corrected energies (green) are obtained by including the ZPE issuing from B2PLYP-D3/m-aug-cc-pVTZ anharmonic vibrations

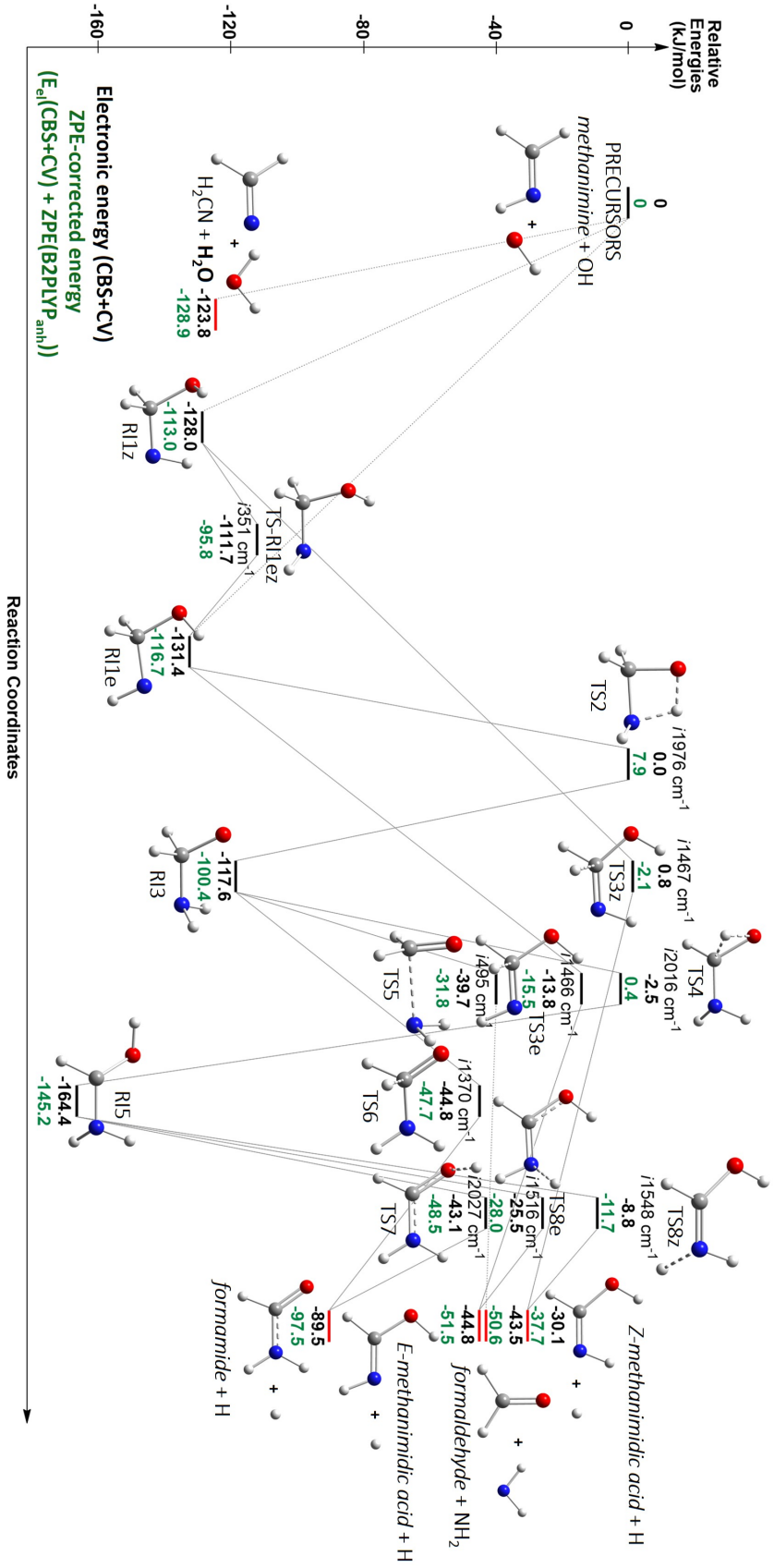

Figure 25: Proposed path for the approach of $\cdot NH_2$ and formamide. Relative electronic CCSD(T)/CBS+CV energies in black. Energies in kJ/mol

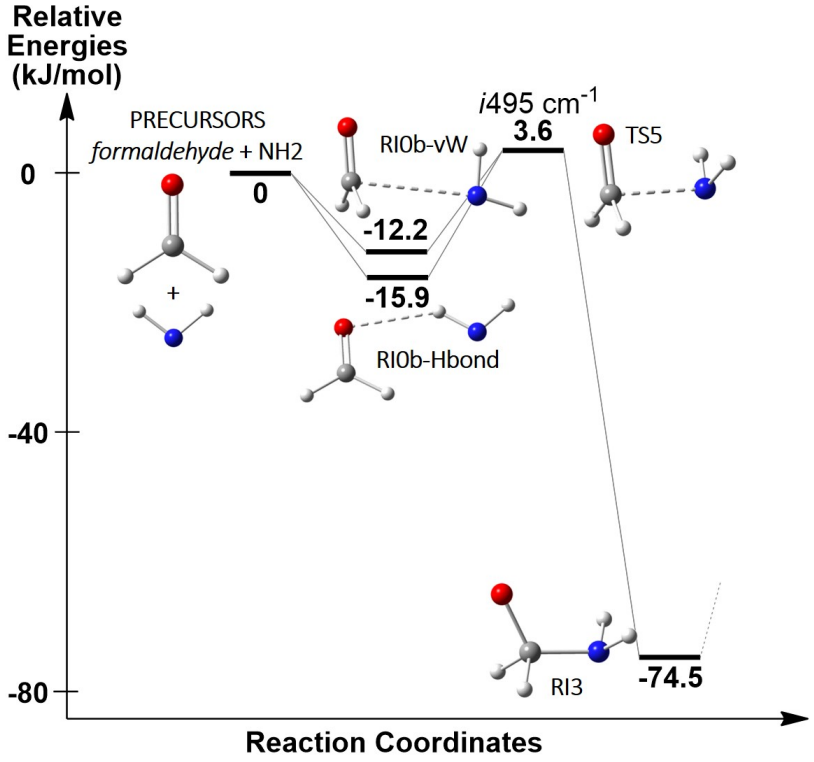

Therefore, capture theory seems appropriate to describe this step. Fig. 26 displays the possible path of the $CH_2O + \cdot NH_2 \rightarrow NH_2CHO + H$ formation reaction (skipping again details about the approach step) and the relative electronic (CCSD(T)/CSB+CV) and zero-point corrected energies (ZPE at the B2PLYP-D3/m-aug-cc- pVTZ level) of all minima and transition states. In the case of the intermediate RI3, the hindered NH2 rotation needs to be carefully managed, using the GC method presented in Chapter 2.

The overall zero point energy (ZPE) is then obtained by summing ZPE_{GVPT2} [50] of the other modes with the ZPE_{HR}, i.e. the first eigenvalue of the HR spectra. This strategy comes naturally considering Eq. 73. After the formation of the intermediate RI3, hydrogen loss can be observed, leading to formamide and the $\cdot H$ radical through the transition state TS6 that has a barrier of 73.2 kJ/mol. The rotation around the C-N bond in RI3 can lead to another energy minimum, which forms again formamide through the same transition state TS6. The products were found 46 kJ/mol more stable than the reactants.

Let us now have a deeper insight into the hindered rotation occurring in the intermediate RI3 that we mentioned above. Fig. 27 shows the potential energy profile along the ϕ dihedral angle, which describes the NH2 hindered rotation

Figure 26: Proposed reaction path for formamide formation. Electronic energies (black) are at the CCSD(T)/CBS+CV level and the ZPE corrected energies (green) are obtained by including the ZPE issuing from B2PLYP-D3/m-aug-cc-pVTZ anharmonic vibrational calculations. All energies are given in kJ/mol.

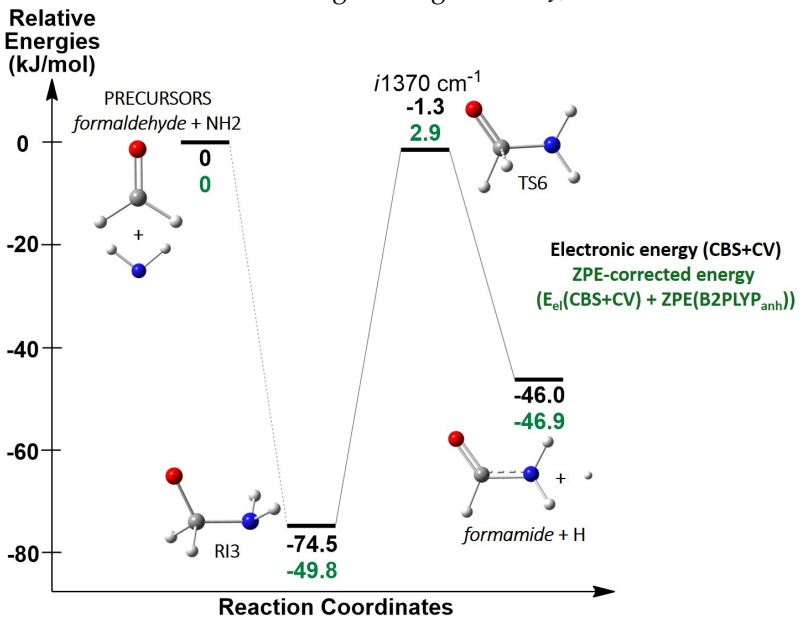

Figure 27: Potential energy profile along the ϕ dihedral angle (NH_2 rotation) for the intermediate RI3 obtained at the B2PLYP-D3/maug-cc-pVTZ level.

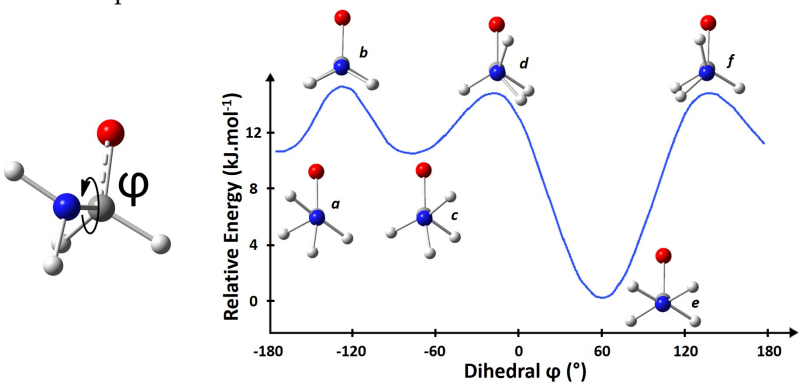

In addition to the absolute energy minimum, the potential energy surface shows two additional equivalent local minima. All these minima correspond to staggered conformations and are connected by three transition states, corresponding to eclipsed conformations. The equivalent conformers *a and c are separated by b, which is the highest transition state, with a barrier of ca. 3.8 kJ/mol. The most stable conformer (e) is found to be about 10.5 kJ/mol more stable than the other minima. The d and f equivalent transition states rule the c to e and e to a transformations and have a relative energy about 14.6 kJ/mol higher than the most stable conformer e.*

6.3 KINETICS CALCULATION

The master equation approach needed for the calculation of rate constant of formation ofthe products has been performed by direct solution of the Eq. 84, without symmetrization. In both additions, the rate of back dissociation of the initial complex (using the principle of detailed balance) at a particular energy is proportional to the DOS per unit volume of the reactants.

As the translational component of reactants DOS (Eq. 168) is proportional to the square root of the translational energy, at low energies the back dissociation of the initial complex is suppressed due to the reactant density of states tending to zero.

In the methanimine and ·OH addition mechanism, at low energies the initial van der Waals complex RIo in Fig. 23 is present with the chance to either rearrange to HOCH2NH (with subsequent possible formation of methanimidic acid) or eliminate a water molecule forming the H_2CN radical, passing through TSo_a and TSo_b respectively.

The other two possible products (formamide+H or formaldehyde+NH_2) have negligible rates due to the fact that more than one step is required to reach them from the original complex and that one of these steps consists in overpassing the high energy TS2.

Both transition states corresponding to these channels lie $\approx$ 4.5 kJ/mol below the reactant zero point energy. However, the TS leading to water elimination presents a higher SOS than the second one at low energies, leading to a low-energy dominance of H_2O elimination.

This can be seen in Figs. 28 and 29 as a constant ratio of around 8 between the rate constants of water elimination and methanimidic acid formation. It is to be noted that Z-methanimidic acid has a much lower rate of formation than its E-isomer. This is essentially due to the fact that the corresponding transition state is rather lower in energy. Moreover, as the two isomers of HOCH2NH (which dissociate to the corresponding isomers of methanimidic acid) equilibrate rapidly between themselves and the E-isomer is more stable, this is another factor contributing to this effect.

As the energy increases, the reactant density of states increases rapidly and this brings about a rapid increase in the rate of redissociation of the complex. Indeed, the two next highest rate constants diminish with increasing energy

Figure 28: Microcanonical rate constant as a function of energy in kJ/mol.

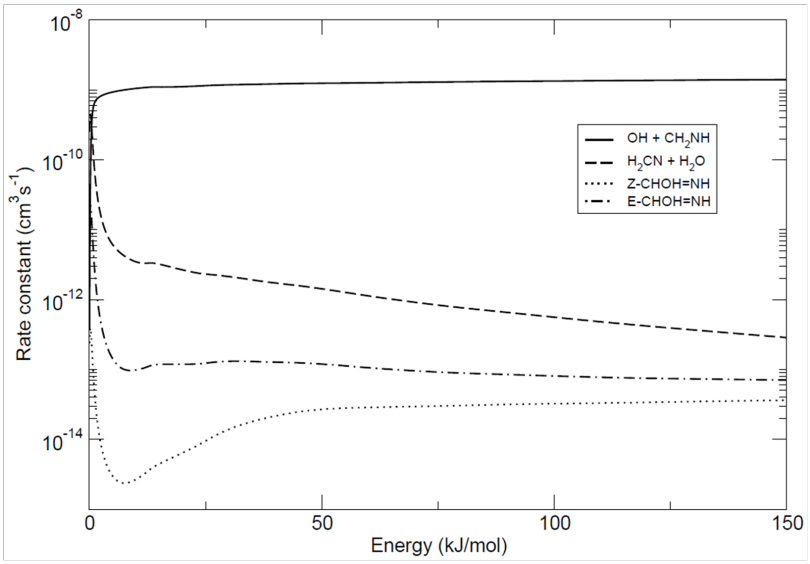

Figure 29: Thermal rate constant as a function of temperature.

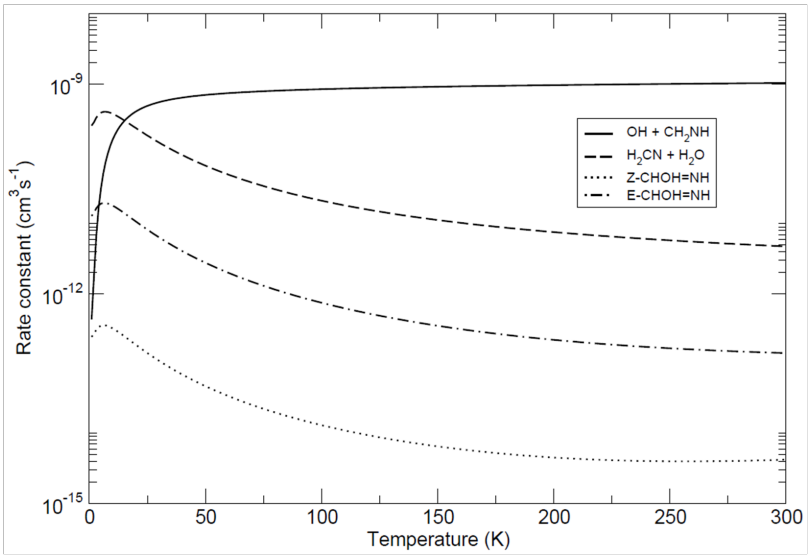

because of this effect (on the other hand, the rate constant of Z-methanimidic acid continues to increase slightly). The same effects are also seen in the canonical rate constants, albeit smeared out due to Boltzmann averaging. Despite the predominance of redissociation, H_2CN and E-methanimidic acid formation remain important processes up to 300K (with rate constants above 10^{-11} cm^3s^{-1}).

On the other hand, the formamide and $\cdot NH_2$ addition has no such high energy TS: in a previous paper [143], a similar RRKM study was performed on the $\cdot NH_2$+H_2CO reaction, based on calculations at the CBS-QB3 level of theory. This enabled us to assure that, even at low temperatures, the formation of formamide through this reaction was largely predominant over the back-dissociation.

In Fig. 30, we show the thermal rate constant calculated by RRKM calculations at different level of quantum electronic calculation, CBS-QB3, CCSD(T)/CBS+CV and CCSD(T)/CBS+CV+fT+fQ. The rate constant drops

Figure 30: Rate constants for the formation of formamide starting from the addition of $\cdot NH_2$ and formaldehyde reaction using the CBS-QB3, CCSD(T)/CBS+CV and CCSD(T)/CBS+CV+fT+fQ energies.

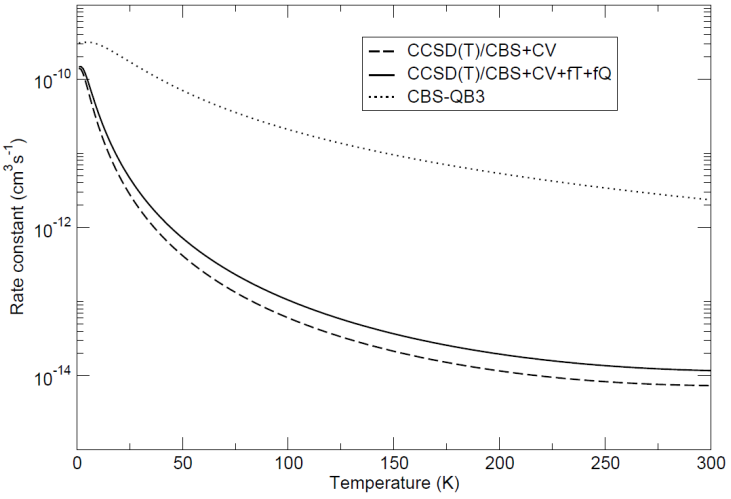

from 3.1×10^{-10} to 7.6×10^{-11} cm^3s^{-1} at 5 K, which is explained by a higher barrier for the transformation of RI3 into formamide + H (represented by TS6), but the formamide formation still predominates at low temperatures since the rate constant of back-dissociation is too law.

Moreover, when including the full-T (CBS+CV+fT) and full-Q (CBS+CV+fT+fQ) corrections, the TS6 relative energy that was found at -1.3 kJ/mol drops to -2.3 and -2.8 kJ/mol respectively, which leads to slightly higher rate constants (9.9×10^{-11} cm^3s^{-1} at 5 K with CCSD(T)/CBS+CV+fT+fQ energies).

With these calculations, we have provided new insights concerning the formation of formamide in the molecular clouds of the ISM. Our computations allowed us to suggest two reaction paths combined to probable mechanisms

concerning this formation. In both cases, $\cdot OH+CH_2NH$ and $\cdot NH_2+H_2CO$, the addition step does not involve significant barriers and can therefore occur in space. While RRKM calculations confirmed the effectiveness of the $\cdot NH_2+H_2CO$ reaction (since, once this first addition has been done, formamide formation largely predominates over back-dissociation at low energies), the $\cdot OH+CH_2NH$ reaction leads preferentially to other products of prebiotic interest such as methanimidic acid and the H_2CN radical. Together with the specific interest of the studied system, the reliability, robustness, and reasonable computational cost of the proposed computational strategy paves the route toward the study of larger systems of interest for astrochemistry and astrobiology.

This computational strategy can be also applied without any restrictions to the calculation of gas phase thermal rate constants in every field of scientific and industrial research for molecule with up to 20-30 atoms. For even larger molecular systems, hybrid schemes can be implemented, where harmonic and anharmonic schemes are both used.

Part III

APPENDIX

****

A

POTENTIAL ENERGY SURFACE

By (single) Potential Energy Surface (PES) the community of physical chemists means the eigenvalue $\epsilon_1(\mathbf{R})$ of the electronic Hamiltonian in Eq. 12, that we rewrite here

$$\hat{H}_{el} = -\frac{1}{2}\sum_{i=1}^{N_i}\nabla_i^2 + \sum_{a>b}\frac{Z_a Z_b}{|\mathbf{R}_a - \mathbf{R}_b|} + \sum_{i>j}\frac{1}{|\mathbf{r}_i - \mathbf{r}_j|} - \sum_{a,i}\frac{Z_a}{|\mathbf{R}_a - \mathbf{r}_i|} \quad (184)$$

Varying at will the geometry of a molecule $\mathbf{R}$, under the hypothesis that the Born-Oppenheimer approximation is always correct, we can obtain a surface (the PES) of $N_{PES} = 3N_{atom} - 6$ dimensions. On this surface, the atoms move defining trajectories: all the information about the system, its dynamical evolution is described by these curves.

This task is extraordinarily demanding both for its computational cost and for the human labour involved, mainly for three reasons:

- *Using a uniform grid of N points for each DOF (the number of DOFs is supposed equal to M) leads to a number of quantum chemistry calculation points of N^M, that becomes unfeasible for most molecules with more than 4 or 5 atoms. Non-uniform, symmetry adapted grids can also be implemented, but the number of points versus the number of atoms still scale unfavourably;*
- *The level of theory of each calculation may vary, due to convergence problems or inconsistency between different calculations;*
- *Fitting procedures to obtain smooth functional forms of the PES can create further error and are not obvious for multidimensional surfaces.*

Many algorithms [144] have been proposed to overcome these drawbacks, but the computational costs and the memory requirement remain the main reasons why full PES of medium size molecules are not available. Moreover, it is easy to note that many regions of the PES are not explored during the evolution, because the electronic potential is too high even if tunnelling effects play a crucial role in dynamics [145].

However, since no formulae are available for the accurate evaluation of multidimensional tunnelling effects, we have not any simple criteria to exclude some regions of the PES in particular with a priori *considerations.*

The most convenient strategy to decrease the total number of quantum chemistry calculations for the estimation of the thermal rate constant is the TST, which implies the existence of a Reactive Mode where the reaction takes place.

The motion along the Reactive Mode changes at infinity the molecular identity of the ensemble of atoms that we are studying and it is impossible, as far as we know, to introduce a model potential which can be both accurate and general, like inverse harmonic or Eckart barrier[45].

The reactive motion, as well some other types of low frequency motions (see Section 2.5), can be better described as a LAM: in Appendix B, we present the derivation of Eq. 56.

B

INTRODUCTION OF CURVES IN $\mathbb{R}^N$

We are interested in finding a path (also called curve), $\zeta(t)$, that connects some stationary points on the PES, i.e.

$$\frac{\partial V}{\partial x_i} = 0 \qquad \forall i \in [1, 2, \ldots 3N] \tag{185}$$

which can be reactants, products, intermediates or Transition States. Here, x_i are the Cartesian nuclear coordinates. The Newton classical law of motion is

$$\frac{d}{dt}(m_a \dot{x}_i) = -\frac{\partial V}{\partial x_i} \qquad \forall i \in \mathbb{R}^{3N} \tag{186}$$

and we start our treatment of LAMs assuming that the path they follow can be described by Eq. 186 [60].

We introduce the concept of intrinsic motion*, i.e. a motion that takes place at an infinitesimal velocity: even if calculated in the frame of classical mechanics, we can build a quantum mechanical Hamiltonian on this curve, using, for example, the DVR representation.*

This assumption means that the trajectory, or curve, that the molecule follows in $\mathbb{R}^{3N}$ can be found by integration of Eq. 186 with the consistent boundary conditions, $\dot{x}_i = 0$.

We first note that Eq. 186 has six solutions that are identically zero, related to translations and external rotations, plus another one related to the curve itself, because we expect that the energy along the LAM varies slowly along the curve (otherwise, it should be treated as a vibration).

These properties can be summarized by three equations

$$\sum_{i=1}^{3N} \sqrt{m_a}\,\xi_i = 0 \tag{187}$$

$$\sum_{i=1}^{3N} \zeta_i(s) \times \xi_i = 0 \tag{188}$$

$$\sum_{i=1}^{3N} \zeta_i'(s) \cdot \xi_i = 0 \tag{189}$$

where m_a is the mass of the atoms, $a \in [1, N]$, $\zeta_i(s)$ is the curve and ξ_i is the displacement from the curve. The first and the second are the Eckart-Sayvetz conditions (see Eq. 37 and Eq. 38 in Section 2.3). The third, Eq. 189, represents the orthogonality between the curve and its displacement in the remaining $3N - 7$ dimensions.

Applying the Eckart-Sayvetz conditions, we can reduce our investigation to a $\mathbb{R}^{3N-6}$ *space: for a small time interval* δt*, the velocity variation* $\delta \dot{x}$ *along the IRC can be found by integration*

$$m_a \dot{x}_i = -\frac{\partial V_i}{\partial x_i} \qquad \forall i \in \mathbb{R}^{3N-6} \tag{190}$$

For the sake of compactness, we use mass weighted Cartesian coordinates in bold vectorial notation $\dot{\mathbf{X}}$ *and* $\mathbf{V}$*. Accordingly, the previous equation becomes*

$$\dot{\mathbf{X}} = -\frac{\partial \mathbf{V}}{\partial \mathbf{X}} \tag{191}$$

The infinite ensemble of solutions of Eq. 191 is called meta-IRC, while the specific solution passing through reactants, TS and products is called IRC. The IRC is a curve, a differentiable path in the 3N-6 *mass-weighted Cartesian coordinate space and can be identified as the Minimum Energy Path (MEP), the steepest descent path along the BO potential.*

Differential curves are generated by a differential map $\zeta(t)$*, a set of differentiable functions* $(\zeta_1(t), \zeta_2(t), \dots \zeta_{3N}(t))$*, where the variable* $t \in I, I = (a, b)$*.*

This definition implies a correspondence law that associates (or maps) each $t \in I$ *into a point* $\zeta(t) \in \mathbb{R}^{3N-6}$ *[146]*

$$\zeta(t) = (\zeta_1(t), \zeta_2(t), \dots, \zeta_{3N-6}(t)), \quad \zeta(t) \in \mathbb{R}^{3N-6} \tag{192}$$

The derivative (or tangent vector, or velocity vector) is defined as

$$\zeta'(t) = (\zeta_1'(t), \zeta_2'(t), \dots \zeta_{3N-6}'(t)) \tag{193}$$

If $\zeta'(t)$ *exists and it is everywhere nonzero, then the curve is called* regular*. After setting the starting point of the regular curve* ζ *at* $t = 0$ *the arc length* $s(t)$ *is defined as*

$$s(t) = \int_0^t |\zeta'(t)| dt \tag{194}$$

where

$$|\zeta'(t)| = \sqrt{\sum_{i=1}^{3N-6} (\zeta_i'(t))^2} \tag{195}$$

is the length of the tangent to $\zeta(t)$*. Note that, sometimes, it can happen that the parameter* t *is the arc length measured from some point and therefore* $ds/dt = 1$*. This is not true for HR, since the variable* $t = \phi \in I = [0, 2\pi]$*, while the curve* $s(t)$ *is moving in a general* $\mathbb{R}^{3N-6}$ *space and its length depends on the magnitude of the reduced mass of the HR.*

The key role of the parameter t *is to guide our research of the IRC but if we merely follow the definition of the LAM (an internal rotation, a bond stretching etc.) the coupling between the LAM itself and the other vibrations*

makes Eq. 189 not satisfied. This inconvenience implies that the definition of internal coordinate (as an example, Eq. 55) cannot be used to calculate the set of differentiable functions $\zeta_i(t)$ and $\zeta_i'(t)$.

Thus, in order to find a computational strategy to calculate the IRC and its arc length $s(t)$, we need to perform a relaxed scan along the LAM in order to satisfy, at least variationally, Eq. 189: in this way, we obtain a series of points in the mass weighted Cartesian coordinates $X_i \in \mathbb{R}^{3N-6}$.

Then, we need a numerical strategy to evaluate locally the arc length $s(t)$, which is related with the metric tensor $g_{i,j}$ by the following equation [147]

$$ds^2 = \sum_{i,j}^{3N-6} g_{i,j}\, dX_i dX_j \tag{196}$$

where X_k are, again, the mass weighted Cartesian coordinate. The metric tensor is written as

$$g_{i,j} = \sum_{t=1}^{3N-6} \frac{\partial \zeta_t}{\partial X_i}\frac{\partial \zeta_t}{\partial X_j} \tag{197}$$

Since the energy of the molecular system is a conservative quantity, the Hamiltonian along the curve must be invariant under any change of coordinates; Podosky [148] and later Schaad [149] show that the coordinate independent Hamiltonian is written as

$$\hat{H} = -\frac{\hbar^2}{2}\sum_{i,j}^{3N-6} g^{1/4}\frac{\partial}{\partial s_i} g^{-1/2} g_{i,j}\frac{\partial}{\partial s_j} g^{1/4} + V(s) \tag{198}$$

where g is the determinant of the metric tensor.

If we assume that, for small displacements along the curve, the metric tensor remains constant, the Hamiltonian can be simplified to

$$\hat{H} = -\frac{\hbar^2}{2}\sum_{i,j}^{3N-6} g_{i,j}\frac{\partial^2}{\partial s_i \partial s_j} + V(s) \tag{199}$$

If the IRC is separable from the other vibrational modes the total nuclear Hamiltonian can be written as a sum of a monodimensional IRC and the remaining vibrations, $\hat{H} = \hat{H}_{IRC} + \hat{H}_{\perp}$, where $\hat{H}_{IRC}$ is written as

$$\hat{H}_{IRC} = -\frac{\hbar^2}{2} g_{i,i}\frac{\partial^2}{\partial s_i^2} + V(s) \tag{200}$$

In this form, Eq. 199 is also called Reaction Path Hamiltonian [59].

Comparing Eq.199 with the standard expression for the Hamiltonian, it is clear that the inverse of the metric matrix is the reduced mass of the LAM.

Now, the computational strategy used to solve the curvilinear differential equation 200 requires to set the reduced mass to unity [63]; in this way, the arc length ds can be calculated for a monodimensional motion (compare with

Eq. 196) as the finite difference of the mass weighted Cartesian coordinates of two consecutive geometries i, $i+1$ *of the relaxed scan*

$$|ds|^2 = |\mathbf{X}_{i+1} - \mathbf{X}_i|^2 \tag{201}$$

This result is achieved by normalization of the gradient of the potential in Eq. 191 in mass weighted coordinates

$$\dot{\mathbf{X}} = \frac{\partial \mathbf{V}}{\partial \mathbf{X}} \cdot \frac{1}{|\partial \mathbf{V}/\partial \mathbf{X}|} \tag{202}$$

which is Eq. 56. Nevertheless, from the local, approximate knowledge of the arc length we obtain another definition for the reduced mass of a monodimensional LAM

$$\mu(s) = \left(\frac{ds}{dx}\right)^2 \tag{203}$$

In this method, the information about the variation of the reduced mass (a well known problem that interests different fields of scientific research) is stored in the discrepancy between $V(s)$*, the potential along the curve expressed in mass-weighted Cartesian coordinates, and* $V(x)$*, the potential in Cartesian coordinates.*

Equation 56 becomes indeterminate at any extremum point along the closed curve $\zeta(s)$*, but it can be shown [62] that even at these points the solution can be deduced from the knowledge of the second and third coefficients of the Taylor expansion of the PES, that we can perform automatically in the frame of VPT2 [50].*

[1] *Friedrich G Helfferich.* Kinetics of multistep reactions, *volume 40. Elsevier, 2004.*

[2] *Terrell L. Hill.* Introduction to Statistical Thermodynamics. *Dover Publications, 1986.*

[3] *William H. Miller, Rigoberto Hernandez, Nicolas C. Handy, Dylan Jayatilaka, and Andrew Willetts. Ab initio calculation of anharmonic constants for a transition state, with appliacion to semiclassical transition state tunneling probabilities.* Chemical Physics Letters, *174:62, 1990.*

[4] *Antonio Fernàndez-Ramos, James A. Miller, Stephen J. Klippenstein, and Donald G. Truhlar. Modelling the kinetics of bimolecular reactions.* Chem. Rev., *106:4518–4584, 2006.*

[5] *M. Karplus, R. N. Porter, and R. D. Sharma. Exchange reactions with activation energy. I. Simple Barrier Potential for (H, H_2).* The Journal of Chemical Physics, *43(9):3259–3287, 1965.*

[6] *Micheal Victor Berry and K. E. Mount. Semiclassical approximations in wave mechanics.* Rep. Prog. Phys., *35:315–397, 1972.*

[7] *Sally Chapman, Bruce C. Garrett, and William H. Miller. Semiclassical eigevalues for nonseparable system: Nonperturbative solution of the hamilton-jacobi equation in actionangle variables.* Journal of Chemical Physics, *64:502, 1976.*

[8] *Eric J. Heller. Timedependent approach to semiclassical dynamics.* The Journal of Chemical Physics, *62(4):1544–1555, 1975.*

[9] *Srihari Keshavamurthy and William H. Miller. A semiclassical model to incorporate multidimensional tunneling in classical trajectory simulations using locally conserved actions.* Chemical Physics Letters, *205(1):96 – 101, 1993.*

[10] *William H. Miller. Including quantum effects in the dynamics of complex (i.e., large) molecular systems.* The Journal of Chemical Physics, *125(13), 2006.*

[11] *Rudolph A. Marcus. At the birth of modern semiclassical theory.* Molecular Physics, *110:513, 2012.*

[12] *Michele Ceotto, Yu Zhuang, and William L. Hase. Accelerated direct semiclassical molecular dynamics using a compact finite difference hessian scheme.* The Journal of Chemical Physics, *138(5), 2013.*

[13] *Oliver Weingart, Annapaola Migani, Massimo Olivucci, Michael A. Robb, Volker Buss, and Patricia Hunt. Probing the photochemical funnel of a retinal chromophore model via zero-point energy sampling semiclassical dynamics.* The Journal of Physical Chemistry A, *108(21):4685–4693, 2004.*

[14] *William H. Miller. Quantum dynamics of complex molecular systems.* Proc. Natl. Acad. Sci. U.S.A., *102:6660–6664, 2005.*

[15] *M.S. Child.* Molecular Collision Theory. *Academic Press Inc., 1974.*

[16] *Wolfgang Domcke, David R Yarkony, and Horst Koppel.* CONICAL INTERSECTIONS. Electronic Structure, Dynamics and Spectroscopy. *Advanced Series In Physycal Chemistry. World Scientific, 2004.*

[17] *Micheal Baer.* Beyond Born-Oppenheimer Electronic Nonadiabatic Coupling Terms and Conical Intersections. *Wiley Interscience, 2006.*

[18] *A. D. Mcnaught and Wilkinson A.* IUPAC. Compendium of Chemical Terminology, 2nd ed. (the Gold Book). *WileyBlackwell; 2nd Revised edition edition, 1997.*

[19] *Max Born.* Mechanic of Atom. *G. Bell and Sons, LTD, 1927.*

[20] *Lokenath Debnath and Mikusinski Piotr.* Introduction to Hilbert Spaces with Applications, 3rd Edition. *Elsevier, 2005.*

[21] *Jeremy N. Harvey. Understanding the kinetics of spinforbidden chemical reactions.* Phys. Chem. Chem. Phys., *9:331–343, 2007.*

[22] *M. J. Frisch, G. W. Trucks, H. B. Schlegel, G. E. Scuseria, M. A. Robb, J. R. Cheeseman, G. Scalmani, V. Barone, B. Mennucci, G. A. Petersson, H. Nakatsuji, M. Caricato, X. Li, H. P. Hratchian, A. F. Izmaylov, J. Bloino, G. Zheng, J. L. Sonnenberg, M. Hada, M. Ehara, K. Toyota, R. Fukuda, J. Hasegawa, M. Ishida, T. Nakajima, Y. Honda, O. Kitao, H. Nakai, T. Vreven, Jr. Montgomery, J. A., J. E. Peralta, F. Ogliaro, M. Bearpark, J. J. Heyd, E. Brothers, K. N. Kudin, V. N. Staroverov, R. Kobayashi, J. Normand, K. Raghavachari, A. Rendell, J. C. Burant, S. S. Iyengar, J. Tomasi, M. Cossi, N. Rega, N. J. Millam, M. Klene, J. E. Knox, J. B. Cross, V. Bakken, C. Adamo, J. Jaramillo, R. Gomperts, R. E. Stratmann, O. Yazyev, A. J. Austin, R. Cammi, C. Pomelli, J. W. Ochterski, R. L. Martin, K. Morokuma, V. G. Zakrzewski, G. A. Voth, P. Salvador, J. J. Dannenberg, S. Dapprich, A. D. Daniels, O. Farkas, J. B. Foresman, J. V. Ortiz, J. Cioslowski, and D. J. Fox.* Gaussian Development Version, Revision H.30. *Gaussian Inc., Wallingford CT, 2009.*

[23] *James C. Keck. Variational theory of chemical reaction rates applied to three-body recombinations.* The Journal of Chemical Physics, *32(4):1035–1050, 1960.*

[24] *Donald G. Truhlar and Bruce C. Garrett. Variational transition-state theory.* Accounts of Chemical Research, *13(12):440–448, 1980.*

[25] *Donald G. Truhlar, A. D. Isaacson, and B. C. Garret. Generalizated transition state.* Theory of Chemical Reaction Dynamics, *-:65–137, 1985.*

[26] *Donald G Truhlar.* Variational Transition State Theory with Multudimensional Tunneling, *reviews in Computational Chemistry. Wiley, 2007.*

[27] *Vasilios S. Melissas and Donald G. Truhlar. Interpolated variational transition-state theory and semiclassical tunneling calculations of the rate constant of the reaction* $oh + c_2h_6$ *at 200-3000 k.* J. Phys. Chem, *pages 875–886, 1994.*

[28] *Wei-Peng Hu, Liu Yi-Ping, and Donald G. Truhlar. Variational transition-state theory and semiclassical tunnelling calculations with interpolated corrections : A new approach to interfacing electronic structure theory and dynamics for organic reactions.* Faraday Trans., *90:1715–1725, 1994.*

[29] *Jingzhi Pu, José C. Corchado, and Donald G. Truhlar. Test of variational transition state theory with multidimensional tunneling contributions against an accurate full-dimensional rate constant calculation for a six-atom system.* J. Chem. Phys., *115:6266, 2001.*

[30] *Philip Pechukas. Transition state theory.* Ann. Rev. Phys. Chem., *32:159–177, 1981.*

[31] *A. GonzalezLafont, T. N. Truong, and D. G. Truhlar. Interpolated variational transitionstate theory: Practical methods for estimating variational transitionstate properties and tunneling contributions to chemical reaction rates from electronic structure calculations.* Journal of Chemical Physics, *95:8875, 1991.*

[32] *E. Wigner. On the quantum correction for thermodynamic equilibrium.* Phys. Rev., *40:749–759, Jun 1932.*

[33] *S. Wiggins, L. Wiesenfeld, C. Jaffé, and T. Uzer. Impenetrable barriers in phase-space.* Phys. Rev. Lett., *86:5478–5481, Jun 2001.*

[34] *Donald McQuarrie.* Statistical Mechanics. *Harper & Row, 1976.*

[35] *Nicholas J. B. Green.* Unimolecular Kinetics. *Comprehesive Chemical Kinetics. Volume 39. Elsevier, 2003.*

[36] *Fueno Takayuki.* The Transition State: a Theoretical Approach. *Kodansha, 1999.*

[37] *M. G. Evans and M. Polanyi. Some applications of the transition state method to the calculation of reaction velocities, especially in solution.* Transactions of Faraday Society, *31:875, 1935.*

[38] *Henry Eyring. The activated complex in chemical reactions.* The Journal of Chemical Physics, *3(2):107–115, 1935.*

[39] *E. Jr Bright Wilson, J. C. Decius, and Paul C. Cross.* Molecular Vibrations. *McGraw-Hill, Inc, 1955.*

[40] *Han Keli and Chu Tianshu.* Reaction Rate Constant Computations.Theories and Applications. *RSC Theoretical and Computational Chemistry Series, 2014.*

[41] *R. A. Marcus. Lifetimes of active molecules. i.* The Journal of Chemical Physics, *20(3):352–354, 1952.*

[42] *R. A. Marcus. Lifetimes of active molecules. ii.* The Journal of Chemical Physics, *20(3):355–359, 1952.*

[43] *R. A. Marcus. Unimolecular dissociations and free radical recombination reactions.* The Journal of Chemical Physics, *20(3):359–364, 1952.*

[44] *Jingjing Zheng, Tao Yu, Ewa Papajak, I. M. Alecu, Steven L. Mielke, and Donald G. Truhlar. Practical methods for including torsional anharmonicity in thermochemical calculations on complex molecules: The internal-coordinate multi-structural approximation.* Phys. Chem. Chem. Phys., *13:10885–10907, 2011.*

[45] *Carl Eckart. Some studies concerning rotating axes and polyatomic molecules.* Phys. Rev., *47:552–558, Apr 1935.*

[46] *Aaron Sayvetz. The kinetic energy of polyatomic molecules.* The Journal of Chemical Physics, *7(6):383–389, 1939.*

[47] *Richard N. Zare. Wiley, New York, 1988.*

[48] *Wendell Forst.* Theory of Unimolecular Reactions. *Academic Press, 111 Fifth Avenue, New York, New York 10003.*

[49] *W. Forst and Z. PrÃ¡Å¡il. Exclusion of disallowed states from state density and its effect on unimolecular rate.* The Journal of Chemical Physics, *53(8):3065–3075, 1970.*

[50] *Vincenzo Barone, Malgorzata Biczysko, and Julien Bloino. Fully anharmonic ir and raman spectra of medium-size molecular systems: accuracy and interpretation.* Phys. Chem. Chem. Phys., *16:1759–1787, 2014.*

[51] *Chunyang Pend, Phylippe Y Ayala, and Bernhard H. Schlegel. Using redundant imternal coordinates to optimize equilibrium geometries and transition states.* J. Comp. Chem., *17:49, 1996.*

[52] *Nicholas C. Handy, S. M. Colwell, and William H. Miller. Semi-classical methods for vibrational energy levels of triatomic molecules.* Faraday Disc. Chem. Soc, *62:29, 1977.*

[53] *William H. Miller. Semi-classical theory for non-separable systems: Construction of good action-angle variables for reaction rate constants.* Faraday Discussions Chem. Soc., *62:40, 1977.*

[54] *Thanh Lam Nguyen, John F. Stanton, and John R. Barker. A practical implementation of semiclassical transition state theory for polyatomics.* Chemical Physics Letters, *499(1-3):9–15, 2010.*

[55] *Alberto Baiardi, Julien Bloino, and Vincenzo Barone. Accurate simulation of resonance-raman spectra of flexible molecules: An internal coordinates approach.* Journal of Chemical Theory and Computation, *11(7):3267–3280, 2015. PMID: 26575763.*

[56] *P. Pulay and G. Fogarasi. Geometry optimization in redundant internal coordinates.* The Journal of Chemical Physics, *96(4):2856–2860, 1992.*

[57] *Jon Baker, Alain Kessi, and Bernard Delley. The generation and use of delocalized internal coordinates in geometry optimization.* The Journal of Chemical Physics, *105(1):192–212, 1996.*

[58] *D. Skouteris, D. Calderini, and V. Barone. Methods for calculating partition functions of molecules involving large amplitude and/or anharmonic motions.* Journal of Chemical Theory and Computation, *12(3):1011–1018, 2016.*

[59] *William H. Miller, Nicholas C. Handy, and Adam John E. Reaction path hamiltonian for polyatomic molecules.* J. Chem. Phys, *72:99, 1980.*

[60] *S. Kato and Kenichi Fukui. Reaction ergodography. methane-tritium reaction.* Journal of American Chemical Society, *98:6395, 1976.*

[61] *Kenichi Fukui. The path of chemical reactions - the irc approach.* Acconuts of Chemical Research, *14:363, 1981.*

[62] *Michael Page and James W. McIver. On evaluating the reaction path hamiltonian.* The Journal of Chemical Physics, *88(2):922–935, 1988.*

[63] *W.Robert Daasch, Scott Werden, David Feller, and Ernest R. Davidson. Can any information about reaction paths be obtained from the reduced mass?* Journal of Molecular Structure: THEOCHEM, *103:177 – 181, 1983.*

[64] *J. C. Light, I. P. Hamilton, and J. V. Lill. Generalized discrete variable approximation in quantum mechanics.* The Journal of Chemical Physics, *82(3):1400–1409, 1985.*

[65] *C. Clay Marston and Gabriel G. Balint Kurti. The fourier grid hamiltonian method for bound state eigenvalues and eigenfunctions.* The Journal of Chemical Physics, *91(6):3571–3576, 1989.*

[66] *Daniel T. Colbert and William H. Miller. A novel discrete variable representation for quantum mechanical reactive scattering via the S matrix kohn method.* The Journal of Chemical Physics, *96(3):1982–1991, 1992.*

[67] *R. Meyer. Trigonometric interpolation method for OneDimensional QuantumMechanical problems.* The Journal of Chemical Physics, *52(4), 1970.*

[68] *T Beyer and Swinehart F.* Assoc. Comput. Mach., Commun., *16:379, 1973.*

[69] *Stephen E. Stein and B. S. Rabinovitch. Accurate evaluation of internal energy level sums and densities including anharmonic oscillators and hindered rotors.* The Journal of Chemical Physics, *58(6):2438–2445, 1973.*

[70] *Fugao Wang and D. P. Landau. Efficient, multiple-range random walk algorithm to calculate the density of states.* Phys. Rev. Lett., *86:2050–2053, Mar 2001.*

[71] *Siddhartha Chib and Edward Greenberg. Understanding the metropolis-hastings algorithm.* The american statistician, *49(4):327–335, 1995.*

[72] *Christoph Junghans, Danny Perez, and Thomas Vogel. Molecular dynamics in the multicanonical ensemble: Equivalence of Wang Landau sampling, statistical temperature molecular dynamics, and metadynamics.* Journal of Chemical Theory and Computation, *10(5):1843–1847, 2014. PMID: 26580515.*

[73] *Alessandro Laio and Michele Parrinello. Escaping free-energy minima.* Proceedings of the National Academy of Sciences, *99(20):12562–12566, 2002.*

[74] *Jaegil Kim, John E. Straub, and Thomas Keyes. Statistical-temperature monte carlo and molecular dynamics algorithms.* Phys. Rev. Lett., *97:050601, Aug 2006.*

[75] *Thanh Lam Nguyen and John R. Barker. Sums and densities of fully coupled anharmonic vibrational states: A comparison of three practical methods.* The Journal of Physical Chemistry A, *114(10):3718–3730, 2010. PMID: 20170143.*

[76] *Thomas Vogel, Ying Wai Li, Thomas Wüst, and David P. Landau. Scalable replica-exchange framework for wang-landau sampling.* Phys. Rev. E, *90:023302, Aug 2014.*

[77] *Craig A. Taatjes and Stephen J. Klippenstein. Kinetic isotope effects and variable reaction coordinates in barrierless recombination reactions.* The Journal of Physical Chemistry A, *105(37):8567–8578, 2001.*

[78] *Stephen J. Georgievskii, Yuri andKlippenstein. Transition state theory for multichannel addition reactions: multifaceted dividing surfaces.* The Journal of Physical Chemistry A, *107(46):9776–9781, 2003.*

[79] *James A. Miller and Stephen J. Klippenstein. Master equation methods in gas phase chemical kinetics.* The Journal of Physical Chemistry A, *110(36):10528–10544, 2006. PMID: 16956234.*

[80] *David R. Glowacki, Chi-Hsiu Liang, Christopher Morley, Michael J. Pilling, and Struan H. Robertson. Mesmer: An open-source master equation solver for multi-energy well reactions.* The Journal of Physical Chemistry A, *116(38):9545–9560, 2012. PMID: 22905697.*

[81] *Don L. Bunker and W. L. Hase. On non-rrkm unimolecular kinetics: Molecules in general, and ch3nc in particular.* The Journal of Chemical Physics, *59(9), 1973.*

[82] *Scott R. Vande Linde and William L. Hase. Non-rrkm kinetics in gas-phase sn2 nucleophilic substitution.* The Journal of Physical Chemistry, *94(16):6148–6150, 1990.*

[83] *Upakarasamy Lourderaj and William L. Hase. Theoretical and computational studies of non-rrkm unimolecular dynamics.* The Journal of Physical Chemistry A, *113(11):2236–2253, 2009. PMID: 19243125.*

[84] *David J. Tannor. Introduction to quantum mechanics: A time-dependent perspective.* Journal of Chemical Education, *85(7):919, 2008.*

[85] *William H. Miller. Beyond transition-state theory: a rigorous quantum theory of chemical reaction rates.* Accounts of Chemical Research, *26(4):174–181, 1993.*

[86] *William H. Miller. Quantum mechanical transition state theory and a new semiclassical model for reaction state constants.* J. Chem. Phys., *61:1823, 1974.*

[87] *William H. Miller, Steven D Schwartz, and John W Tromp. Quantum mechanical rate constant for bimolecular reactions.* J. Chem. Phys., *79:4889, 1983.*

[88] *William H. Miller. Unified statistical model for complex and direct reaction mechanisms.* Journal of Chemical Physics, *65:2216, 1976.*

[89] *Tsunenobu Yamamoto. Quantum statistical mechanical theory of the rate of exchange chemical reactions in the gas phase.* The Journal of Chemical Physics, *33(1), 1960.*

[90] *Tae Jun Park and J. C. Light. Quantum flux operators and thermal rate constant: Collinear h+h2.* J. Chem. Phys., *88:4897, 1988.*

[91] *Tamar Seideman and William H. Miller. Transition state theory, siegert eigenstates, and quantum mechanical reaction rates.* The Journal of Chemical Physics, *95(3), 1991.*

[92] *Uwe Manthe. Calculation of initial state-selected reaction probabilities by a minimal number of wavepackets.* Chemical Physics Letters, *241(5-6):497–501, 1995.*

[93] *Tamar Seideman and William H. Miller. Calculation of the cumulative reaction probability via a discrete variable representation with absorbing boundary conditions.* Journal of Chemical Physics, *96:4412, 1992.*

[94] *Manthe Uwe, Seideman Tamar, and William H. Miller. Full-dimensional quantum mechanical calculation of the rate constant for* $h_2 + oh\ h_2o + h$. Journal of Chemical Physics, *99:10078–10081, 1993.*

[95] *Uwe Manthe and William H. Miller. Cumulative raction probability as eigenvalue problem.* J. Chem. Phys., *99:3412, 1993.*

[96] *FermÃn Huarte-Larrañaga and Uwe Manthe. Calculating initial-state-selected reaction probabilities from thermal flux eigenstates: A transition-state-based approach.* The Journal of Chemical Physics, *123(20), 2005.*

[97] *Gerd Schiffel and Uwe Manthe. A transition state view on reactive scattering: Initial state-selected reaction probabilities for the* $h + ch4 \rightarrow h2 + ch3$ *reaction studied in full dimensionality.* The Journal of Chemical Physics, *133(17), 2010.*

[98] *H. Tal—Ezer and R. Kosloff. An accurate and efficient scheme for propagating the time dependent schrödinger equation.* The Journal of Chemical Physics, *81(9):3967–3971, 1984.*

[99] *D. Kosloff and R. Kosloff. A fourier method solution for the time dependent schrÃ¶dinger equation as a tool in molecular dynamics.* Journal of Computational Physics, *52(1):35 – 53, 1983.*

[100] *Ronnie Kosloff. Time-dependent quantum-mechanical methods for molecular dynamics.* The Journal of Physical Chemistry, *92(8):2087–2100, 1988.*

[101] *Leonard Schiff.* Quantum Mechanics*. McGraw-Hill Book company, 1968.*

[102] *Eric J. Heller. Frozen gaussians: A very simple semiclassical approximation.* The Journal of Chemical Physics*, 75(6), 1981.*

[103] *R. B. Gerber, V. Buch, and Mark A. Ratner. Time-dependent self-consistent field approximation for intramolecular energy transfer. i. formulation and application to dissociation of van der waals molecules.* The Journal of Chemical Physics*, 77(6), 1982.*

[104] *H.-D. Meyer, U. Manthe, and L.S. Cederbaum. The multi-configurational time-dependent hartree approach.* Chemical Physics Letters*, 165(1):73 – 78, 1990.*

[105] *Eric J. Heller. Time dependent variational approach to semiclassical dynamics.* The Journal of Chemical Physics*, 64(1), 1976.*

[106] *A. Raab. On the dirac-frenkel/mclachlan variational principle.* Chemical Physics Letters*, 319(5-6):674 – 678, 2000.*

[107] *Hans-Dieter Meyer, Fabien Gatti, and Graham A. Worth.* Multidimensional Quantum Dynamics: MCTDH Theory and Applications*. Wiley-VCH Verlag GmbH & Co. KGaA, 2009.*

[108] *M.H. Beck, A. JÃ€ckle, G.A. Worth, and H.-D. Meyer. The multiconfiguration time-dependent hartree (mctdh) method: a highly efficient algorithm for propagating wavepackets.* Physics Reports*, 324(1):1 – 105, 2000.*

[109] *Graham A. Worth and Irene Burghardt. Full quantum mechanical molecular dynamics using gaussian wavepackets.* Chemical Physics Letters*, 368(3-4):502 – 508, 2003.*

[110] *D. Skouteris and V. Barone. A new gaussian mctdh program: Implementation and validation on the levels of the water and glycine molecules.* The Journal of Chemical Physics*, 140(24), 2014.*

[111] *I. Burghardt, H.-D. Meyer, and L. S. Cederbaum. Approaches to the approximate treatment of complex molecular systems by the multiconfiguration time-dependent hartree method.* The Journal of Chemical Physics*, 111(7), 1999.*

[112] *Sophya Garashchuk and Tijo Vazhappilly. Wavepacket approach to the cumulative reaction probability within the flux operator formalism.* The Journal of Chemical Physics*, 131(16), 2009.*

[113] *Vincenzo Barone. Vibrational zero-point energies and thermodynamic functions beyond the harmonic approximation.* J. Chem. Phys.*, 120:3059, 2004.*

[114] *Jingjing Zheng and Donald G. Truhlar. Quantum thermochemistry: Multistructural method with torsional anharmonicity based on a coupled torsional potential.* Journal of Chemical Theory and Computation, *9(3):1356–1367, 2013. PMID: 26587598.*

[115] *Antonio Fernández-Ramos. Accurate treatment of two-dimensional non-separable hindered internal rotors.* The Journal of Chemical Physics, *138(13), 2013.*

[116] *D. G. Truhlar and A. D. Isaacson. Simple perturbation theory estimates of equilibrium constants from force fields.* Journal of Chemical Physics, *94:357, 1991.*

[117] *Frank Matzkies and Uwe Manthe. Accurate reaction rate calculations including internal and rotational motion: A statistical multiconfigurational time-dependent hartree approach.* The Journal of Chemical Physics, *110(1), 1999.*

[118] *Stefan Grimme. Semiempirical gga-type density functional constructed with a long-range dispersion correction.* Journal of computational chemistry, *27(15):1787–1799, 2006.*

[119] *J. T. Hougen. Strategies for advanced applications of permutation-inversion groups to the microwave spectra of molecules with large amplitude motions.* Journal of Molecular Spectroscopy, *256:170–185, August 2009.*

[120] *Sophie Blasco and David Lauvergnat. Quantum study of the internal rotation of methanol in full dimensionality* $(1+11\mathrm{d})$*: a harmonic adiabatic approximation.* Chemical Physics Letters, *373(3-4):344 – 349, 2003.*

[121] *J. C. A. Bobyens, D. C. Levendis, Michael I. Bruce, and Michael L. Williams. Crystal structure of osmocene, os(*η*-c5h5)2.* Journal of Crystallographic and Spectroscopic Research, *16(4):519–524, 1986.*

[122] *J. Bodenheimer, E. Loewenthal, and W. Low. The raman spectra of ferrocene.* Chemical Physics Letters, *3(9):715 – 716, 1969.*

[123] *J. Bodenheimer. The raman spectra of ruthenocene.* Chemical Physics Letters, *6(5):519 – 520, 1970.*

[124] *Camille Latouche, Federico Palazzetti, Dimitrios Skouteris, and Vincenzo Barone. High-accuracy vibrational computations for transition-metal complexes including anharmonic corrections: Ferrocene, ruthenocene, and osmocene as test cases.* Journal of Chemical Theory and Computation, *10(10):4565–4573, 2014. PMID: 26588150.*

[125] *John P. Perdew, Kieron Burke, and Yue Wang. Generalized gradient approximation for the exchange-correlation hole of a many-electron system.* Phys. Rev. B, *54:16533–16539, Dec 1996.*

[126] *P. Jeffrey Hay and Willard R. Wadt. Ab initio effective core potentials for molecular calculations. potentials for the transition metal atoms sc to hg.* The Journal of Chemical Physics, *82(1), 1985.*

[127] *Richard B. McClurg, Richard C. Flagan, and William A. Goddard III. The hindered rotor density-of-states interpolation function.* The Journal of Chemical Physics, *106(16), 1997.*

[128] *James P. Ferris and William J. Hagan. Hcn and chemical evolution: The possible role of cyano compounds in prebiotic synthesis.* Tetrahedron, *40(7):1093 – 1120, 1984.*

[129] *Nadia Balucani. Elementary reactions of n atoms with hydrocarbons: first steps towards the formation of prebiotic n-containing molecules in planetary atmospheres.* Chem. Soc. Rev., *41:5473–5483, 2012.*

[130] *Fanny Vazart, Danilo Calderini, Dimitrios Skouteris, Camille Latouche, and Vincenzo Barone. Reassessment of the thermodynamic, kinetic, and spectroscopic features of cyanomethanimine derivatives: A full anharmonic perturbative treatment.* Journal of Chemical Theory and Computation, *11(3):1165–1171, 2015. PMID: 26579765.*

[131] *Stefan Grimme. Semiempirical hybrid density functional with perturbative second-order correlation.* The Journal of Chemical Physics, *124(3), 2006.*

[132] *J. Troe and V.G. Ushakov. Anharmonic rovibrational numbers and densities of states for* HO_2, H_2CO, *and* H_2O_2. The Journal of Physical Chemistry A, *113(16):3940–3945, 2009.*

[133] *Jeffrey L. Bada and Henderson James Cleaves. Ab initio simulations and the miller prebiotic synthesis experiment.* Proceedings of the National Academy of Sciences, *112(4):E342, 2015.*

[134] *Yassin A. Jeilani, Huyen Thi Nguyen, Beatriz H. Cardelino, and Minh Tho Nguyen. Free radical pathways for the prebiotic formation of xanthine and isoguanine from formamide.* Chemical Physics Letters, *598:58 – 64, 2014.*

[135] *Samanta Pino, Judit E Sponer, Giovanna Costanzo, Raffaele Saladino, and Ernesto Di Mauro. From formamide to rna, the path is tenuous but continuous.* Life, *5(1):372–384, 2015.*

[136] *Pilar Redondo, Carmen Barrientos, and Antonio Largo. Some insights into formamide formation through gas-phase reactions in the interstellar medium.* The Astrophysical Journal, *780(2):181, 2014.*

[137] *Brant M. Jones, Christopher J. Bennett, and Ralf I. Kaiser. Mechanistical studies on the production of formamide (h2ncho) within interstellar ice analogs.* The Astrophysical Journal, *734(2):78, 2011.*

[138] *Akbar Mohamad Ali and John R. Barker. Comparison of three isoelectronic multiple-well reaction systems: Oh + ch2o, oh + ch2ch2, and oh + ch2nh.* The Journal of Physical Chemistry A, *119(28):7578–7592, 2015. PMID: 25839620.*

[139] *C. Kahane, Ceccarelli. C., A. Faure, and E. Caux. Detection of formamide, the simplest but crucial amide, in a solar-type protostar.* The Astrophysical Journal Letters, *763(2):L38, 2013.*

[140] *Fanny Vazart, Camille Latouche, Dimitrios Skouteris, Nadia Balucani, and Vincenzo Barone. Cyanomethanimine isomers in cold interstellar clouds: Insights from electronic structure and kinetic calculations.* The Astrophysical Journal, *810(2):111, 2015.*

[141] *John D. Watts, JÃŒrgen Gauss, and Rodney J. Bartlett. Coupled-cluster methods with noniterative triple excitations for restricted open-shell hartree-fock and other general single determinant reference functions. energies and analytical gradients.* The Journal of Chemical Physics, *98(11), 1993.*

[142] *J. F. Stanton, J. Gauss, M. E. Harding, and P. G. Szalay.*

[143] *Z. Kaňuchová, R. G. Urso, G. A. Baratta, J. R. Brucato, M. E. Palumbo, and G. Strazzulla. Synthesis of formamide and isocyanic acid after ion irradiation of frozen gas mixtures.* Astronomy and Astrophysics.

[144] *Timothy Hollebeek, Tak-San Ho, and Herschel Rabitz. A fast algorithm for evaluating multidimensional potential energy surfaces.* The Journal of Chemical Physics, *106(17), 1997.*

[145] *Mohsen Razavy.* Quantum theory of tunneling. *World Scientific, 2003.*

[146] *Manfredo P. Do Carmo.* Differential Geometry of Curves and Surfaces. *Prentice–Hall, Instituto de Matematica Pura e Aplicada (IMPA) Rio de Janeiro, Brazil, 2nd edition, 1976.*

[147] *Akitomo Tachibana and Kenichi Fukui. Differential geometry of chemically reacting systems.* Theoretica chimica acta, *49(4):321–347, 1978.*

[148] *Boris Podolsky. Quantum-mechanically correct form of hamiltonian function for conservative systems.* Phys. Rev., *32:812–816, Nov 1928.*

[149] *L.J. Schaad and Jiani Hu. The schrÃ¶dinger equation in generalized coordinates.* Journal of Molecular Structure: THEOCHEM, *185:203 – 215, 1989.*